

6-2020

Functional heterogeneity and metabolic adaptation of fibroblasts in cancer

Lisa Becker

Follow this and additional works at: https://digitalcommons.library.tmc.edu/utgsbs_dissertations



Part of the [Medicine and Health Sciences Commons](#)

Recommended Citation

Becker, Lisa, "Functional heterogeneity and metabolic adaptation of fibroblasts in cancer" (2020). *The University of Texas MD Anderson Cancer Center UTHealth Graduate School of Biomedical Sciences Dissertations and Theses (Open Access)*. 1015.

https://digitalcommons.library.tmc.edu/utgsbs_dissertations/1015

This Thesis (MS) is brought to you for free and open access by the The University of Texas MD Anderson Cancer Center UTHealth Graduate School of Biomedical Sciences at DigitalCommons@TMC. It has been accepted for inclusion in The University of Texas MD Anderson Cancer Center UTHealth Graduate School of Biomedical Sciences Dissertations and Theses (Open Access) by an authorized administrator of DigitalCommons@TMC. For more information, please contact digitalcommons@library.tmc.edu.

FUNCTIONAL HETEROGENEITY AND METABOLIC ADAPTATION OF
FIBROBLASTS IN CANCER

by

Lisa Maria Becker, BS, MS

APPROVED:



Raghu Kalluri, MD., Ph.D.
Advisory Professor



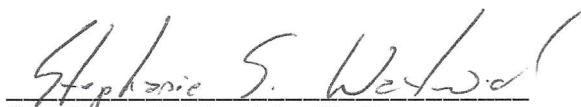
Menashe Bar-Eli, Ph.D.



Jonathan Kurie, M.D.



Samuel Mok, Ph.D.



Stephanie Watowich, Ph.D.

APPROVED:

Dean, The University of Texas

MD Anderson Cancer Center UTHealth Graduate School of Biomedical Sciences

FUNCTIONAL HETEROGENEITY AND METABOLIC ADAPTATION OF FIBROBLASTS IN CANCER

A

THESIS [DISSERTATION]

Presented to the Faculty of

The University of Texas

MD Anderson Cancer Center UTHealth

Graduate School of Biomedical Sciences

in Partial Fulfillment

of the Requirements

for the Degree of

DOCTOR OF PHILOSOPHY

by

Lisa Maria Becker, BS, MS
Houston, Texas

May, 2020

DEDICATION

I am dedicating this thesis to my grandfather Willi Fetsch – he would explode with pride!

I am also dedicating this thesis to my parents Helmut Becker and Regina Fetsch-Becker. None of my achievements thus far would have been possible without the support of my parents. I cannot put in words how thankful I am for all the sacrifices they have made for me. They brought me up to become the person I am today. They have always been my greatest supporters and their unwavering confidence in me has been essential for my success.

WIDMUNG

Ich widme diese Arbeit meinem Großvater Willi Fetsch – er würde vor Stolz platzen!

Ebenso widme ich diese Arbeit meinen Eltern Helmut Becker and Regina Fetsch-Becker. Keines meiner Ziele in meinem Leben hätte ich ohne die unermüdliche Unterstützung meiner Eltern erreicht. Ich kann nicht in Worte fassen, wie dankbar ich bin, für alle Opfer, die meine Eltern für mich erbracht haben. Sie haben mich zu dem Menschen gemacht, der ich heute bin. Schon immer waren sie meine größten Fans und ihre unerschütterliche Zuversicht in mein Können war untentbehrlich für meinen Erfolg.

ACKNOWLEDGEMENTS

First and foremost, I would like to thank Dr. Raghu Kalluri for mentoring me over the past 5 years. I have grown enormously as a scientist, and also as a person under his guidance and mentorship. He has taught me how to think critically about my work, how to face and overcome challenges in my project and how to present my work in written and oral formats – all hallmarks of a good and successful scientist. But how you teach someone is very unique and determines how well a person gets trained. When I first started working in Raghu's lab, I oftentimes wondered why he does not tell me more outright what to do, how to solve a specific problem, or which direction to move forward into, and instead provided a few suggestions and then left me with the words 'think about it'. This has given me the opportunity to really freely pursue what I am passionate about, but more importantly, it forced me to deeply think about my work! The small pointers and suggestions he provided, were always just enough to help guiding my thinking process, but allowed me to arrive at a conclusion, or solve the problem on my own. I can appreciate that this form of mentoring might be at times more exhausting for the mentor, as sometimes my thinking process took a while and needed redirecting, but it trained me to think independently and gave me confidence in my own skills and thinking. What was also critical for developing confidence in my own scientific skills, was Raghu constantly forcing me to step out of my comfort zone and take on challenges that I never knew I am capable to face. I have learnt that when I was asked to take over a specific task, such as helping to create and validate transgenic animals, I can trust Raghu that - whatever it is - doing it, is good for me! Whenever faced with such a situation, I would first be afraid of it; but Raghu's utmost confidence in me being able to accomplish the task, made me do it – and I always succeeded. Thus, he has shown me, what I am actually capable of, which I can truly say, is one of the most important things I take away from my PhD and I will forever be grateful for this lesson. Lastly, Raghu has always had my back and supported me in every aspect of my graduate school career. Whether it was me finding myself unfairly treated and he stepping up for me, or whether it was me being frustrated about my experiments - he has shown himself as very supportive and understanding and I was always able to have open conversations with him and received advice and support. I know I have not always been an easy grad student; I am notoriously last minute in asking for his help with anything – and he has always taken the time to help me regardless of my last-minute request. He has always been very accommodating and most understanding, so I could do learn things in a way and at a pace that fits me personally. I truly appreciate his patience and the time and effort he has taken to help me succeed in graduate school and also to prepare me for a future career in research.

Second, I deeply thank Dr. Valerie LeBleu, who I consider as a second mentor in the lab. Val is the most energetic person I have ever met, and I consider myself very lucky to be working with her. Val's way of teaching you how to perform surgery or an experiment, is the most efficient and helpful way I have ever experienced, and it ensures you will not forget anything important. Instead of long explanations, she tells you very specifically - and also demonstrates to you - the critical steps in each experiment that you absolutely must follow precisely. This ensures that you will be able to perform the experiment independently already the next time – because instead of trying to remember hours of someone talking at you trying to explain something, you remember exactly the important steps. One of the important skills as a scientist is being able to teach others in the lab and thanks to her teaching me very well, I know I will be able to train others likewise in my future career. In contrast to her inexhaustible amount of energy, she also has unlimited patience! She has always helped me with literally every problem and issue I had throughout my work. I could come to her office the 20th time in one hour, because I still have a problem with an experiment or the analysis of such (with the less straightforward, more complicated problems), and she still welcomes me with a smile, tells me to sit down and interrupts her own work to make sure to help me. I will be forever thankful for her endless patience with me and her support and the tremendous time and effort she spends helping me with all of my projects. Even after she had left the institution, she has been continuously working with me and is always available for a phone call whenever I have a question. In addition to purely scientific advice, Val taught me much about how to work efficiently, carefully and stringently, how to manage time and also how to avoid getting overwhelmed. Together, Val and Raghu have taught me invaluable lessons about preparing a manuscript and going through the publication process and throughout this process they have always had unrestricted confidence in me, which helped me to grow above all my own expectations.

I would also like to thank my great advisory committee: I have known Dr. Menashe Bar-Eli from the very start in graduate school, as he works in the same department, and just down the hallway from me. He has not only provided me advice as his role as my committee member, but after every journal club or seminar I have presented in the department, he has taken the time to offer his critique and advice. His door has always been open, and even if I just came for a signature for the Cancer Biology program, he would always ask me how things are going and give me a suggestion or two for my project. I greatly appreciate all his advice. Dr. Jonathan Kurie has been a great and very supportive member on my committee. He has met with me several times outside the committee meeting setting and our discussion have always lasted forever. I have

always felt he was as excited about my project as I am myself, which has been a great motivation over the years. I have also enjoyed having Dr. Samuel Mok on my committee, who has always challenged me with great questions that made me think about my project deeply. I have always appreciated his advice and ideas of all the things I can do in my project, and I hope I didn't disappoint him, that I wasn't able to chase them all. When I had to find a new committee member in my fourth year of graduate school, I was so lucky to have Dr. Stephanie Watowich stepping in and commit to being on my advisory committee. I always was a big fan of her teaching while I took her lectures as part of the graduate school program, and I was happy that I was able to benefit more from her teaching while having her on my committee. She was willing to engage with my research that was already at a later stage when she joined my committee and provided new and valuable perspectives. I am very grateful for this. Lastly, I would like to thank Dr. Valerie LeBleu, who served on my committee until she left the institution. She has shown me that her officially stepping down from my advisory committee did not change her role as one of my advisors by continuously offering her help and guidance. I am deeply thankful for this exceptional care for me as her student. Together, I also thank all my committee members for being the most responsive faculty I have ever met. They make a student's life so easy – I am the only one I know, who can schedule her meetings within two days, because everyone always readily responds. It has made all formal things that a student is required to do during graduate school very easy for me and I have never taken that for granted!

Next, I would like to thank all the people directly involved in this work and without who's help and work this would have not been possible:

Drs. Joyce O'Connell, Annie Vo, Margo Cain, Rodrigues Blanco, Desiree Tampe, Lauren Bizarro, Hikaru Sugimoto, Anna McGow, Sughra Raza, John Asara, Sara Lovisa, Kathleen McAndrews, Rafal Zielinski, Philip Lorenzi, Michael Zeisberg, Patricia Philips, Pedro Correa de Sampaio, and Ehsan Ehsanipour were all critically involved in the study of CAF heterogeneity and the metabolic reprogramming of CAFs presented in the first part of this thesis. Joyce, Annie and Margo had built the basis for the project investigating CAFs' metabolic reprogramming and performed a great part of the experiments. I was very lucky to learn from their great discoveries and add more experiments to round up the work.

Drs. Hans Petter Eikesdal, Yingqi Teng, Akane Kizu, Julianne Carstens, Keizo Kanasaki, and Hikaru Sugimoto were collaborators on the study presented in the second part of this thesis that investigates how deregulated TGF β signaling can cause epithelial carcinogenesis of the forestomach. Hans and Yingqi were the leaders of this project and I was lucky to be able to

collaborate with them and expand my knowledge about fibroblasts to a different aspect, as well as a different cancer type.

I also thank all members of the Kalluri lab family, all of whom helped me at some point, if it was with experimental advice, or bringing me some home-cooked food – I am thankful to have had them all by my side. In particular, I would like to thank Drs. Julie Carstens, Sara Lovisa and Pedro Correa de Sampaio. As senior postdocs who have gone through the grad school experience they have always provided me with immense help, whether it was advice on how to perform experiments, how to interpret or analyze my data, or how to keep going when going through frustration! I'm sure I annoyed them more than only once and I thank them for being great mentors and friends. I also need to thank Dr. Olga Volpert for all advice and help she has provided me. I immensely appreciate the friendships in the lab, particularly those of Kebbeh, Mari and Dr. Jena. Kebbeh is an amazing person to be around and a great friend who has always helped me when I needed her- both in and outside the lab! She made sure I have food when working late at the lab and assisted me with experiments whenever I needed help. Mari has always helped me not to forget my European roots and has become a very good friend over the past 5 years. She makes the best red cabbage pasta there is and you can have the best scientific and non-scientific conversations with her over a glass of wine outside in the non-air-conditioned world. When I met Jena at the first day of graduate school, she mentioned she rides horses, so I knew I have to become her friend. Little did I know, that we not only would work in the same lab, become good friends who indeed ride horses together, but also that her entire family here in Houston basically adopted me as their foreign child. Jena, and her parents Leslie and John Tavormina are such welcoming people with the biggest heart. They have provided me with a support system that made being far away from my family much easier. They took me in during Harvey and I'm invited to every holiday. Jena brings me Starbucks before every big event, such as me having to give a presentation or taking an exam. I really appreciate all her thoughtfulness and also all the fun we had together throughout the years. I would also like to thank Drs. Hikaru Sugimoto, Jiha Kim, Toru Miyake, Kate McAndrews, Michelle Kirtley and Janine Hensel for help, training and advice throughout the years.

We have a very supportive graduate program, and I would like to thank the Deans, as well as Brenda Gaughan, Lourdes (Bunny) Perez and Elisabet Lau for all the support and constantly helping me with any questions I have. I have also received financial support from the Rosalie B. Hite fellowship over the past two years, which I am tremendously thankful for.

Thank you to all of my friends outside the lab, who have supported me and who are too many to list them all. Specifically, I want to thank Daniel, who is one of the greatest friends one can ask for. Without him, I am not sure if I had ever gone to graduate school. When I first mentioned graduate school to him, he signed me up for a GRE practice test and ordered me the learning books – which was the push that got me started. He also has edited all my applications to graduate school and then while in graduate school, he has listened to all of my excitement and happiness about my research, but also endured all of my whining and self-doubts in our weekly phone calls. He has been a great source of comfort throughout this experience.

I also need to thank my family and all my friends back home in Germany. My family has always been my rock through every period of my life. Their unconditional love and support helped me through life and through graduate school. I thank my parents Regina and Helmut and my siblings Hanna and Philipp for being so understanding of me being so far away from home and not being able to take part in lots of important things in their lives. Hanna and Philipp are the greatest siblings, who are also my best friends and who always remind me who I am. When being so far away for such a long time you know if you have true friends, and I am lucky to have several of those. I cannot mention all of them, but I thank Anni for texting with me almost every day about literally everything in our lives, and Miri for asking me to be her maid of honor and arranging her wedding according to my schedule so that I could attend – This meant so much to me!

Last, but not least, I thank Linda Middleton and Winston. Linda generously has been letting me ride her horse Winston over the past 3 years, which is an enormous gift as anyone who rides horses would know. Winnie, without knowing, has kept me sane over the years, because the world always looks much better from the back of a horse with your feet off the ground!

FUNCTIONAL HETEROGENEITY AND METABOLIC ADAPTATION OF FIBROBLASTS IN CANCER

Lisa Maria Becker, MS

Advisory Professor: Raghu Kalluri, MD., Ph.D.

The tumor microenvironment is comprised of a multitude of cell types producing a milieu of cytokines, growth factors and an extracellular matrix. Together, this intricate network of cells plays highly critical roles in determining a tumor's potential to progress and metastasize. As the predominant cell types in the tumor microenvironment, cancer-associated fibroblasts (CAFs) are a key component in the regulation of tumor development and progression, but their exact functions in tumorigenesis remain poorly understood. This is partly due to the considerable heterogeneity amongst these cells, which confounds the characterization of their roles within the tumor microenvironment. Nevertheless, recent studies have provided fresh insights in CAFs biology and how these cells contribute to tumorigenesis at different stages, suggesting that CAFs can reshape the tumor immune response via interactions with immune cells, as well as induce tumor angiogenesis and support cancer cell proliferation through modifying tumor metabolism. These reports provided excellent groundwork to further unravel the complex and heterotypic functions of this cell type.

In this work, we identified phenotypically and functionally distinct CAF subtypes critical in mammary carcinoma progression using multiplex staining techniques and genetically engineered mouse models that enables the specific targeting of CAF subtypes. Specifically, the distinct functional roles played by α SMA⁺, FAP⁺ and PDGFR β ⁺ CAFs were characterized. While targeting

FAP⁺ CAFs did not cause any dramatic changes in primary tumor growth or metastasis, depletion of PDGFR β ⁺ CAFs moderately reduced tumor growth and metastasis. On the other hand, α SMA⁺ CAFs-depleted tumors grew significantly slower and showed decreased angiogenesis. Compellingly, despite primary tumor growth stagnation and notably smaller tumors, metastasis to the lungs continued unabated or even slightly increased in mice with tumors lacking α SMA⁺ CAFs. Intriguingly, we observed a down-regulation of tumor metabolites in tumors depleted of α SMA⁺ CAFs. We further examined the metabolic relationship between CAFs and cancer cells to arrive at a mechanistic understanding of the observed metabolic phenotypes in CAFs. Our work demonstrates that CAFs' metabolic reprogramming can be triggered by hypoxia-induced epigenetic modification of HIF-1 α and rate-limiting glycolytic enzymes.

As an extension to this work, we further explored fibroblasts' contributions to cancer initiation. Here, we leveraged a previously reported mouse model in which Tgf β signaling in fibroblasts has shown to modulate epithelial growth, resulting in squamous carcinoma of the forestomach. In our studies, we uncovered a complex feed forward loop, in which the loss of Tgf β receptor 2 in FSP1⁺ fibroblasts leads to a Smad4-dependent up-regulation of HGF production to induce increased proliferation in neighboring epithelial cells. The proliferating epithelial cells release BMP7 which, in turn, promotes fibroblast proliferation. Interestingly, we demonstrated that this signaling cross-talk is specific to FSP1⁺ fibroblasts, highlighting the importance of fibroblast heterogeneity not only in cancer progression, but also in normal tissue homeostasis.

The work presented in this thesis offers novel insights into fibroblast biology at different stages of cancer development and progression. Our studies shed new light on how fibroblast subsets can phenotypically and functionally be defined. We also showed in two settings how fibroblast - epithelial cell interactions are critical for tumor initiation or progression. In one context, we demonstrated the metabolic liaison between CAFs and cancer cells can drive tumorigenesis.

In the second context, we showed an intricate signaling cross-talk between fibroblasts and epithelial cells is required to provoke epithelial carcinogenesis.

LIST OF CONTENTS

APPROVAL PAGE.....	i
TITLE PAGE.....	ii
DEDICATION.....	iii
ACKNOWLEDGMENTS.....	iv
ABSTRACT.....	ix
LIST OF CONTENTS.....	xii
LIST OF FIGURES.....	xvii
LIST OF TABLES.....	xix
CHAPTER 1	
BACKGROUND AND SIGNIFICANCE.....	1
Tumor microenvironment.....	2
Cancer-associated fibroblasts.....	6
CAF heterogeneity.....	8
Glucose metabolism in CAFs.....	10
Dissertation goals and major findings.....	11
CHAPTER 2	
MATERIALS AND METHODS.....	13
Murine cell lines.....	14
Patient-derived cell lines.....	14
Mice.....	15
4T1 orthotopic mammary cancer models.....	16
4T1 intravenous injections in α SMA-vTK mice.....	17

MMTV-PyMT mammary cancer mouse models.....	17
Immunofluorescence on human tissues	18
Immunolabeling of mouse tissues	19
Immunohistochemistry and immunofluorescence on murine mammary carcinoma tissues.....	19
Immunohistochemistry and immunofluorescence on murine forestomach tissues	21
TSA-based multiplex staining on murine mammary carcinoma tissues.....	23
Imaging of FSP1-GFP and α SMA-RFP signal	24
Immunofluorescence analyses of cultured cells	24
Chromogenic in situ hybridization (CISH).....	25
Analysis of immune cell populations in CAF-depleted tumors.....	26
Quantitative real time PCR.....	28
Human and mouse mammary fibroblasts.....	28
Murine forestomach fibroblasts.....	29
Immunoblotting.....	32
Human mammary fibroblasts.....	3
Isolated forestomach fibroblasts and tissues.....	32
5-Azacytidine treatments of hBFs	33
E10 epithelial cell proliferation assays	33
BMP7 stimulation of forestomach fibroblast proliferation	34
¹³ C glucose labeling experiments.....	34
Seahorse Glycolysis Stress Test	35

Statistical analysis	36
CHAPTER 3	
CHARACTERIZATION OF FIBROBLAST HETEROGENEITY IN MURINE MODELS OF MAMMARY CARCINOMA	37
Summary.....	38
Introduction.....	38
CAF heterogeneity in the 4T1 mammary carcinoma mouse model.....	40
CAF heterogeneity in the MMTV-PyMT mammary carcinoma mouse model.....	43
Mesenchymal marker expression in human samples.....	47
Interpretation of findings.....	49
Potential pitfalls and alternate approaches.....	50
Future directions.....	51
CHAPTER 4	
DISTINCT FIBROBLAST SUBTYPES EXHIBIT DIFFERENT FUNCTIONS IN MAMMARY CARCINOMA	53
Summary.....	54
Introduction.....	54
Functions of α SMA ⁺ CAFs in mammary carcinoma progression.....	58
Functions of FAP ⁺ CAFs in mammary carcinoma progression.....	67
Functions of PDGFR β ⁺ CAFs in mammary carcinoma progression.....	69

Interpretation of findings.....	71
Potential pitfalls and alternate approaches.....	76
Future directions.....	78
CHAPTER 5	
CANCER-ASSOCIATED FIBROBLASTS ARE EPIGENETICALLY REPROGRAMMED TOWARD INCREASED GLYCOLYSIS AND FACILITATE MAMMARY CARCINOMA PROGRESSION.....	79
Summary.....	80
Introduction.....	80
CAFs display a glycolytic phenotype.....	83
Breast cancer-derived human CAFs display enhanced glycolytic activity....	86
Cancer cells uptake and utilize CAF-secreted metabolites to fuel their metabolism.....	88
Oscillating oxygen tension results in epigenetic reprogramming of hBFs to attain CAF-like metabolic profiles.....	90
Interpretation of findings.....	94
Potential pitfalls and alternate approaches.....	97
Future directions.....	98
CHAPTER 6	
DEREGULATED SIGNALING IN FIBROBLASTS CAN INITIATE EPITHELIAL TUMORIGENESIS	99
Summary.....	100
Introduction.....	101

Loss of Smad4-mediated signaling in FSP1+ stromal cells lacking TGFB2 abrogates forestomach cancer development.....	103
Mesenchymal FSP1+ stromal cells specifically induce forestomach cancer.....	105
Loss of TGFB2 in FSP1+ stromal cells induces epithelial proliferation via HGF/Met signaling.....	106
BMP7/HGF imbalance in forestomach and epithelium paracrine signaling aggravates forestomach carcinogenic response.....	109
HGF mediated induction of epithelial carcinogenesis is specific to FSP1+ stromal cells	112
Interpretation of findings.....	116
Potential pitfalls and alternate approaches.....	113
Future directions.....	114
CHAPTER 7	
DISCUSSION.....	115
Discussion.....	116
CAF heterogeneity	116
CAFs' altered metabolism	120
Fibroblasts' roles in tumor initiation.....	121
Future directions.....	123
Conclusion	124
BIBLIOGRAPHY.....	126

LIST OF FIGURES

Figure 1. The tumor microenvironment.....	3
Figure 2. CAF subsets with different functions.....	9
Figure 3. α SMA and FSP1 expression in healthy and mammary tumor bearing mice.....	41
Figure 4. Overlaps in CAF marker expression in 4T1 tumors.....	42
Figure 5. 4T1 and MMTV-PyMT tumor histological features.....	43
Figure 6. Expression of CAF markers by different cell types in PyMT tumors.....	44
Figure 7. Expression overlaps of CAF markers in PyMT tumors.....	45
Figure 8. CAF marker expression changes during tumorigenesis in PyMT tumors.....	46
Figure 9. CAF marker expression in patient tissues of different pathologies.....	48
Figure 10. α SMA ⁺ CAFs promote primary mammary carcinoma growth.....	58
Figure 11. α SMA ⁺ CAFs deprived tumors show vascular remodeling.....	59
Figure 12. α SMA ⁺ CAFs depletion can enhance invasion and intravasation and has no effect on lung metastatic outgrowth.....	60
Figure 13. α SMA ⁺ CAFs depletion in PyMT tumors reduce tumor growth and change CAF marker expression patterns.....	62
Figure 14. PyMT transplantation model.....	63
Figure 15. α SMA ⁺ CAF depletion in transplanted PyMT tumors leads to growth stagnation and vascular remodeling.....	64
Figure 16. α SMA ⁺ CAFs depleted tumors show increased tumor associated macrophage infiltration.....	66

Figure 17. Depletion of FAP ⁺ CAFs does not impact primary tumor growth.....	67
Figure 18. FAP ⁺ CAFs depleted tumors exhibit different immune cell composition.....	68
Figure 19. Depletion of PDGFR β ⁺ CAFs impacted tumor immunity.....	70
Figure 20. Glycolytic changes in cancer cells in α SMA ⁺ CAFs depleted tumors....	83
Figure 21. mCAFs are highly glycolytic compared to mNFs.....	84
Figure 22. Abrogation of lactate intake by cancer cells results causes no changes in tumor vasculature.....	85
Figure 23. hCAFs are highly glycolytic compared to hBFs.....	87
Figure 24. Cancer cells incorporate CAFs-derived metabolites in their metabolism.....	89
Figure 25. Chronic hypoxia induces stable expression of HIF-1 α and glycolytic enzymes in hBFs.....	91
Figure 26. Glycolytic CAFs accumulate in hypoxic areas of tumors	93
Figure 27. Proposed model of fibroblast reprogramming.....	94
Figure 28. Loss of SMAD4 together with TGFRB2 in FSP1 ⁺ fibroblasts does not result in forestomach cancer development.....	104
Figure 29. Tumor initiation by conditional loss of TGFRB2 is specific to FSP1 ⁺ fibroblasts.....	105
Figure 30. HGF signaling is elevated in forestomachs of TGFRB2cKO mice.....	106
Figure 31. HGF signaling is elevated in TGFRB2cKO mice.....	107
Figure 32. Elevated HGF signaling in TGFRB2cKO fibroblasts causes Met phosphorylation in neighboring epithelial cells	108

Figure 33. BMP7 signaling is disrupted in TGFB β 2/SMAD4cKO mice.....	109
Figure 34. BMP7 is expressed by epithelial cells and FSP1 fibroblasts express the receptor ALK6.....	110
Figure 35. Forestomach cancer can be initiated through a feed forward loop HGF/BMP7 signaling between fibroblasts and cancer cells.....	111
Figure 36. Epithelial cell- fibroblast crosstalk via BMP7/HGF signaling is specific to FSP1 ⁺ fibroblasts.....	112

LIST OF TABLES

Table 1. Most commonly used CAF markers.....	7
Table 2. Effects of CAF subtype depletion in mammary carcinoma.....	76

CHAPTER 1

BACKGROUND AND SIGNIFICANCE

Tumor microenvironment

After more than 40 years of cancer research, significant progress has been made towards our understanding of the underlying mechanisms of tumorigenesis. Our initial view of tumor formation was based on the simplistic model in which endogenous mutations in specific tumor suppressor genes or oncogenes transform healthy cells into cancerous cells, which then gradually expand into a large tumor mass. This view has evolved over the past three decades into what can be described as a tumor-organ model. In contrast to a mass of cancerous cells, a tumor is now regarded as an organ-like construction encompassing specific cell types and extracellular matrix to provide structure and tissue homeostasis. Although specific gene mutations and chromosomal anomalies can indeed transform healthy cells and eventually lead to their accumulation due to uncontrolled proliferation and enhanced survival, once a tumor reaches a certain mass, oxygen and nutrient availability come into play as a limiting factor for cancer cells at the center of the mass. At this point, cancer cells employ several mechanisms that allow them to receive sufficient support from normal, non-cancerous cells in the host organ. For instance, cancer cells release several angiogenic factors, such as vascular endothelial growth factor (VEGF), fibroblast growth factor (FGF),¹ etc., in order to activate and attract endothelial cells to induce angiogenesis resulting in increased oxygen and nutrients access to the tumor tissue. In order to evade immune surveillance, cancer cells secrete immunosuppressive factors such as transforming growth factor beta ($\text{TGF}\beta$)^{2,3}, or recruit immunosuppressive cells (e.g., T regulatory cells) by prostaglandin E2 (PGE_2) production⁴. Such immunosuppressive cells inhibit T-cell's anti-tumor activities. Additionally, fibroblasts can be activated through platelet-derived growth factor (PDGF), FGF and $\text{TGF}\beta$ secreted by cancer cells^{5,6}. In their activated state fibroblasts facilitate tumor growth and, in later stages, promote metastasis⁵ through various mechanisms. These specialized cell types surrounding the cancer cells, together with factors such as pH, oxygen tension, and interstitial fluid pressure, are referred to as the tumor stroma, or tumor microenvironment (**Figure 1A**). The

tumor microenvironment in which the cancer cells are embedded into plays a critical role in tumor progression and represents a key factor to consider and overcome in developing efficacious anti-cancer therapeutics.

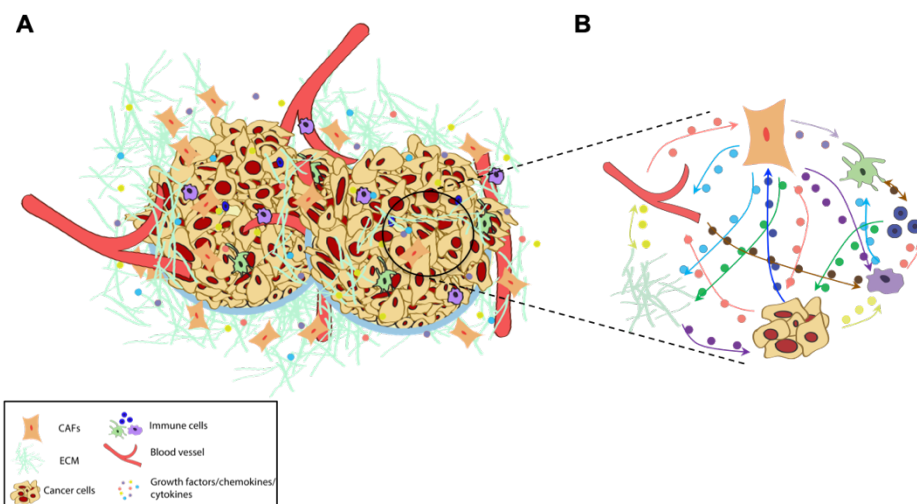


Figure 1 The tumor microenvironment

A. Illustration of the tumor microenvironment **B.** Signaling crosstalk between different cell types in the tumor microenvironment

The tumor microenvironment is a complex interplay of endothelial and perivascular cells, immune cells of various types, fibroblasts, extracellular matrix (ECM) proteins,

cytokines, and growth factors secreted by all participating cells. Mirroring how cancer cells attract and activate stromal cells, stromal cells in turn affect cancer cells through paracrine signaling. Epidermal growth factor (EGF), FGF, TGF β , tumor necrosis factor alpha (TNF α) and interleukins secreted by immune cells stimulate cancer cell growth⁷. Fibroblasts can induce epithelial to mesenchymal transition (EMT) in cancer cells via TGF β and support cancer growth through release of hepatocyte growth factor (HGF), EGF family members, insulin-like growth factor-1 (IGF-1), stromal cell-derived factor-1 (SDF-1 or CXCL12), and a variety of fibroblast growth factors (FGFs)^{8–13}. In addition to their essential functions in angiogenesis, endothelial cells secrete hypoxia-inducible factor 1 alpha (Hif1 α), which facilitates cancer cell metastasis¹⁴.

In addition to active signaling and crosstalk between stromal and cancer cells, different stromal cell types also interact with one another, arbitrating their respective functions and the relative abundance of different subtypes of stromal cells to achieve and maintain homeostasis in

the tumor microenvironment. Fibroblast-derived TGF β not only induces EMT in cancer cells, but also inhibits cytotoxic T-cell functions as well as NK cells¹⁵. Through MMP secretion, immune cells, together with fibroblasts, actively remodel ECM and thereby provide growth support and structure to the tumor organ^{5,16}. ECM degradation and remodeling releases many growth factors and cytokines that are sequestered in these frameworks and can further influence all cells in the tumor microenvironment^{17,18}. Fibroblasts and endothelial cells can influence the functions of immune cells at all stages of tumor progression, thereby actively regulating the immune response to the tumor. In turn, immune cells, specifically myeloid cells release cytokines (VEGF, TNF α , TGF β and others), chemokines (such as IL6 and CXCL12), MMPs and several other soluble factors regulating angiogenesis and tumor vascularization⁷. Fibroblasts within the tumor stroma secrete similar cytokines and growth factors and therefore are also critical regulators of angiogenesis¹¹. As it becomes apparent, the tumor microenvironment is a highly complex signaling network within which a tumor grows (**Figure 1B**).

Over the past two decades, ample evidence confirmed the notion that tumor microenvironment is essential for tumor formation and progression. In the 1980s, studies by Mina Bissell showed that wounding can trigger tumor development in animals infected with tumor initiating viruses and transgenic mice overexpressing oncogenes^{19–21}. Today we know that conditions of excessive wound healing, such as fibrosis elevate the risk for cancer development enormously. For instance, patients with idiopathic pulmonary fibrosis have a significantly higher risk to develop lung cancer than healthy individuals^{22,23}. An additional example are patients with liver cirrhosis that are at higher risk to develop hepatocellular carcinoma²⁴. Together, these studies suggest that tissue remodeling and activation in immune and endothelial cells, as well as fibroblasts are required for a tumor growth. In support of this, clinical studies have correlated increased stromal content with poor prognosis^{25–27}, and functional studies showed that altering components of the tumor microenvironment affects tumorigenesis^{11,28,29}.

How exactly the tumor microenvironment is developed is not fully understood, but several different theories have been postulated. As mentioned above, one possibility is that the cancer cells themselves create their own stroma by attracting stromal cells and hijacking their functions through targeted signaling. An alternative school of thought is that an inflammatory microenvironment provides the necessary niche for tumor formation to develop in the first place. This idea was first forwarded in 1862 by Rudolf Virchow, who observed that tumors develop at sites of previous injury at an increased rate³⁰. This was later supported by the above-mentioned studies using Rous sarcoma virus to induce cancer formation, which was only possible in the presence of tissue injury where active tissue remodeling is taking place^{19,20}. Further supporting this is the fact that conditions of chronic inflammation such as fibrosis are known cancer risk factors²²⁻²⁴. Moreover, irradiation of stroma and subsequent ECM remodeling has been shown to induce tumorigenesis in non-irradiated epithelial tissue^{31,32}. In line with these observations, several studies have suggested that genetic alterations in tumor associated stroma, which were not found in the epithelial carcinoma cells, might also contribute to tumor formation³³⁻³⁵. A few studies have provided direct evidence that mutations in stromal cells, such as fibroblasts can indeed induce epithelial tumorigenesis^{36,37}. Lastly, a line of research attributes the presence of stromal cells within a tumor to failed anti-tumor host responses. This theory supposes that, in early cancer development, the host tissue mounts an anti-tumor immune response in order to clear out damaged cells or to contain the cancerous cells, if the tumor cannot be overcome. Support for this idea comes mainly from post mortem studies, which identified many cancerous lesions in patients who died of cancer-unrelated causes³⁸. In these studies, the presence of cancerous lesions in thyroid glands is so frequent, that it is considered a normal finding³⁹. Such observations suggest that stroma can prevent the growth of tumors from pre-cancerous lesions. Another example is the condition of ductal carcinoma *in situ* (DCIS) of the breast. It is considered a non-invasive breast cancer that remains indolent. Although DCIS lesions often harbor many cancer driver mutations, they develop into invasive carcinomas only in minority of patients

presenting with such lesions⁴⁰. These observations highlight that interplay between stroma and mutated epithelial cells plays a critical role in determining tumor progression. Based on the fact that indolent cancerous lesions are more frequently found in people than the occurrence of cancer, we may conclude that in many cases the stroma is able to contain tumor growth and can indeed also exhibit anti-cancer functions. However, the determinants in tumor microenvironment that are permissive or restrictive to tumor growth remain largely unknown.

In summary, research in the past two decades has firmly established the concept of the tumor microenvironment into which cancer cells are embedded and the plethora of interactions within the tumor microenvironment continues to be unraveled. It is not certain how the tumor microenvironment forms in the first place, but most likely all described scenarios can happen depending on the disease and tissue context.

Cancer-associated fibroblasts

Fibroblasts are the most abundant cell type amongst the different components of the stroma. Paradoxically they are also the least understood. In their normal physiological roles, fibroblasts mediate key processes in the wound healing response. During tissue injury, growth factors and cytokines such as TGF β , PDGF, and EGF are released by the damaged tissue, which activate fibroblasts and induce their differentiation into so-called myofibroblasts^{10,41,42}. Myofibroblasts received their name because of their features that are similar to smooth muscle cells with contractile properties essential for wound closure. These cells are generally identifiable via their expression of alpha smooth muscle actin (α SMA). In their activated state, fibroblasts secrete extracellular matrix proteins, such as collagens, which become part of the granulation tissue and later scars^{41,42}. The wound healing process involves paracrine signaling among fibroblasts, endothelial cells and immune cells, all critical for wound closure. This process is reminiscent of the aforementioned cell-cell interactions in the tumor microenvironment during tumor progression. The parallelism between cancer and the wound healing process had been

recognized as early as 1986, when Harold Dvorak famously referred to tumors as “wounds, that do not heal”, and cancer initiation as “wound healing gone awry”⁴³. It is not surprising that the identification and characterization of the roles fibroblasts play in the tumor microenvironment had been largely drawn from their known functions in the wound healing process. In the context of a tumor, fibroblasts are referred to as cancer-associated fibroblasts or CAFs. CAFs can stem from several different sources, such as resident tissue fibroblasts^{44,45}, bone-marrow derived cells⁴⁶, or normal tissue epithelial cells, in addition to tumor cells themselves by undergoing epithelial to mesenchymal transition (EMT) and transdifferentiation¹⁸. CAFs are defined as activated fibroblasts in the tumor microenvironment that can actively promote tumor growth through their secretion of growth factors, cytokines and ECM proteins. Expression of certain markers, such as α SMA⁴⁷, platelet derived growth factor receptor alpha/beta (PDGFR α/β)⁹ and fibroblast activation protein (FAP)⁴⁸ have been identified as the hallmark to the activated state for these fibroblasts. Numerous other fibroblast-associated proteins such as intermediate filament associated proteins (e.g. Vimentin, Desmin, fibroblast specific protein 1 (FSP1 or S100A4))^{49–52}, transmembrane proteins and receptors (e.g. Neural glial antigen 2 (NG2), discoidin domain-containing receptor 2

(DDR2)^{48,51,52,53,54}, and

Caveolin1 (CAV1))^{55,56}

and ECM molecules (e.g.

CollagenI/III/IV,

Fibronectin)⁸ as well as

growth factors and

cytokines (HGF, VEGF,

SDF1)^{11,29,57} have also

been associated with

CAFs. Table 1

Table 1 Most commonly used CAF markers

CAF marker	References	Other cell types expressing this marker
Alpha smooth muscle actin (α SMA)	47,49,213	Pericytes ²¹⁴ , cancer cells ⁴⁵
Type I Collagen (Col1)	8	Cancer cells, endothelial cells ²¹⁵
Fibroblast activation protein (FAP)	48,51,52	Monocytes ^{121,216}
Vimentin	217,218	Cancer cells ^{s45} , endothelial cells ²¹⁹ , neurons ²²⁰
Platelet derived growth factor receptor alpha (PDGFR α)	221	Cancer cells ^{222,223} , cardiac telocytes ²²⁴
Platelet derived growth factor receptor beta (PDGFR β)	221	Pericytes ²²⁵
Discoidin domain-containing receptor 2 (DDR2)	53,54	Endothelial cells ²²⁶
Desmin	49,227	Smooth muscle cells (e.g. pericytes) ²²⁸
Fibroblast specific protein (FSP1, or S100A4)	229	Activated melanocytes ²³⁰
Neural glial antigen 2 (NG2)	221	Pericytes ²²⁸
Caveolin 1 (CAV1)	55,56	Endothelial cells and adipocytes ^{231,232}

summarizes the most important and most commonly used CAF markers. Notably, none of the

listed markers universal to the entire CAF population, and different teams have used one or a few of these markers in combination to identify CAFs in their studies.

Historically, CAFs were thought to facilitate tumorigenesis in virtually all solid tumors. The first in vivo studies showed CAFs co-implanted with cancer cells into animals (co-called admix experiments) resulted in increased tumor growth compared to cancer cells injected alone or with normal fibroblasts. Further studies demonstrated CAFs secrete various factors such as HGF, EGF, IGF-1, and SDF1, which promote cancer cell proliferation and metastasis^{5,58,59}. Targeting CAFs has been shown to reduce tumor growth and metastasis in breast, colon, lung and pancreatic carcinoma animal models^{60,61}, supporting a growth promoting function for CAFs. However, research in the past few years had changed this view. In colon and pancreatic cancer xenograft models, CAFs have been shown to promote tumor growth via paracrine Hedgehog (Hh) signaling⁶². When Hh signaling was inhibited in the fibroblasts however, pancreatic tumor growth, as well as the survival of mice with stroma-depleted tumors, was reduced in a subsequent study⁶³. When α SMA-expressing CAFs were directly targeted for depletion in a mouse model of pancreatic ductal carcinoma, the tumors exhibited increased invasive abilities, and the survival of the animals was diminished⁶⁴. These studies stand in contrast to the presumption of CAF's tumor growth promoting roles and suggest these cells can also suppress tumor growth in certain contexts. As we continue to unravel CAF functions in tumorigenesis, it becomes increasingly obvious, that the roles they play in the tumor microenvironment are highly diverse and context-dependent.

CAF heterogeneity

The concept of CAF heterogeneity had risen to prominence alongside the new insights in CAFs biology and functions. The multitude of functions and the plethora of distinct signaling pathways involved to elicit such functions led to the concept that, instead of presenting as one cell type with a specific role in tumorigenesis, CAFs are actually comprised of multiple subpopulations, each with distinct functions. The variety of markers used to identify CAFs, as well as the different

reported sources of these cells further support this hypothesis. By categorizing specific CAFs functions into broad areas, different CAF subtypes have been postulated⁶⁵ (**Figure 2**).

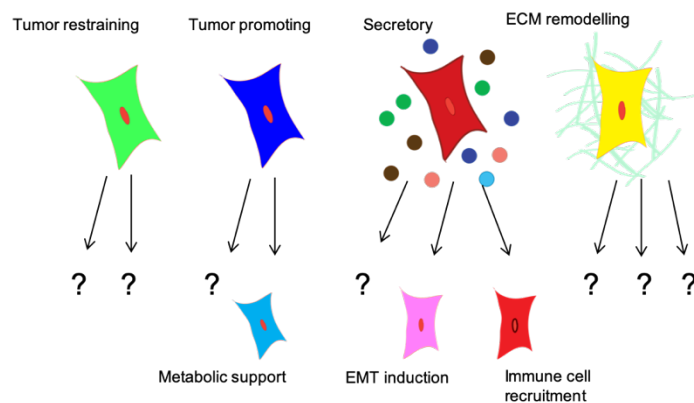


Figure 2 CAF subsets with different functions. Adapted from ⁶⁵ with permission.

Primarily, tumor restraining and tumor promoting CAFs could be regarded as two main CAF subsets. A third subset was proposed in association with a secretory phenotype, releasing increased amounts of signaling molecules that impact immune cells, tumor vasculature and cancer cell

proliferation. CAFs that are predominantly responsible for extracellular matrix remodeling were proposed as a fourth subtype⁶⁵. It is likely that each of these subtypes can be further subdivided into distinct subpopulations. For instance, another subpopulation of tumor-promoting CAFs may be CAFs with specific metabolic features supplying tumors with metabolites to meet their energetic needs. Secretory CAFs might be further defined to describe specialized CAFs responsible for recruiting immune-suppressive cells via the secretion of IL6, IL4 and IL8 or CAFs directly modifying cancer cell proliferation and invasiveness via specific signaling mediators such as TGF β ⁵⁸ (**Figure 2**). While these fine-grained functional subsets of CAFs have been proposed, how these subsets can be uniquely identified by means of molecular markers remains largely undetermined. Some functional studies attributed expression of a specific marker, or the lack thereof, to a specific function. For instance, the lack of Caveolin in fibroblasts has been associated with increased lactate production that can feed into cancer cells' metabolism⁶⁶. On the other hand, Caveolin-expressing CAFs are associated with ECM remodeling and the enhancement of tumor invasiveness⁵⁶. In addition, analyses of patient tumor tissues have attributed expression of specific CAF markers to different clinical outcomes. For instance, Collagen and FAP have been identified as predictors of poor outcome in patients with pancreatic cancer, whereas α SMA was

correlated with favorable outcome⁶⁷. While these studies suggest that specific mesenchymal markers can be used for CAF subtype identification, whether single markers can sufficiently define a CAF subtype, or whether markers can provide meaningful subtype identity only in the context of co-expressing additional CAF markers remain open questions. Studies aiming to discover distinct CAF subtypes should also take into consideration that CAFs likely can change their phenotypes dynamically in a context-dependent manner, such as the stage of tumorigenesis. Moreover, it is unknown whether different origins or locations of CAFs correspond with different CAF markers and/or functions. There is an increased urgency to answer these questions as more studies utilizing mesenchymal markers are emerging in the CAF field.

Glucose metabolism in CAFs

A specific example of a tumor promoting pathway involves CAFs functioning as metabolic support cells for proliferating cancer cells. Highly proliferative cells, such as cancer cells, present with enhanced glycolytic rates. In physiological conditions, cells metabolize glucose into pyruvate (glycolysis), which gets shuttled through the tricarboxylic acid cycle (TCA or Krebs cycle) in the mitochondria⁶⁸. This process creates NADH, which feeds into the electron transport chain (ETC). The ETC consists of several complexes (complex I-V), through which electrons pass. This process, which absolutely requires oxygen, produces large amounts of ATP (34 mol ATP per mol of glucose)⁶⁸.

When oxygen in tissues is sparse, the pyruvate produced by the glycolytic pathway is converted into lactate, resulting in only 2 mol of ATP per mol of glucose. Although energetically less efficient, the conversion of pyruvate to lactate releases NAD^+ , which fuels continuous glycolysis and a cell can repurpose the intermediates of glycolysis for nucleotide biosynthesis via the pentose phosphate pathway⁶⁸.

In the 1920s Otto Warburg observed that cancer cells present with enhanced glycolytic rates, metabolizing glucose to lactate regardless of oxygen availability. This phenomenon is

referred to as the Warburg effect, and was initially thought to result from dysfunctional mitochondria in cancer cells. Subsequent research disproved this hypothesis and it is now believed that the enhanced demand for biosynthetic products necessary for cancer cell growth and divisions causes these cells to change their metabolism preference to this less efficient, but much faster way for energy production⁶⁹.

Similar to cancer cells' altered metabolism, CAFs have been proposed to undergo metabolic reprogramming toward aerobic glycolysis and have been suggested to participate in a tumor-promoting lactate shuttle with cancer cells ("Reverse Warburg Effect")⁷⁰⁻⁷³. Here, the glycolytic CAFs are suggested to secrete lactate, which is taken up by cancer cells to fuel their own energetic needs. A few possible mechanisms of how this metabolic relationship develops had been proposed, but the precise details of how such metabolic programming of CAFs emerges and how it is sustained are not well understood. Of note, crosstalk between cancer cells and CAFs involving additional metabolites, such as glutamine, have been proposed as cancer growth supporting mechanisms⁷⁴.

Dissertation goals and major findings

CAFs are a heterogeneous cell population that exhibits a plethora of functions critical for tumor development and progression. In this work, we aimed to further unravel novel functions of CAFs in the context of CAF heterogeneity. The majority of our studies focuses on mammary carcinoma, which consists up to 80% of stroma, suggestive of the tremendous relevance of CAFs in this cancer type. In order to address CAF heterogeneity, we employed multiplex staining techniques to identify distinct CAF subsets in mammary tumors based on the expression patterns of several CAF markers and their overlaps. This method enabled us to identify phenotypically distinct subsets, whose functions were subsequently assessed in transgenic animal models of mammary carcinoma that allowed for specific targeting of CAFs. These functional studies confirmed that phenotypically distinct CAF subtypes also differed in their functions in the tumor

microenvironment. A particularly intriguing observation from CAF targeting studies was these cells' impact on tumor metabolism. Here, we sought to further investigate the metabolic relationships between CAFs and breast cancer cells, thus uncover the underlying mechanisms of this metabolic reprogramming in CAFs. Our studies suggest the glycolytic, CAF-like phenotype can be induced in normal fibroblasts by exposing them to chronic hypoxic conditions.

Having observed that normal fibroblasts can gain CAF-like functions via altered metabolism, we further aimed to investigate how other changes in fibroblasts might influence epithelial cells. Here, we were interested not in how cancer growth is sustained, but rather if indeed changes in fibroblasts in healthy tissues can initiate tumorigenesis in the neighboring epithelium. We used a well-established model that showed disrupted TGF β signaling in fibroblasts can lead to development of carcinogenesis of the forestomach. Deciphering the underlying signaling mechanisms revealed an intricate feed forward signaling loop between fibroblasts and cancer cells that plays a critical role in cancer initiation.

In summary, in this thesis different aspects of CAF biology were investigated. We uncovered distinct CAF subtypes with differing roles in mammary carcinoma progression and further specifically explored CAFs' roles in providing metabolic support for cancer cells. Here, the hypoxia dependent reprogramming of fibroblasts was identified as a mechanism driving the glycolytic phenotype of CAFs. Lastly, the complex signaling between epithelial cells and fibroblasts that can lead to cancer initiation was elucidated. In this context, we not only further elucidated the intricate interactions between fibroblasts and epithelial cells, but showed that already in this state distinct fibroblast subtypes can be identified.

CHAPTER 2

MATERIALS AND METHODS

Parts of the methods section are taken verbatim from previously published work:

Eikesdal, H. P.*, Becker, L. M.*, Teng, Y.*, Kizu, A., Carstens, J. L., Kanasaki, K., Sugimoto, H., LeBleu, V. S., Kalluri, R. (2018). **BMP7 Signaling in TGFB β 2-Deficient Stromal Cells Provokes Epithelial Carcinogenesis**. *Molecular Cancer Research*, 16(10), 1568-1578. <https://doi.org/10.1158/1541-7786.mcr-18-0120>

Vo, A. P. Glucose Metabolism in Cancer-Associated Fibroblasts. *Harvard Univ.* (2013). doi:10.1029/91JD03139

Becker, L. M.*, O'Connell, J. T.*, Vo, A. P., Cain, M. P., Tampe, D., Bizarro, L., Sugimoto, H., McGow, A. K., Asara, J. M., Lovisa, S., McAndrews, K. M., Zielinski, R., Lorenzi, P. L., Zeisberg, M., Raza, S., LeBleu, V. S., and Kalluri, R. **Epigenetic Reprogramming of Cancer Associated Fibroblasts Deregulates Glucose Metabolism and Facilitates Progression of Breast Cancer**. *Cell Reports*, 31(9), 107701. <https://doi.org/10.1016/j.celrep.2020.107701>

Murine cell lines

4T1 Balb/c mammary tumor epithelial cells (ATCC) were grown in Dulbecco's Modified Eagle's Medium supplemented with 10% fetal calf serum and penicillin/streptomycin (each 100U/ml). In same experiments, 4T1 were modified to express GFP and luciferase (GFP luc). 4T1 cells were validated by STR analysis and confirmed negative for mycoplasma. Mouse normal mammary fibroblasts and cancer-associated fibroblasts were grown from tissues obtained from MMTV-PyMT mice^{75,76}. Tissues were minced into 1 mm³ pieces and digested overnight in 300U Type I collagenase per ml of RPMI-1640 media containing 20% fetal bovine serum (FBS) with 100U/ml penicillin/streptomycin and 250ng/ml amphotericin (PSA) (complete media). Fibroblasts were subsequently allowed to grow out of the tissue pieces maintained in complete media.

To isolate fibroblasts from forestomaches, the forestomaches of wild-type (wt), TGFB2cKO, and TGFB2/SMAD4cKO mice were collected, minced into small pieces, and digested with 400 units/ml of collagenase IV (Worthington) in Dulbecco Minimal Essential Medium (DMEM, Cellgro) at 37C for 24 hours in a cell incubator. Next day, the medium was replaced with DMEM, supplemented with 20% fetal bovine serum (FBS), 100 units/mL of penicillin and 100 mg/mL of streptomycin (Cellgro). The cells were grown at 37C in a humidified chamber and 5% CO₂ under sterile tissue culture conditions and passaged when they reached 80% confluency. The resulting fibroblast cell cultures at passages 4 to 6 were used for all the experiments. The fibroblast cultures were confirmed for the presence of FSP1 protein by immunostaining.

Patient-derived cell lines

Human benign mammary fibroblasts and cancer-associated fibroblasts were grown from breast biopsy tissue samples obtained as part of an institutionally approved clinical study at Boston's Brigham and Women's Hospital. The breast biopsies were either ultrasound-guided (Ultrasound

core needle biopsy = US-CNB) or stereotactically-guided (Stereo-CNB) core needle biopsies. In Stereo-CNB, the biopsy target was always microcalcifications, but the core samples provided for this study did not contain calcifications, as determined by x-ray. All patients (n=499) were female and between 18 and 88 years of age (median age of 51 years). The tissues were mounted into O.C.T mounting media and frozen for subsequent immunolabeling studies or processed for fibroblast propagation. For the latter, after an ethanol and subsequent phosphate-buffered saline (PBS) wash, 1 mm³ pieces were digested overnight in 300 U Type I collagenase per ml of RPMI-1640 media containing 20% fetal bovine serum (FBS) with 100 U/ml penicillin/streptomycin and 250 ng/ml amphotericin (PSA) (complete media). Fibroblasts were subsequently allowed to grow out of the tissue pieces and maintained in complete media. These patient-derived fibroblasts were isolated by previous lab members at Harvard Medical School.

Mice

α SMA-vTK, and PDGFR β -vTK have been previously described^{77,78}. FAP-vTK mice have been created by Dr. Toru Miyake in the Kalluri lab. Tg(S100a4-cre)1EgnYunkJ (FSP1-Cre) and FSP1-GFP mice were a kind gift from E. G. Neilson (Northwestern)³⁶. Tgfb2^{tm1.2Hlm} (Tgfb2^{flloxE2}) mice were a kind gift from H. L. Moses (Vanderbilt)⁷⁹. Smad4^{tm1.1Rdp} (Smad4^{flloxE8/9}) mice⁸⁰ were kindly provided by R. A. DePinho (MDACC). R26R-LSL-EYFP (R26R-EYFP) reporter mice⁸¹ were kindly provided by B. G. Neel (Harvard). The α SMA-Cre and α SMA-RFP mice were previously described^{77,82}. Mice strains employed in these studies include control (wt) mice which include both Cre-negative littermates of *TGFBR2*^{ckO} and *TGFBR2/SMAD4*^{ckO} strains or Cre-positive littermates with heterozygous loss of *TGFBR2*. Control mice for experiments with α SMA-vTK, PDGFR β -vTK and FAP-vTK mice were littermates vTK⁻ mice. The FSP1-GFP and α SMA-RFP strains were bred to generate the double transgenic strain. Both male and female young and adult mice were studied in the studies involving *TGFBR2*^{ckO} and *TGFBR2/SMAD4*^{ckO} mice; whereas only female

adult mice were used for experiments involving mammary carcinoma. The genetic backgrounds were C57Bl/6, Balb/c, sv129 or a mixture of these backgrounds. Animal studies were carried out at the Beth Israel Deaconess Medical Center and at the MD Anderson Cancer Center and approved by the Institutional Animal Care and Use Committee of each institution.

4T1 orthotopic mammary cancer models

Adult virgin female mice (~8 weeks of age) were used for orthotopic implantation of 1×10^6 4T1 mammary epithelial cancer cells, as previously described. When the average combined tumor volume reached $\sim 500 \text{ mm}^3$ (14 days post cancer cell implantation), α SMA-vTK and WT control mice received daily intraperitoneal (i.p.) injections with 50 mg/kg of ganciclovir (GCV). Tumors were measured every 2 to 3 days using Vernier callipers. Mice were euthanized when the average tumor volume reached 1500 to 2000 mm^3 in the control group (24 days post cancer cell implantation). When probing for glycolytic fibroblasts in different tumor stages, mice were sacrificed when tumors reached $\sim 50\text{-}80 \text{ mm}^3$, $\sim 150\text{-}250 \text{ mm}^3$, $\sim 400\text{-}500 \text{ mm}^3$, $\sim 700\text{-}900 \text{ mm}^3$, $1200\text{-}1500 \text{ mm}^3$, respectively. For each stage, tumors from 4-6 mice were obtained. At time of sacrifice, mice were injected with hypoxyprom to probe for pimonidazole adduct formation in tumor tissues. To ascertain metastatic burden in lungs of mice with a tumor volume of 500 mm^3 , 1×10^6 4T1 cells were injected in the right mammary fat pad and volume was monitored until sacrifice when tumor volume reached 500 mm^3 . To measure α SMA expression in animal tissues, α SMA-RFP mice⁷⁷ were crossed to *S100A4-GFP* mice⁸³ and subsequently implanted with 4T1 carcinoma cells as described above. 5 μ m sections from formalin fixed paraffin-embedded lung tissues were stained with hematoxylin and eosin. Slides were scanned using Aperio Digital Scanner (Department of Veterinary Medicine and Surgery at MDACC). Metastases were identified by histopathological analysis and metastatic area was quantified with Aperio eSlide Manager and Aperio Image Scope v12.3.2.8013 as a percentage of the total area of the lung. While performing

tumor measurements and lung metastasis analysis, the operator was blinded to the experimental groups the mice were stratified into or to their genotypes.

4T1 intravenous injections in α SMA-vTK mice

0.5×10^6 4T1 mammary carcinoma cells were injected intravenously (retroorbital route) in α SMA-vTK and WT control mice. GCV treatment was started 2 days prior cancer cell injection and continued until the endpoint of the experiment (10 days after cancer cell injection). Lung metastases were quantified as described above.

MMTV-PyMT mammary cancer mouse models

MMTV-PyMT transgenic mice spontaneously develop tumors at 8-12 weeks of age in their mammary fat pads⁷⁶. For studies on tumor progression, mice were sacrificed when tumors reached a combined volume of approximately 800 mm³. The single tumors were measured, harvested and paraffin embedded. In total, 24 tumors from 11 distinct mice were used for analyses. For depletion studies, MMTV-PyMT mice were crossed to α SMA-vTK mice to obtain MMTV-PyMT; α SMA-vTK transgenic mice. In these animals, GCV treatment was started when the combined tumor volume reached ~500 mm³ and continued until endpoint of the experiment (20 days post GCV treatment start). For the transplantation experiments, MMTV-PyMT mice were sacrificed when combined tumor volume reached ~1000 mm³. Individual tumors were collected and tumors of ~0.8 g were chosen for transplantation. These were cut into small pieces of ~1 mm³ and implanted into the right mammary fat pads of recipient α SMA-vTK, FAP-vTK or PDGFR β -vTK⁷⁸ mice (one piece/fat pad). Each donor tumor was distributed to five recipient mice. GCV treatment was started once the tumors reached ~400 mm³ in recipient mice and continued until the endpoint of the experiment (20 days post GCV treatment start). In all experiments, tumors

were measured every other day with Vernier calipers. Lung metastases in MMTV-PyMT; α SMA-vTK mice, as well as in the transplantation model were quantified as described above.

Immunofluorescence on human tissues

For human tissues, 5 μ m cryosections were fixed in acetone at 4°C for 5 minutes (min). After incubating with blocking solution (1% BSA in PBS) for 20 min at room temperature (RT), primary antibodies against extracellular matrix proteins or other stromal markers were applied followed by FITC-conjugated secondary antibodies. Subsequently, sections were incubated with a CK8 antibody, which was visualized by Cy3-anti-rat IgG secondary antibody. Sections were incubated with individual antibodies for 1 hour (h) at RT. For staining with α SMA and CAIX, primary α SMA antibody was followed by Cy3-conjugated secondary antibody incubation. For the subsequent incubation with CAIX antibody, a FITC-conjugated secondary antibody was used. The following primary antibodies were used: CK8 (Throma-1; the University of Iowa, 1:50), Collagen I (SouthernBiotech 1310-01; 1:200), Collagen III (SouthernBiotech 1330-01; 1:200), Laminin 1 (Sigma L9393; 1:200), Tenascin C (Abcam ab108930; 1:200), α SMA (Sigma F3777; 1:200), FSP1 (a gift from Dr. Eric Neilson, Vanderbilt Univ.; 1:500), CD31 (DAKO, JC70A; 1:50), CAIX (Novus Biologicals 1:100) and NG2 (Millipore AB5320; 1:200). FITC anti-goat IgG (Jackson ImmunoResearch 705-095-147; 1:200), FITC anti-rabbit IgG (Jackson ImmunoResearch 711-095-152; 1:200), Rhodamine anti-rabbit IgG (Jackson ImmunoResearch 711-295-152; 1:200), FITC anti-rat IgG (Jackson ImmunoResearch 712-095-153; 1:200), and Rhodamine anti-rat IgG (Jackson ImmunoResearch 712-295-153; 1:200) secondary antibodies were utilized. The slides were washed with PBS three times for 10 min and mounted with Vectashield plus DAPI. Staining was visualized on a Zeiss AxioSkop 2 fluorescent microscope and the images were taken with Axiovision Rel 4.8 software. FITC staining and stromal area were quantified in 3 to 5 visual fields per sample using the NIH Image J Analysis Software, where the same threshold was used for all

compared conditions. Collagen I, III and tenascin C staining was determined as a ratio of FITC staining signal/ stromal area for each visual field. Laminin1 staining was assessed as a ratio of FITC signal/perimeter length around tumor or epithelial structures. CD31, NG2, α SMA and FSP1 positive cells only within the stroma were quantified as a ratio of individual marker positive cell number/ stromal area per visual field. In case of NG2-covered microvessels (CD31⁺), the numbers were calculated as a percentage out of all microvessels per visual field.

Immunolabeling of mouse tissues

Immunohistochemistry and immunofluorescence on murine mammary carcinoma tissues

Immunohistochemistry on paraffin-embedded mouse tissues for α SMA and Hypoxyprobe was performed using the Vector M.O.M. kit (Vector Laboratories, BMK-2202). Slides were deparaffinized, rehydrated and microwaved for 15 min at 98°C in citrate buffer (pH 6), before incubated with Hydrogen-peroxide (Fisher H325-100; 15 min at RT). Tissues were blocked with M.O.M. blocking reagent (prepared according to manufacturer's recommendations) for 30 min at RT, before incubated with primary antibody (α SMA DAKO M0851; 1:100, or Hypoxyprobe HPI Inc., 1:50) over night at 4°C. After washing 3x3 min with TBS, secondary antibody (part of M.O.M. kit) incubation followed for 30 min at RT. Subsequently, slides were washed (TBS, 3x 3 min) and incubated with ABC reagent (Vector Laboratories, VECTASTAIN® Elite® ABC HRP Kit, PK-6100; prepared as recommended by manufacturer) for 30 min at RT. After another wash, incubation with DAB (Life Technologies, 750118) for 4 min at RT followed, before tissues were counter stained with Hematoxylin (30 s incubation, Sigma-Aldrich GHS316-500ML). Slides were dehydrated before coverslipping. Immunofluorescence stainings on paraffin-embedded mouse tissues were performed using Tyramide Signal Amplification (TSA) technology (Perkin Elmer) as previously described⁸⁴. In short, tissues were deparaffinized, rehydrated and microwaved for 15 min at 98°C in citrate buffer (pH 6) for antigen retrieval (AR; number of 15 min-long ARs varied

by antibody; described below). After blocking with 1% BSA in TBST for 10 min at RT, sections were incubated with primary antibody for 1 h at RT. A secondary antibody incubation followed using a horseradish peroxidase (HRP)-conjugated polymer (Biocare) for 10 min, before incubation with TSA reagent (Opal reagent, 1:50, Perkin Elmer; 10min at RT). In between steps, slides were washed with TBST 3x3 min. An additional antigen retrieval followed the immunolabeling to wash off antibodies. In case of co-immunolabeling with additional antibodies, the same procedure was repeated for each antibody. The following antibodies were used: CK8 (Throma-1; the University of Iowa, 1:50, 3 ARs), α SMA (DAKO M0851; 1:2000; 4 ARs), FBP1 (Abcam ab109020; 1:50; 2 ARs), PKM2 (Cell Signaling, CS #4053; 1:800, 2 ARs), HK2 (CS #2867; 1:200; 2 ARs), Lyve1 (Angio Bio Co 11-034; 1:100, 1 AR), GLUT1 (Abcam ab115730, 1:200, 4 ARs) CAIX (Novus Biologicals NB100-417; 1:1000; 2 ARs with Tris-EDTA buffer, pH 9.0, 0.05% Tween (TE buffer)). Co-immunolabeling of tissues for CD31, PDGFR β and α SMA was performed in a similar procedure, without usage of TSA technology. Tissue sections were subjected to a 30 min AR using TE buffer before blocking with 4% Aurion Cold Water Fish Skin Gelatine (Electron Microscopy Sciences, 25560) for 1h at RT. Incubation with primary antibodies: CD31 (Dianova, DIA 310; 1:400), α SMA (DAKO M0851; 1:400), PDGFR β (Thermo Fisher, MA5-15143; 1:100) (1h at RT) was followed by 30 min incubation with secondary antibodies: goat anti-rabbit Alexa Fluor (Invitrogen, A11034, 1:250), donkey anti-mouse Alexa Fluor (Invitrogen, A3157, 1:250), goat anti-rat Alexa Fluor (Invitrogen, A11007, 1:250). All immunofluorescence labeling experiments were followed by a 5-minute incubation with DAPI (Life Tech) before mounted using Fluoroshield mounting media (Sigma Aldrich, F618). OCT-embedded tissues from α SMA-RFP; S100A4-GFP mice were fixed with acetone at 4°C for 5 min, before slides were mounted with Vectashield + DAPI. Immunofluorescence images were acquired either with Vectra Multispectral Imaging System version 2 (Perkin Elmer), or Zeiss AxioSkop 2. Immunoreactive scores (IRS) were obtained from the sum of distribution and intensity scores for each section. Sections were

evaluated for staining intensity throughout the entire tissue section and ranked on a scale of 1 to 4 (or adapted to 1-5, depending on the respective experiment) with the section with the lowest staining intensity being scored 1; and the section with the highest staining intensity being scored 4/5. Distribution scores were determined similarly determining the staining distribution in the entire tissue section. The distribution score and intensity score were added together to make up the final score. IRS scores were quantified while blinded to genotype or experimental group the tissues belonged to. All quantifications were performed on pictures taken with identical exposure settings. For representative pictures shown in the figure, in some cases picture contrast and brightness were enhanced.

Immunohistochemistry and immunofluorescence on murine forestomach tissues

Tissues were fixed in formalin, paraffin embedded, and 4 mm sections were prepared. Briefly, sections were deparaffinized and rehydrated, before antigen retrieval at 98C for 1 hour in 0.01 mol/L citrate buffer (pH 6.0). After blocking with diluted serum from the secondary antibody host for 30 minutes, the slides were incubated overnight (4C) with the primary antibody. After blocking endogenous peroxidase activity for 20 minutes with 3% hydrogen peroxide (Sigma), a biotinylated anti-goat or anti- rabbit secondary antibody was applied for 30 minutes (Vector Laboratories). The antigen–antibody complex was revealed by incubating with avidin–biotin–peroxidase (ABC) for 30 minutes according to the manufacturer's instructions (Vector Laboratories, VECTASTAIN® Elite® ABC HRP Kit, PK-6100). Staining was visualized by incubation with diamino-benzidine tetrahydrochloride (Vector Laboratories) for 2 to 10 minutes, as appropriate. The sections were then counter- stained with hematoxylin (Fisher) where appropriate, dehydrated and mounted with Entellan (Electron Microscopy Services). Parallel sections were run for all the experiments without primary antibody, to ensure the specificity of the immunoreactions. The above protocol was also used for ALK6 and FSP1 and CD45 and FSP1 double staining, with the following modifications: Blocking was performed with diluted donkey serum. The goat anti-ALK6 or rat anti-CD45 antibody

was added as the first antibody and incubated overnight at 4°C, followed by a biotinylated donkey anti-goat or anti-rat secondary antibody (Jackson Immuno- Research) and ABC reagent. Staining was visualized by incubating for 20 minutes with 3-amino-9-ethylcarbazole (AEC, Vector Laboratories), before washing thoroughly and adding an avidin– biotin blocking solution (Vector). Thereafter, the tissue sections were blocked again with diluted donkey serum, before adding a rabbit anti-FSP1 polyclonal antibody for 60 minutes, followed by a biotinylated goat anti-rabbit antibody. The antigen–antibody complex was revealed by incubation with avidin–biotin–alkaline phosphatase for 30 minutes according to the manufacturer's instructions (Vectastain ABC-AP Kit, Vector Laboratories). Staining was visualized by incubating for 30 minutes with Vector Blue (Vector Laboratories). The sections were then dehydrated and mounted with Vectamount AQ (Vector Laboratories).

Co-immunofluorescence staining was performed using the TSA-based staining technique as described above. After tissue were prepared as described above, an additional fixation step was added using formaldehyde:methanol (1:10) prior to antigen retrieval.

For immunolabeling for CK5, mouse tissues were fixed overnight at 4°C in 4% paraformaldehyde (PFA); then transferred into 30% sucrose/phosphate buffered saline (PBS, Cellgro) for at least 24 hours. After rinsing with PBS, the tissues were embedded in OCT compound (Sakura) and frozen in liquid nitrogen. Cryosections (10 µm) were prepared, blocked with 1% bovine serum albumin (BSA, Sigma), before incubating with a rabbit anti-CK5 antibody for 60 minutes. Thereafter a TRITC-conjugated donkey anti-rabbit secondary antibody (Jackson) was applied for 60 minutes to detect the CK5 positive cells. The sections were then mounted with Vectashield with DAPI and analyzed by fluorescence microscopy. EYFP positive cells were visualized directly, without the need for antibody staining.

The following antibodies were used: For immunohistochemistry: Goat anti-BMP7 (Santa Cruz Biotechnology, sc-6899, dilution: 1:25), goat anti-ALK2 (R&D, AF637, 1:50), rabbit anti-ALK3 (Santa Cruz Biotechnology, sc-20736, 1:150), goat anti-ALK6 (Santa Cruz Biotechnology, sc-

5679, 1:150), rat anti-CD45 (R&D, MAB114, 1:50), rabbit anti-CK5 (Abcam, ab24647, 1:1200), rabbit anti-CK20 (Abcam, ab53120, 1:200), rabbit anti-Met (phosphorylated Tyr1001, Abcam, ab61024, 1:50), rabbit anti-S100A4/FSP1 (gift from E.G. Neilson, 1:450), rabbit anti-HGF (Santa Cruz Biotechnology, sc-7949, 1:50), rabbit anti-Ki67 (Abcam, ab15580, 1:500), and rabbit anti-p63 (phosphorylated Ser160/162, Cell Signaling Technology, #4981, 1:100). Anti-CD45 is a monoclonal antibody; all other antibodies are polyclonal. For immunofluorescence: anti-CK5 (Abcam, ab24647, 1:300), anti-S100A4/FSP1 (DAKO, A5114; Opal 690 1:50, 2ARs), anti-Ki67 (Thermo Scientific, RM-9106-S, 1:500, Opal 520, 1:200, 3 ARs). Anti-Ki67 is rabbit monoclonal; all other antibodies are rabbit polyclonal.

Immunofluorescence pictures (400x) were taken of representative forestomach epithelium and stroma by one observer (Hikaru Sugimoto.), and the pictures were given random numbers. The number of Ki67 positive cells in the forestomach were counted by another observer (Hans Petter Eikesdal), blinded to the mouse genotype. Ki67 positive cells in the epithelium (FSP1 negative), and in the stroma (FSP1 positive) were summarized for the whole tissue section framed within the picture, and from at least three separate mice per genotype. After unblinding by the first observer (Hikaru Sugimoto.), the number of Ki67 positive cells in the epithelium (FSP1 negative) and the stroma (FSP1 positive) were compared between the three genotypes.

TSA-based multiplex staining on murine mammary carcinoma tissues

TSA-based multiplex immunolabeling was performed as described above (*Immunohistochemistry and immunofluorescence on murine mammary carcinoma tissues*). The panels used are listed in below, which includes the number of 15 min antigen retrievals was used for each antibody, as well as concentration for primary antibodies and the Opal fluorescent reagent. It also informs about which Opal fluorescent reagent was used in conjunction with which antibody. Data analysis was performed using Inform Software. For each marker, detection thresholds determined

positivity. An R script created by Ehsan Ehsanipour in the Kalluri lab then summarized for each cell which expression thresholds were met and therefore was positive for which markers.

Antibodies used:

Antigen	Company and Lot #	Number of AR (15 min each)	AR Buffer	Concentration	Secondary reagent	Opal	Opal concentration
FAP	Abcam ab53066	1	TE	1:100*	Biocare Rabbit	Opal 570	1:100
FSP1	Dako	2	Citrate	1:8000	Biocare Rabbit	Opal 650	1:100
CK8	Throma-1; the University of Iowa	3	Citrate	1:50	Rat Polymer	Opal 620	1:400
α SMA	Dako M0851	4	Citrate	1:2000	Biocare Mouse on mouse polymer	Opal 690	1:100
Vimentin	CS5741	5	Citrate	1:200	Biocare Rabbit	Opal 520	1:100
CD31	Dianova Dia-310	6	Citrate	1:50*	Rat Polymer	Coumarin	1:50
Ki-67	Thermo	7	Citrate	1:500	Biocare Rabbit	Opal 540	1:400

*primary antibody was used with Aurion 4% Cold water fish gel instead of 1% BSA

Imaging of FSP1-GFP and α SMA-RFP signal

Tissues from FSP1-GFP; α SMA-RFP double transgenic and wt mice were fixed in 4% PFA overnight at 4°C; then transferred into 30% sucrose/PBS for at least 24 hours. After rinsing with PBS, the tissues were embedded in OCT compound and frozen in liquid nitrogen. Cryosections (7.5 μ m) were prepared, hydrated with a brief wash in PBS, mounted with Vectashield with DAPI and analyzed by fluorescence microscopy. Both the GFP and RFP transgene could be visualized directly by fluorescence microscopy.

Immunofluorescence analyses of cultured cells

Primary forestomach fibroblasts were grown to sub-confluency on eight-well BD Falcon culture slides and fixed in ice-cold methanol (–20°C). After blocking with 1% donkey serum, the cells were incubated with the primary antibody overnight at 4°C. Subsequently, the immunoreactions

were detected by rhodamine-conjugated secondary antibodies (Jackson ImmunoResearch), mounted with Vectashield with DAPI (Vectorlabs) and analyzed by fluorescence microscopy. Parallel wells were run for all the experiments without primary antibody, to assure the specificity of the immunoreactions. The following antibodies were used: Anti-ALK6 (Santa Cruz, sc-25455, 1:50), anti-Met (phosphorylated Tyr1001, Abcam, ab61024, 1:50), anti-FSP1 (gift from E.G. Neilson, 1:150), anti-HGF α (Santa Cruz, sc-7949, 1:50), anti-Tgfbr2 (Santa Cruz, sc-220, 1:100). All antibodies are polyclonal.

Chromogenic in situ hybridization (CISH)

Sense and anti-sense oligonucleotide probes (Operon) for HGF and BMP7 RNA were designed and labeled with digoxigenin using the DIG oligonucleotide 3'-End Labeling Kit (Roche). Glass slides were coated with a 2% solution of 3-aminopropyl-triethoxy-silane (Sigma) and washed with acetone and DEPC-water before use. Cryosections (14 μ m) were applied to the coated slides, fixed immediately with 4% PFA, permeabilized with 0.2M HCl and proteinase K, fixed again in 4% PFA, and then incubated 3 hours in hybridization buffer (50% formamide, 2x SSC, 50mM phosphate buffer, 1x Denhard's solution, 5% sodium dextran). Thereafter, the sections were incubated in hybridization buffer with either the sense or anti-sense DIG-labeled probes, overnight at 37°C. The next day the sections were washed in washing buffer (100 mM Tris HCl, pH 7.5, 150 mM NaCl), and incubated 30 minutes with blocking buffer (Roche DIG High Prime DNA Labeling and Detection Starter kit I), before adding an alkaline phosphatase-conjugated anti-DIG antibody (Roche) for 60 minutes at 37°C. After repeated washes, the sections were equilibrated in detection buffer (100 mM Tris HCl, pH 9.5, 100 mM NaCl) and the immunoreaction was visualized by incubating with NBT/BCTP color substrate (Roche) for three hours. The color reaction was stopped using TE-buffer and the sections were mounted using Vectashield. Parallel sections were run with sense and anti-sense oligonucleotide probes, with or without DIG antibody, and with or

without NBT/BCTP color substrate, to assure the specificity of the in situ RNA hybridization and of the immunoreaction.

Sequences of the CISH oligonucleotide primers:

HGF sense: CAGTGTTTCAGAAAGTTGAATGCATGACCTGC

HGF anti-sense: GCAGGTCATGCATTCAACTTCTGAACACTG

BMP7 sense: AGCGATTTGACAACGAGACCTTCCAGATCACAGTCTATCAGGTGC TCCAG

BMP7 anti-sense: CTGGAGCACCTGATAGACTGTGATCTGGAAGGTCTCGTTGTCAAA
TCGCT

Analysis of immune cell populations in CAF-depleted tumors

Tumors were collected and transferred into cold RPMI/10% FBS and kept on ice. Subsequently, tumors were cut into small pieces and placed in C-tubes (gentle MACS, Miltenyi Biotech) in digestion buffer 0.1 mg/ml Liberase and 0.2 mg/ml DNaseI in RPMI. The pre-installed program: m_imp Tumor_02 was run on GentleMACS octo dissociator. Homogenized samples were incubated in C-tubes at 37C for 30 min at 150 rpm before the second program m_impTumor_03 was run twice on the dissociate. Samples were strained through 100 µm mesh into 50-ml conical tube and 5 ml and RPMI (10mM M EDTA, 10% FBS (pH8.0) was added. FACS buffer (1% FBS in PBS) was added to wash before pelleting the cells by spinning 5 min at 600g. The wash step was repeated before sample was layered on Histopaque (Sigma Aldrich) and spun at 700g for 20 min. The white interphase was collected, pelleted and resuspended in FACS buffer. Samples were stained in 96 well plates. Plate was spun 2 minutes at 800g at 4C, before cell pellets were resuspended in 100 µl staining mix (FACS buffer + 1/5 of final volume BV Buffer + 50 µg/ml CD16/32 block + surface antibodies + viability dye). Primary antibody incubation lasted 30 min on ice before spinning the plate again and washing twice with 200 µl FACS buffer. Cells were permeabilized and fixed with FoxP3 Fix-perm (Biolegend) for 1-12 h at 4C before washing with

FoxP3 Fix Perm wash (Biolegend) and incubation with intracellular antibodies. After 2 additional washes with FoxP3 Fix Perm wash, pellets were resuspended in 200 µl of BD Cytofix, incubated on ice for 30 min (covered with foil) and washed with FACS buffer before flow cytometry analysis on Fortessa X-20. Samples were run at 7,000 – 10,000 events/sec (do not exceed 20,000 events/sec) and up to 2,500,000 events were recorded per sample. Analysis was performed with FlowJo software.

Antibody panels:

T-cell panel

Marker	Color	Dilution	Cat # (Clone)
PD1 (CD 279)	PerCP-Cy5.5	1/100	BioLeg 135208 (29F.1A12)
GranzB	APC	1/100	Invitrogen GRB05 (GB11)
CD8	BV650 (Qdot 655)	1/200	BioLeg 100742 (53-6.7)
CD45	Pac Blue	1/100	Bio Legend 103126 (30-F11)
Live/dead	780 (APC-Cy)	1/1000	eBio 65-0865-14
CD11b	BV711	1/400	BD 563168 (M1/70)
Ki67	A488	1/100 (i)	BD 558616 (B56)
CD49b	PE	1/100	eBio 12-5971-81
CD4	BV605	1/200	BioLeg 100548 (RM4-5)
Foxp3	A700	1/50 (i)	eBio 56-5773-82 (FJK-16s)
CD3	PE-Cy	1/200 (i)	eBio 25-0031-82 (145-2c11)

Macrophage panel:

Marker	Color	Dilution	Cat # (Clone)
CD11b	BV711	1/400	BD 563168 (M1/70)
Ly6C	APC	1/200	BD 560595 (AL-21)
Ly6G	PE-Cy7	1/200	BD 560601 (1A8)
CD45	Pac Blue	1/100	Bio Legend 103126 (30-F11)
PDL1 (B7-H1)	PE (=CD274)	1/100	eBio 12-5982-83 (MIH5)
CD19	BV650 (Qdot 655)	1/100	BioLeg 115541 (6D5)
Live/Dead	780 (APC-Cy7)	1/1000	eBio 65-0865-14
CD3	A700	1/50 (i)	eBio 56-0032-82 (17A2)
PD1	PerCP-Cy5.5	1/100	BioLeg 135208 (29F.1A12)

CD11c	PE-CF594	1/50	BD 562454 (HL3)
Ki67	A488	1/100 (i)	BD 558616 (B56)

(i) means this is an intracellular antibody used in the second round of staining after permeabilization.

Quantitative real time PCR

Human and mouse mammary fibroblasts

Primers were used with SYBR Green PCR Master Mix in a 7300 Sequence Detector System (Applied Biosystems) and measurements were standardized to expression of the housekeeping genes, either acidic ribosomal phosphoprotein PO (ARP/ 36B4), 18s, or β -actin. Fold-change in gene expression was determined using the ddCt method. Technical triplicates were used, and statistical analyses computed on the dCt that compared biological replicates (cell lines from distinct mice or biopsies). Primer sequences are below:

Gene	Species	Primer sequences
<i>SLC2A1 (GLUT1)</i>	H. Sapiens	F 5' AAGGTGATCGAGGAGTTCTACA 3' R 5' ATGCCCCAACAGAAAAGATG 3'
<i>Hk2</i>	M. Musculus	F 5' GGAACCGCCTAGAAATCTCC 3' R 5' GGAGCTCAACCAAAACCAAG 3'
<i>HK2</i>	H. Sapiens	F 5' TTTGACCACATTGCCGAATGC 3' R 5' GGTCCATGAGACCAGGAAACT 3'
<i>LDHA</i>	H. Sapiens	F 5' CAGCCCGAACTGCAAGTTG 3' R 5' CCCCATCAGGTAACGGAATC 3'
<i>Pkm</i>	M. Musculus	F 5' GCCGCCTGGACATTGACTC 3' R 5' CCATGAGAGAAATTCAGCCGAG 3'
<i>PKM</i>	H. Sapiens	F 5' ATGTCGAAGCCCGATAGTGAA 3' R 5' TGGGTGGTGAATCAATGTCCA 3'
<i>PFKL</i>	H. Sapiens	F 5' GCTGGGCGGCACTATCATT 3' R 5' TCAGGTGCGAGTAGGTCCG 3'
<i>Slc16a3 (Mct4)</i>	M. Musculus	F 5' GGGGCCTACTGCTCAACTG 3' R 5' CGGTCTCGGAAGACACTCAG 3'

<i>SLC16A3</i> (MCT4)	H. Sapiens	F 5' TGACTGGACAGGTATCCTTGAG 3' R 5' AGTAGTGGAATGTGGTGGCTA 3'
<i>HIF1A</i>	H. Sapiens	F 5' CTGCCACCACTGATGAATTA 3' R 5' GTATGTGGGTAGGAGATGGA 3'
<i>Arp/36b4</i>	M. Musculus	F 5' GGAGCCAGCGAGGCCACACTGCTG 3' R 5' CTGGCCACGTTGCGGACACCCTCC 3'
<i>ACTB</i> (β -Actin)	H. Sapiens	F 5' CATGTACGTTGCTATCCAGGC 3' R 5' CTCCTTAATGTCACGCACGAT 3'
<i>18s</i>	M. Musculus	F 5'-GTAACCCGTTGAACCCCAT-3' R 5'-CCATCCAATCGGTAGTAGCG-3'

Murine forestomach fibroblasts

Primary forestomach fibroblasts were plated on 6-well plates (Falcon), at 150,000 cells per well, and starved 24 hours in DMEM with 0.1% FBS. Thereafter the media was changed to DMEM with 0.1% FBS with or without Activin A (50 ng.ml⁻¹) or 100 ng.ml⁻¹ BMP7 (R&D), and the cells were treated for 24 hours. Then the cells were washed with warm (37°C) PBS, and RNA was isolated with Trizol, as described in the Invitrogen product manual, followed by DNase (Invitrogen) treatment. RNA concentration was measured using an Eppendorf BioPhotometer. Reverse transcription of 0.5 µg of RNA from each sample was performed with Superscript II™ reverse transcriptase (Invitrogen) or Multiscribe™ reverse transcriptase (Applied Biosystems), followed by RNase treatment, before running PCR (35 cycles) with the below primers.

Primer sequences:

Gene	Sequence
Activin A forward	5' TGGAGCAGACCTCGGAGATCATC 3'
Activin A reverse	5' AAGCACTAGACTGGCACCCTC 3'
Activin B forward	5' TCCGAGATCATCAGCTTTGCAG 3'
BMP2 forward	5' ATCTGTACCGCAGGCACTCAGG 3'
BMP2 reverse	5' TGTGTGGTCCACCGCATCACAG 3'

BMP4 forward	5' AGCCATGCTAGTTTGATACCTG 3'
BMP4 reverse	5' AAGCAGAGCTCTCACTGGTCC 3'
BMP6 forward	5' TGCTGGATCTCTACAACGCCCTG 3'
BMP6 reverse	5' ACAGTCCTTGTAGACGCGGAACTC 3'
BMP7 forward	5' TGGACAACGAGGTGCACTCCAG 3'
BMP7 reverse	5' TGGTTGCTGGTGGCTGTGATATC 3'
HGF forward	5' ACCAAACTTCTGCCGGTCCTGTTG 3'
HGF reverse	5' ATCATGGAATTCCAAGGCTGGC 3'
β -actin forward	5' TGGCATTGTTACCAACTGGG 3'
β -actin reverse	5' AGTTTCATGGATGCCACAGG 3'
CCL5 forward:	5' TCACCATCATCCTCACTGCAGC 3'
CCL5 reverse	5' TCTCTGGGTTGGCACACACTTG 3'
CTGF forward	5' ATGTCAGTGCGCAGCCGAAGCAG 3'
CTGF reverse	5' AGTCTGCAGAAGGTATTGTCATTG 3'
EGF forward	5' AAGCAAGGCGATTTGGATAGCC 3'
EGF reverse	5' TTCGCAGTACTTCCGGTCTCGG 3'
FGF2 forward	5' ACTACAACTCCAAGCAGAAGAGAG 3'
FGF2 reverse	5' TCAGCTCTTAGCAGACATTGGAAG 3'
FGF10 forward	ATGTGGAAATGGATACTGACAC 3'
FGF10 reverse	5' TCATGGCTAAGTAATAGTTGCTG 3'
GM-CSF forward	5' ATTGTGGTCTACAGCCTCTCAGC 3'
GM-CSF reverse	5' AGGTGGTAACTTGTGTTTCACAGTC 3'
HB-EGF forward	5' ACTGGATCCACAAACCAGCTGC 3'
HB-EGF reverse	5' TGAGAAGTCCCACGATGACAAG 3'

IGF1 forward	5' AGATACACATCATGTCGTCTTCAC 3'
IGF1 reverse	5' TTCTGAGTCTTGGGCATGTCAG 3'
IGF2 forward	5' AAGTCGATGTTGGTGCTTCTC 3'
IGF2 reverse	5' TCACTGATGGTTGCTAGACATC 3'
IL-6 forward	5' ACTGATGCTGGTGACAACCACG 3'
IL-6 reverse	5' AGCTTATCTGTTAGGAGAGC 3'
KGF forward	5' ATACTGACACGGATCCTGCCAAC 3'
KGF reverse	5' TGCATAGAGTTTCCCTTCCTTG 3'
NGF forward	5' TGGATGGCATGCTGGACCCAAGC 3'
NGF reverse	5' ATGAACCTCCAGGCAGCCTGC 3'
SDF1 α forward	5' AGTCAGCCTGAGCTACCGATG 3'
SDF1 α reverse	5' TAAAGCTTTCTCCAGGTACTC 3'
SFRP1 forward	5' AGCGAGTACGACTACGTGAGC 3'
SFRP1 reverse	5' ACCGTTCTTCAGGAACAGCACAA 3'
TNC forward	5' TGTCCCCTCCCAAAGACCTTATTG 3'
TNC reverse	5' TCGGGTGTTGTTTTTCACAATGTGC 3'
TGF α forward	5' ACAGCTCGCTCTGCTAGCGCTG 3'
TGF α reverse	5' TTCTCATGTCTGCAGACGAGG 3'
TGF β 1 forward	5' ACTCTCCACCTGCAAGACCATCGAC 3'
TGF β 1 reverse	5' TGGTAGAGTTCCACATGTTGCTCC 3'
Wnt1 forward	5' TCTACTACGTTGCTACTGGCAC 3'
Wnt1 reverse	5' TTGCACTCTTGGCGCATCTCAGAG 3'
Wnt3 forward	5' TCCTCGCTGGCTACCCAATTTG 3'
Wnt3 reverse	5' GTGCTTGTTTCATAGCTG 3'

Immunoblotting

Human mammary fibroblasts

Cells were lysed with RIPA buffer using standard protocol. Protein concentrations were determined by BCA Protein Assay (Thermo Scientific) with a microplate reader at 562 nm. Wes system (Protein Simple) was utilized and assay was performed according to manufacturer's recommendations with the following antibodies: HIF1 α antibody (Novus Biologicals, AF1935, 1:10), β -Actin (Sigma Aldrich, A3854, 1:100). Band intensities were quantified using the Compass Software (Protein Simple).

Isolated forestomach fibroblasts and tissues

Cells and tissues were homogenized and lysed with protein lysis buffer (50 mM Tris HCl, pH 7.5, 150 mM NaCl, 0.1% SDS, 1% deoxycholate, 1% Triton X-100) containing a protease inhibitor cocktail (Roche). Protein concentrations were measured by a bicinchoninic acid (BCA) assay (Pierce), and 30 μ g of protein was loaded per lane for the whole tissue immunoblots and 15 μ g of protein was loaded per lane for the cell culture immunoblots. For the BMP7 stimulation experiment, primary forestomach fibroblasts were plated on 6-well plates (Falcon), at 150 000 cells per well, and starved 24 hours in DMEM with 0.1% FBS. Thereafter, the cells were either harvested directly or the media was changed to DMEM with 0.1% FBS with 100 ng/ml⁻¹ of BMP7, and the cells were treated for 24 or 48 hours before harvesting protein. The protein lysates were fractionated using SDS-PAGE gel electrophoresis, transblotted to PVDF membranes by semi-dry technique, before performing coomassie staining to assure equal protein loading. Thereafter, the membranes were blocked with 5% fat-free dry milk for 60 minutes, before immunoblotting overnight with the primary antibody. The immobilized antibody was detected using the appropriate horseradish peroxidase-conjugated secondary antibody (Sigma) and ECL (Pierce). The

immunoreaction was visualized using Hyblot autoradiography films (Denville). Immunoblots for actin were performed for all samples to assure equal protein loading. The intensity of the bands from uncropped blots were quantified using ImageJ software. The areas under each peak for the proteins of interest were normalized to those of actin in each blot. The following antibodies were used: Rabbit anti-Actin (Sigma, A2066, 1:2500), rabbit anti-Akt (phosphorylated Ser473, Cell Signaling, #4060, 1:1000), mouse anti-BMP7 (Sigma, B2555, 1:2000), rabbit anti-ERK1/2 (phosphorylated Thr202/Tyr204, Cell Signaling, #9101, 1:500), mouse anti-HGF (Assay Designs, #905-165, 1:5000), rabbit anti-PTEN (Cell Signaling, #9559, 1:1000), rabbit anti-Smad1/5 (phosphorylated Ser463/465, Cell Signaling, #9516, 1:1000), rabbit anti-Smad2 (phosphorylated Ser465/467, Cell Signaling, #3101S, 1:1000). BMP7, HGF, phosphorylated-Akt, phosphorylated-Smad1/5, and PTEN are monoclonal antibodies; all other antibodies are polyclonal.

5-Azacytidine treatments of hBFs

hBFs were seeded in 10 cm plates (100,000 cells/plate). 3 days after seeding media was replaced with media containing 3 μ M 5-Azacytidine. Media was replaced with fresh 5-Azacytidine containing media after 24 h. After 48 h, cells were harvested. hBF # 33 and # 38 were used in 3 independent experiments (biological replicates) and hBF #120 was used in 2 independent experiments (biological replicates). These experiments were performed by Joyce Tse O'Connell.

E10 epithelial cell proliferation assays

Primary forestomach fibroblasts were grown to sub-confluency in DMEM with 20% FBS. Thereafter, the media were changed to DMEM with 0.1% FBS, and the cells were incubated for 48 hours. Then, the conditioned media were sterile filtered (0.22 μ m, Fisherbrand) and stored at -80°C until further use. E10 epithelial cell lines were used to determine the influence of

conditioned fibroblast media on epithelial cell function. The E10 lung epithelial cell line was a kind gift from A. Malkinson (UCHSC). The E10 cells were grown in CMRL-1066 Medium (Gibco), supplemented with L-glutamine (0.15 g.L^{-1} , Cellgro), 10% FBS, 100 units. ml^{-1} of penicillin and $100 \text{ }\mu\text{g.ml}^{-1}$ of streptomycin. The cells were seeded at 1,800 cells per well in 96-well plates (Falcon) and allowed to attach overnight in CMRL-1066 with 10% FBS. Next, the E10 cells were serum starved in DMEM with 0.1% FBS for 24 hours, before culturing for 48 hours with the conditioned fibroblast media, with or without the Met inhibitor SU11274 ($10\mu\text{M}$, kind gift from Pfizer). The surviving cell number was assessed by methylene blue assay, as described previously⁸⁵. Multiple rows of eight wells were subsequently analyzed. Cells were regularly tested and negative for mycoplasma.

BMP7 stimulation of forestomach fibroblast proliferation

Primary forestomach fibroblasts were seeded at 2,000 cells per well in 96-well plates and allowed to attach overnight in DMEM with 20% FBS. Thereafter, the cells were serum starved in DMEM with 0.1% FBS for 24 hours, before treating for 48 hours with 0, 1, 10 or 100 ng.ml^{-1} recombinant human BMP7 (BMP7, R&D) in DMEM with 0.1% FBS. The surviving cell number was assessed by methylene blue assay, as previously described.

^{13}C glucose labeling experiments

hCAFs were incubated in media (10% FBS (dialyzed, Thermo Scientific), 2 mM L-glutamine (Gibco), 2.5 mM $^{13}\text{C}_6$ glucose in glucose-free DMEM) containing uniformly ^{13}C labeled glucose ([U- ^{13}C] glucose, Cambridge Isotope Laboratories) for 48 h to allow labeling of all glucose-derived metabolites in the cells. The cells were washed four times with PBS and processed for mass spectrometry as described above, or, after incubation in media containing [U- ^{13}C] glucose, washed three times with PBS to remove any residual [U- ^{13}C] glucose before incubation with media containing unlabeled glucose (10% FBS, 2 mM L-glutamine, 2.5 mM glucose in DMEM) to collect

conditioned media (CM), which contained labeled secreted metabolites. The CM metabolites were extracted and measured (as described above) or fed to MDA-MB-231 cells for 24 h. MDA-MB-231 cells were then washed four times with PBS and processed for mass spectrometry as described above. Unlabeled MDA-MB-231 cells, as well as unlabeled hCAFs served as controls. If false positive rate in controls exceeded 5% (for metabolites secreted by hCAFs) or 10% (for metabolites in hCAFs and MDA-MB-231 cells), metabolites were excluded. These experiments were performed by Margo Cain and data analysis was done by myself.

Seahorse Glycolysis Stress Test

Glycolysis stress tests were performed using a Seahorse XF96 analyzer (Agilent). The assays were performed according manufacturer's instructions. Specifically, microplates (part of Agilent product pack 102416-100) were coated with 10 µg/ml rat tail Collagen I (Corning 354249) before mouse fibroblasts (10,000 cells/well) and human fibroblasts (8000cells/well) were seeded. Assays were performed 2 days after seeding to allow cells to attach to the plate. 24 h before the assay, cartridge (part of Agilent product pack 102416-100) was filled with H₂O and placed in a non-CO₂ incubator. After overnight incubation, H₂O was replaced with Calibrant (part of Agilent product pack 102416-100), and placed back in a non-CO₂ incubator. Seahorse XF prep station was used to replace cell culture media with Base Media (Agilent, 102353-100) supplemented with 2 mM Glutamine (Gibco; pH of media adjusted to 7) 45 min prior to the assay. After media change, cells were placed in non-CO₂ incubator. 10 min before start of the assay, medium was replaced once again using Seahorse XF prep station, to ensure correct baseline readings. Assay was performed with a standard protocol: for each stage, 3 measurements were taken; for each measurement, media was mixed for 3 min and the measurement lasted 4 min. After baseline measurements, glucose (10 mM final concentration, Agilent 103020-100) was injected from port A. After 3 measurements, Oligomycin (3 µM final concentration, Agilent 103020-100) was injected from port

B and measurements were repeated. Lastly, 2 deoxy-glucose (100 mM final concentration, Agilent 103020-100) was injected from port C and 3 measurements followed before assay ended. Data was analyzed with Seahorse Wave software. After the assay, cells were fixed to the plates with 4% paraformaldehyde (Electron Microscopy Sciences 15710-S) and stained with DAPI (Life Tech). Subsequently, pictures were taken of each well (5 pictures in 20x magnification) and % DAPI positive area was quantified with ImageJ software to determine cell density, which was used to normalize ECAR values. Glycolysis, glycolytic capacity and glycolytic reserve were determined as recommended in the Seahorse XF User Manual: *Glycolysis*: last rate measurement before glucose injection is subtracted from the max rate measurement before oligomycin injection. *Glycolytic capacity*: last rate measurement before glucose injection is subtracted from the max rate after oligomycin injection. *Glycolytic reserve*: glycolysis is subtracted from glycolytic capacity.

Statistical analysis

For comparison between two groups, a one-tailed or two-tailed unpaired *t*-test (with Welch's correction when appropriate) or Mann-Whitney test was performed, as listed in the figure legend. For comparison between three groups, an ordinary one-way ANOVA test was used. A *P* value < 0.05 was used to define statistical significance.

CHAPTER 3

CHARACTERIZATION OF FIBROBLAST HETEROGENEITY IN MURINE MODELS OF MAMMARY CARCINOMA

This work has been done with the help and in collaboration with Drs. Ehsan Ehsanipour, Pedro Correa de Sampaio, Julie Carstens, Hikaru Sugimoto and Patricia Philips. Some of the data shown in this chapter was generated by Joyce Tse O'Connell and Hikaru Sugimoto (indicated in figure legends) and is shown with their permission.

Parts of the work in this chapter has been published previously and is taken verbatim from the publication:

Becker, L. M.*; O'Connell, J. T.*; Vo, A. P., Cain, M. P., Tampe, D., Bizarro, L., Sugimoto, H., McGow, A. K., Asara, J. M., Lovisa, S., McAndrews, K. M., Zielinski, R., Lorenzi, P. L., Zeisberg, M., Raza, S., LeBleu, V. S., and Kalluri, R. **Epigenetic Reprogramming of Cancer Associated Fibroblasts Deregulates Glucose Metabolism and Facilitates Progression of Breast Cancer**. Cell Reports, 31(9), 107701. <https://doi.org/10.1016/j.celrep.2020.107701>

Summary

CAFs are now widely recognized as a heterogeneous cell population, comprised of multiple functionally distinct subsets. Several recent studies have identified breast cancer CAF subtypes based on the expression patterns of different mesenchymal markers. However, the majority of CAF populations remains to be identified. More importantly, phenotypically-defined CAF populations need to be further attributed to specific functions to provide new insight into their specific roles in tumorigenesis. This chapter describes a project in which we leveraged multiplex immunofluorescent staining technology to catalogue overlapping expression patterns of different mesenchymal markers in two mammary carcinoma rodent models. Based on differential marker expression, we defined several distinct CAF populations and constructed a comprehensive map of the evolution of CAF marker composition in the TME during tumor initiation and progression. Surprisingly, the majority of CAFs was identified by expression of single markers, with little overlap in the expression patterns of the four different markers tested. Phenotypically defining these CAF subtypes served as the basis for several follow-up studies to further characterize their functions which are presented in Chapter 4.

Introduction

Several studies aiming to unravel CAF heterogeneity in breast cancer had been published in recent years. Sugimoto et al. investigated the expression pattern of six major CAF makers in 4T1 mouse mammary tumors by measuring co-expression of marker pairs. NG2, α SMA and PDGFR β showed significant overlap (80-90%) in their expression patterns, whereas FSP1 displayed expression restricted to a single, distinct CAF population. In contrast, Vimentin and Collagen1 (Col1) were shown to be ubiquitous mesenchymal markers⁸⁶. RNA sequencing analyses were used to identify three distinct CAF subpopulations in the MMTV-PyMT transgenic model of mammary carcinoma. Vascular CAFs (vCAFs), developmental CAFs (dCAFs), and

matrix CAFs (mCAFs) were each associated with a distinct gene expression signature, and immunolabeling evidence suggested unique origins for these subpopulations. Commonly used CAF markers such as α SMA, FAP and FSP1 were found in all discovered CAF subsets, and therefore not useful in further resolving CAF subsets on the level of gene expression. Instead, protein expression of more restricted CAF markers such as PDGFR α , Nidogen2, and scrapie-responsive protein 1 (SCRG1) could each define a unique CAF subset (mCAFs, vCAFs, dCAFs, respectively). Although no functional characterization experiments were performed in this study, the abundance of vCAFs and mCAFs in patient-derived samples were observed to be correlated with increased risk of developing metastatic disease⁸⁷. A follow-up study compared the described subsets in mammary fat pads as well as in early and late stage MMTV-PyMT tumors and demonstrated dynamic changes in CAF populations through tumorigenesis using multiplex immunolabeling. In addition, gene expression signatures were determined for early and late stage CAFs. Early stage CAF signatures were correlated with more positive patient outcome, while late stage CAFs signatures were associated with disease features such as increased NF κ B signaling which is itself linked to increased risk for developing metastases⁸⁸.

Clinical studies have suggested increased stromal content as a predictor of improved outcome in ER⁺ breast cancer, whereas in triple negative breast cancer it is a predictor of poor outcome^{25–27,89}. Recently, a paper described “reactive stroma”, a stroma subtype characterized by high level of protein expression of Caveolin-1, Collagen VI, and α SMA, as well as a higher cell density in the stromal compartment independent of molecular subtypes. This subtype predicted favorable clinical outcome in estrogen receptor (ER)⁺/ human epidermal growth factor receptor 2 (HER2)⁻ breast cancers, but had no prognostic value in triple-negative cases⁹⁰. A very thorough flow cytometry-based study using patient-derived fibroblasts was successful in identifying four CAF subsets based on the differential expression patterns of CD29, FAP, α SMA, PDGFR β , FSP1, and CAV1. Subsequent in vitro experiments demonstrated two of the identified subsets interacting

with different immune cell populations, thereby promoting an immunosuppressive microenvironment⁹¹.

As it becomes obvious, several breast CAF subsets have been identified using RNA sequencing, multiplex immunolabeling or flow cytometry in transgenic animal models and patient tissues. The variety of marker sets used in these studies and the inconsistency in observed differential expression pattern highlights the difficulty of CAF subset identification and highlights a need for more standardized determination of CAF populations. In an effort to further unravel the complexity of heterogeneous CAF marker expression, we used Tyramide Signal Amplification (TSA)-based multiplex immunolabeling to probe for different mesenchymal markers in tissue sections from two distinct animal models of mammary carcinoma. Specifically, expression overlaps of α SMA, Vimentin, FSP1, FAP were investigated. α SMA is the most commonly used marker to identify CAFs and FSP1 had already been shown to uniquely label a distinct CAF population in mammary carcinoma⁹². While the prominent CAF marker FAP is thought to specifically label activated fibroblasts, Vimentin presents a more ubiquitous fibroblast marker. We hypothesized that we would be able to identify distinct CAF populations by the differential expression patterns of these 4 markers.

CAF heterogeneity in the 4T1 murine mammary carcinoma model

To confirm the distinct, minimally overlapping expression pattern of α SMA and FSP1 in CAFs, we utilized α SMA-RFP;S100A4-GFP transgenic mice, which express RFP and GFP that are respectively driven by α SMA and FSP1 (S100A4) promoters. RFP and GFP expression was assayed in healthy tissues of α SMA-RFP;S100A4-GFP mice, or in tumors and metastatic lungs of α SMA-RFP;S100A4-GFP mice bearing 4T1 tumors. α SMA⁺ stromal cells comprised the majority of stromal cells in the mammary fat pads (~80%) and in the lungs (~62%) of healthy mice, as well as in tumors (~94%) and metastatic lungs (~66%) of 4T1 tumors bearing mice when

compared to FSP1⁺ stromal cells (~17% in the mammary fat pad, ~22% in the lungs, ~2% in 4T1 tumors, and ~28% in metastatic lungs) (**Figure 3A**). Stromal cells or CAFs (in tumors and metastatic lungs) double positive for α SMA and FSP1 were rare, consistent with our previous report using immunohistochemistry⁸⁶ and direct visualization of GFP (FSP1) and RFP (α SMA) in

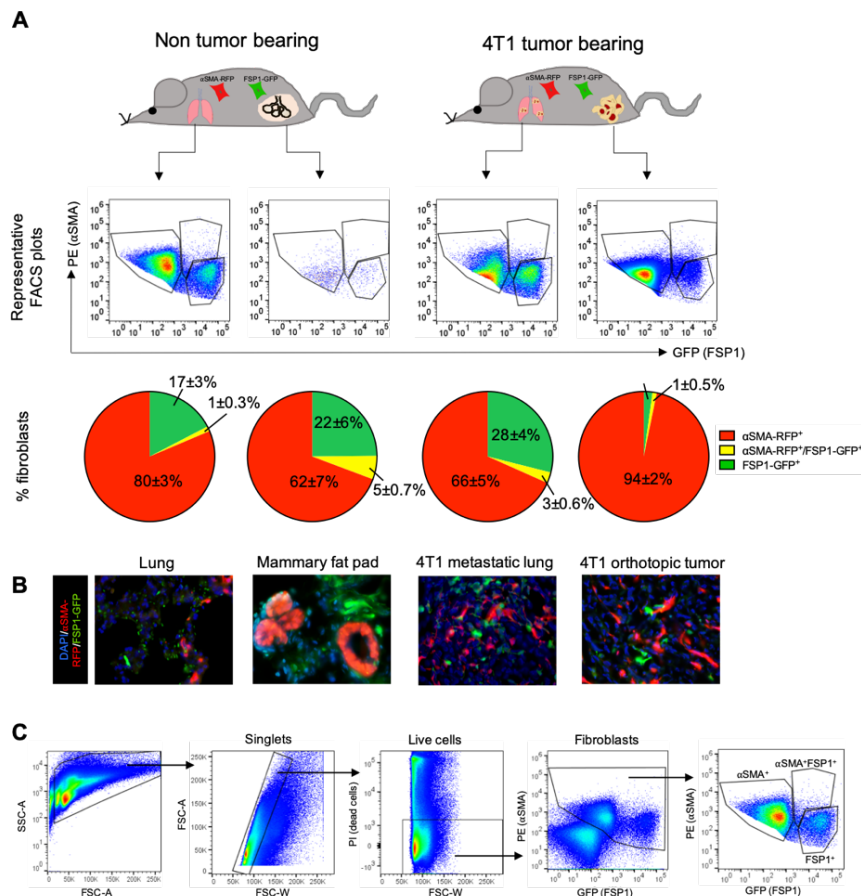


Figure 3. α SMA and FSP1 expression in healthy and mammary tumor bearing mice

A. α SMA-RFP;*S100A4*-GFP transgenic mice were implanted with 4T1 mammary carcinoma cells. Expression of RFP and GFP was analyzed in tumors and metastatic lungs of the mice, as well as in mammary fat pads and lungs of healthy control animals. FACS blots with quantification are shown. **B.** Representative tissue sections. Scale bar: 16 μ m. **C.** Gating strategy used in (A). n = 3 healthy and 4 tumor bearing mice. Experiment performed by Joyce Tse O'Connell and panels are reproduced with permission. A similar experiment using α SMA-RFP mice is shown in doctoral dissertation of Joyce Tse O'Connell⁹⁶.

tissue sections (**Figure 3B**).

Following the identification of distinct α SMA⁺ and FSP1⁺ CAF subsets, expression of additional CAF markers was tested in the same populations. To detect CAF subsets that can be identified by expression of either a single mesenchymal marker or a combination of multiple markers, we used TSA-based multiplex immunolabeling to probe for fibroblast markers α SMA, Vimentin (Vim), FSP1, FAP and non-fibroblast markers CK8

and CD31 on a single tissue section of excised 4T1 mammary tumors. CAFs were defined as non-epithelial (CK8⁻), non-endothelial (CD31⁻) cells that expressed at least one of the mesenchymal markers tested. A CD45 antibody for detection of mesenchymal marker expression by immune cells was not included, due to the limitation of 8 fluorescence filters used to unmix the channels. However, immune cells were excluded based on their shape and size in the analysis using the Inform program. In end-stage (~2000mm³) 4T1 tumors, the majority of CAFs were single-positive for one of the four mesenchymal markers probed (**Figure 4**). FSP1 was observed to label a very minor CAF subset in these tumors (<0.05%) in comparison to α SMA which was more widely expressed (~20%). Vimentin was ubiquitously expressed in end-stage tumor CAFs (~95%), with Vimentin single-positive (s+, Vim^{s+}) CAFs being the most abundant CAF subset (~80%), followed by α SMA⁺Vim⁺ (~14%) and α SMA^{s+} CAFs (3%). 10-20% of each population were co-expressing Ki67 (data not shown).

The minimal expression overlap between FSP1 and α SMA observed in the transgenic animals (α SMA-RFP; S100A4-GFP) was confirmed with multiplex immunolabeling. Note however, that a direct comparison of CAF abundance assayed using different approaches can present with

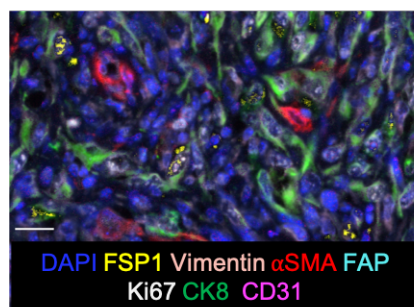
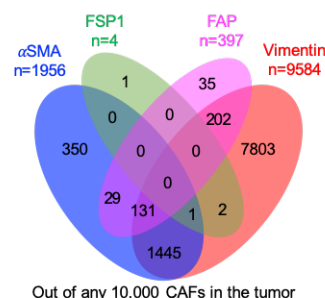


Figure 4. Overlaps in CAF marker expression in 4T1 tumors

4T1 mammary tumors were stained for FSP1, Vimentin, α SMA, FAP, CK8, CD31, Ki67 and DAPI. Representative picture of the staining and Venn diagram of expression overlaps of α SMA, FSP1, Vimentin and FAP is shown. Numbers represent the number of cells in any 10,000 CAFs (CK8⁻CD31⁻) in the tumor. The analysis is the average of 9 individual tumors. Scale bar: 20 μ m.



difficulties, as discussed later in this chapter.

4T1 mammary carcinomas are thought to mimic TNBC. As clinical studies investigating the prognostic properties of stroma often compare TNBC to hormone-receptor positive

breast cancers, we further expanded our experiments to include the MMTV-PyMT transgenic

mammary carcinoma mouse model (referred to as PyMT) representing the ER+, luminal B subtype.

CAF heterogeneity in the MMTV-PyMT murine mammary carcinoma model

4T1 and PyMT-derived mammary tumors differ not only in their molecular subtype, but also in their histological features. 4T1 tumors present with large necrotic areas and less differentiated tissue compared to PyMT tumors. Hypoxia is also increased in 4T1 tumors (**Figure 5**).

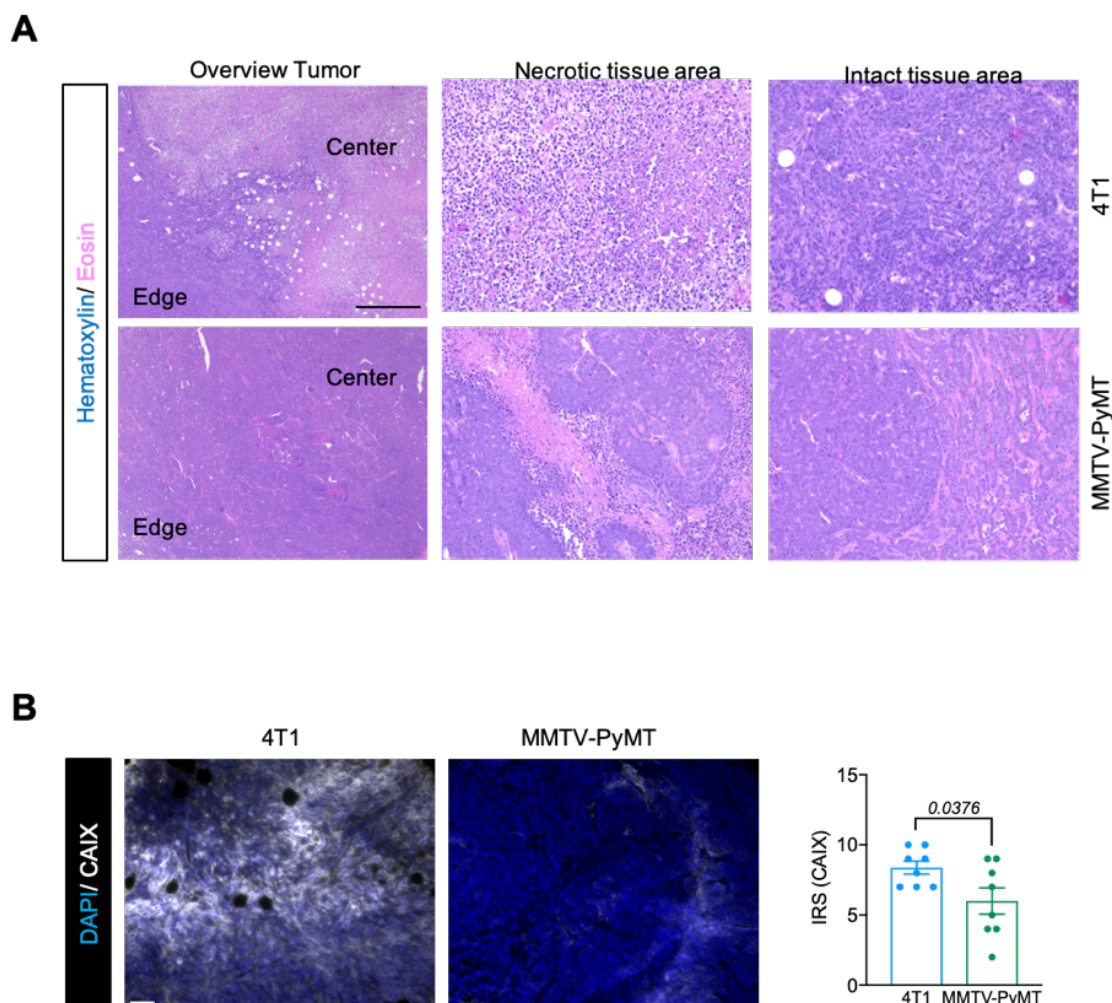


Figure 5 4T1 and MMTV-PyMT tumor histological features

A. H&E stained 4T1 and MMTV-PyMT (PyMT) tumors with representative pictures of edge and center, as well as necrotic and intact tissue. **B.** Assessment of hypoxia with CAIX staining in 4T1 and PyMT tumors with representative pictures and quantification. Scale bars = 50µm.

In PyMT tumors, expression of CAF markers by non-fibroblast cells was determined by two (2) multiplex immunolabeling panels: In both panels, CK8 and CD31 served as control markers for epithelial and endothelial cells, and Ki67 was used to measure proliferation. Panel1 includes α SMA and FAP; whereas Panel2 includes Vimentin and FSP1 (**Figure 6**). All CAF markers were expressed by cancer cells (15% - 40%), but the majority of CAF marker expression (>50% for all markers except Vim (45%)) were in the CAFs. Proliferative index differed depending on the markers tested, but was similar to the 4T1 model ~10-25% depending on the marker (data not shown).

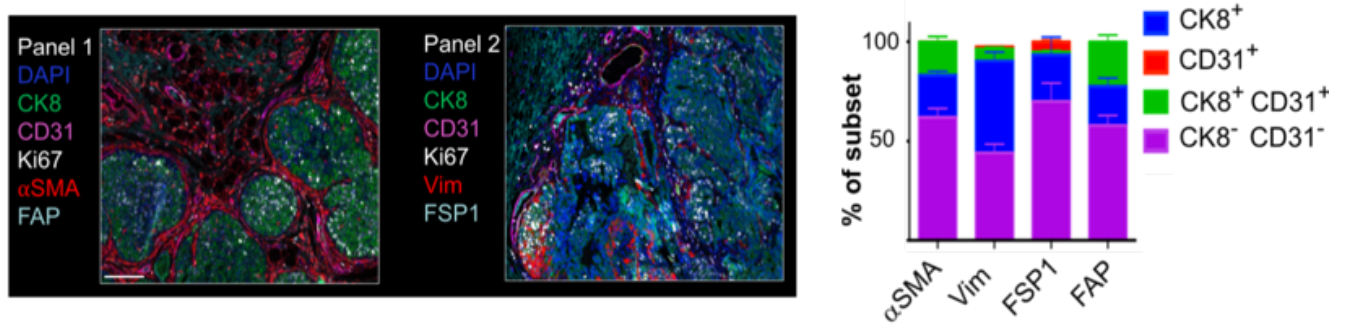


Figure 6 Expression of CAF markers by different cell types in PyMT tumors

Two TSA-based multiplex panels were used to determine expression of FSP1, Vimentin, α SMA and FAP by epithelial (CK8) and endothelial (CD31) cells. Mesenchymal marker expression by immune cells were excluded based on size (see methods). Scale bar: 20 μ m.

We subsequently measured the expression overlaps of α SMA, Vimentin, FSP1, and FAP in PyMT tumors using TSA-based multiplex staining. Surprisingly, only a small fraction (<10%) of CAFs co-expressed multiple markers simultaneously and the majority of the cells expressed a single CAF marker (single-positive; ^{s+}). The most abundant CAFs in PyMT tumors expressed only α SMA (α SMA single positive: α SMA^{s+}) (49% of all CAFs), followed by Vim^{s+} CAFs (23%). FSP1 and FAP were expressed only in a minority of CAFs (**Figure 7A**).

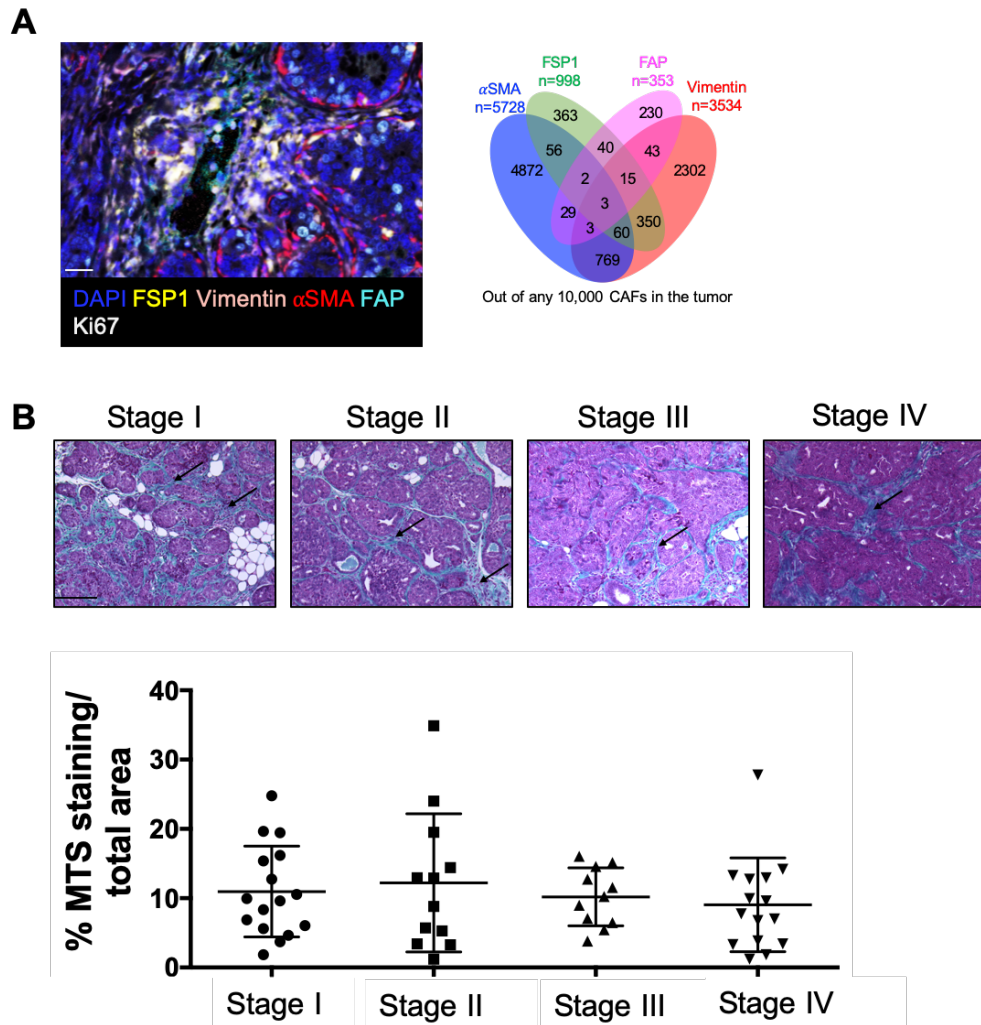


Figure 7 Expression overlaps of CAF markers in PyMT tumors

A. Representative picture of TSA-based multiplex staining of FSP1, FAP, Vimentin, α SMA, Ki67 and DAPI in PyMT tumors. Scale bar: 20 μ m. **B.** Quantification of stromal area via Mason Trichrome staining (MTS) at different stages of tumorigenesis. Scale bar: 50 μ m. Arrows indicate stromal areas.

Tumors from PyMT transgenic mice represent an excellent system to model multi-stage progression of human disease delineated by histological features. To describe and resolve the population dynamics of distinct CAF subsets in disease progression, we staged the tumors into four groups based on tumor volume. Stromal content (as assessed by Mason Trichrome Straining (MTS)) remained unchanged as tumors progressed (**Figure 7B**). We next measured the

abundance of the major CAF populations we had identified specifically in these groups, using healthy mammary fat pads as a baseline (**Figure 8B-C**).

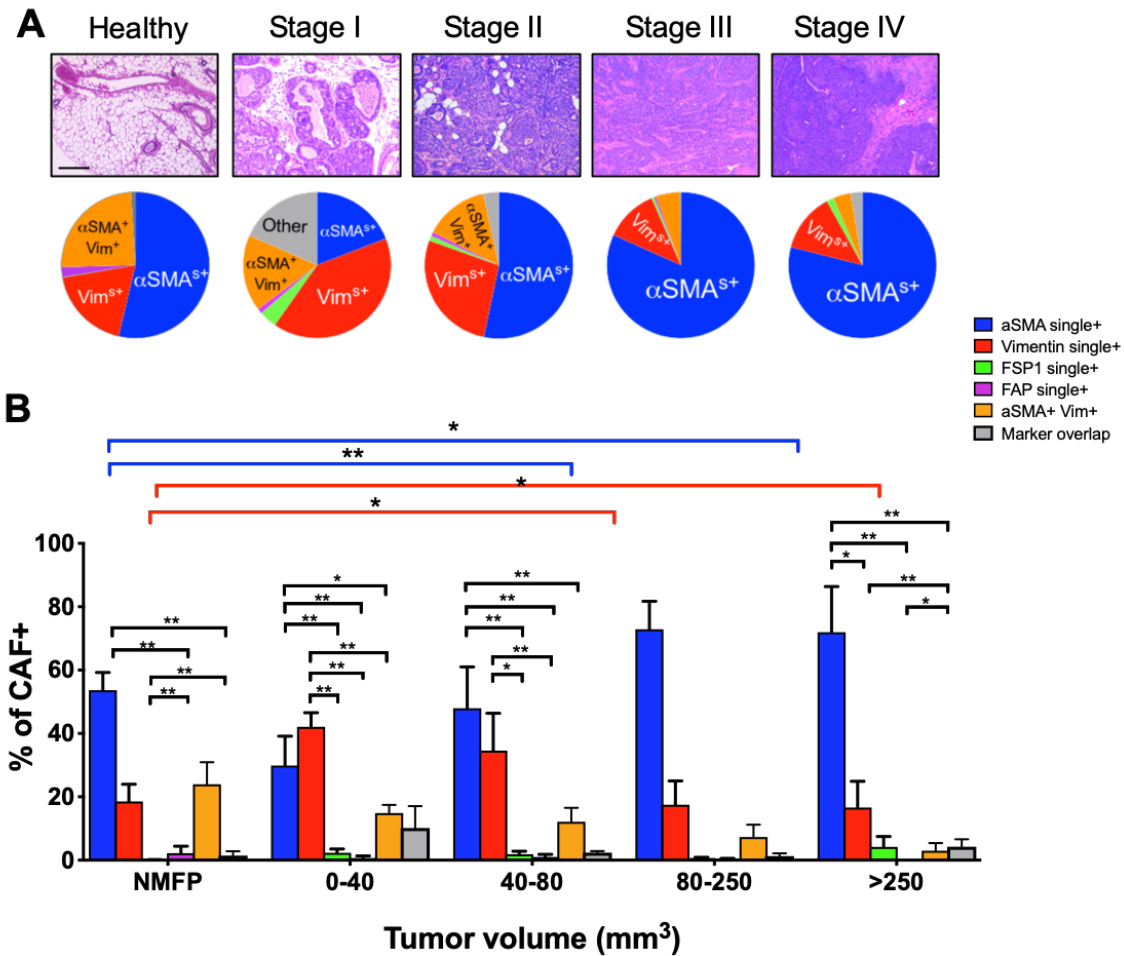


Figure 8 CAF marker expression changes during tumorigenesis in PyMT tumors.

A. Expression of the largest identified CAF subsets based on expression of αSMA, FAP, FSP1 and Vimentin in tumors of different stages. Representative H&E pictures of tumors at different stages are shown. Scale bar: 50μm **B.** Quantification of **A**. Note, that stages in **A**. refer to tumors of different volumes in **B**.

In healthy tissues, αSMA⁺, Vim⁺ and αSMA⁺Vim⁺ stromal cells represented the largest fibroblast populations. Changes in the distribution of different populations were readily observable in early stage tumors (**Figure 8A-B**). Notably, healthy mammary fat pads contain 5% fibroblasts (by cell number), whereas in tumors, up to 20% of cells were CAFs irrespective of their staging (data not shown). In early-stage tumors, Vimentin⁺ CAFs were the most abundant, with their abundance decreasing in larger, later-stage tumors. In contrast, αSMA⁺ CAFs were less

abundant in early stage tumors but the population expanded as the tumors progressed. The percentage of cells co-expressing multiple CAF markers, including $\alpha\text{SMA}^+\text{Vim}^+$ also decreased with tumor growth. In tumors \leq Stage 2, $\alpha\text{SMA}^{\text{s}+}$, $\text{Vim}^{\text{s}+}$ and $\alpha\text{SMA}^+\text{Vim}^+$ CAF populations were similar in size. As the tumors progressed beyond Stage 2, $\alpha\text{SMA}^{\text{s}+}$ CAFs outpaced all other populations (**Figure 8A-B**).

In summary, our approach successfully identified distinct CAF subsets by expression of single mesenchymal markers or combination of multiple co-expressed markers. Most CAFs were found to express only one of the four markers tested. Next, we sought to validate our findings in human breast cancer tissues.

Mesenchymal marker expression in human samples

In collaboration with Sughra Raza from the Brigham and Women's hospital in Boston, MA, we established a collection of patient samples from a large patient cohort (**Figure 9A**). Tissue biopsies were isolated from patients with benign pathologies (~65%), such as fibroadenomas or calcifications, and breast cancer (~35%, **Figure 9A**) with varying mammographic breast densities (**Figure 9A**). A total of 499 biopsies were collected from patients between 18 and 88 years of age (Median age: 51 years). All cancer cases were 82% White, 10% Hispanic/Latino, 3% Black/African American, 2% Asian and 3% not indicated. Amongst the patients with benign pathologies, 77% were White, 10% Hispanic/Latino, 9% Black/African American, 2% Asian, 0.3% American Indian/Alaska Native and 2% not indicated.

As TSA-based multiplex staining was unsuccessfully applied to preserved human samples, we opted to investigate the expression of stromal markers individually. CK8 staining was used as an epithelial cell marker to exclude non-stromal mesenchymal marker expression from our results. ECM proteins Collagen I, Collagen III and tenascin expression was increased in cancer tissues when compared to benign tissues. Laminin expression, in contrast, was decreased

in breast cancer samples. FSP1 and α SMA expression was upregulated in cancer samples. In agreement with previous studies probing for tumor angiogenesis, CD31 expression was also increased; whereas pericyte coverage of CD31 vessel was decreased (**Figure 9**).

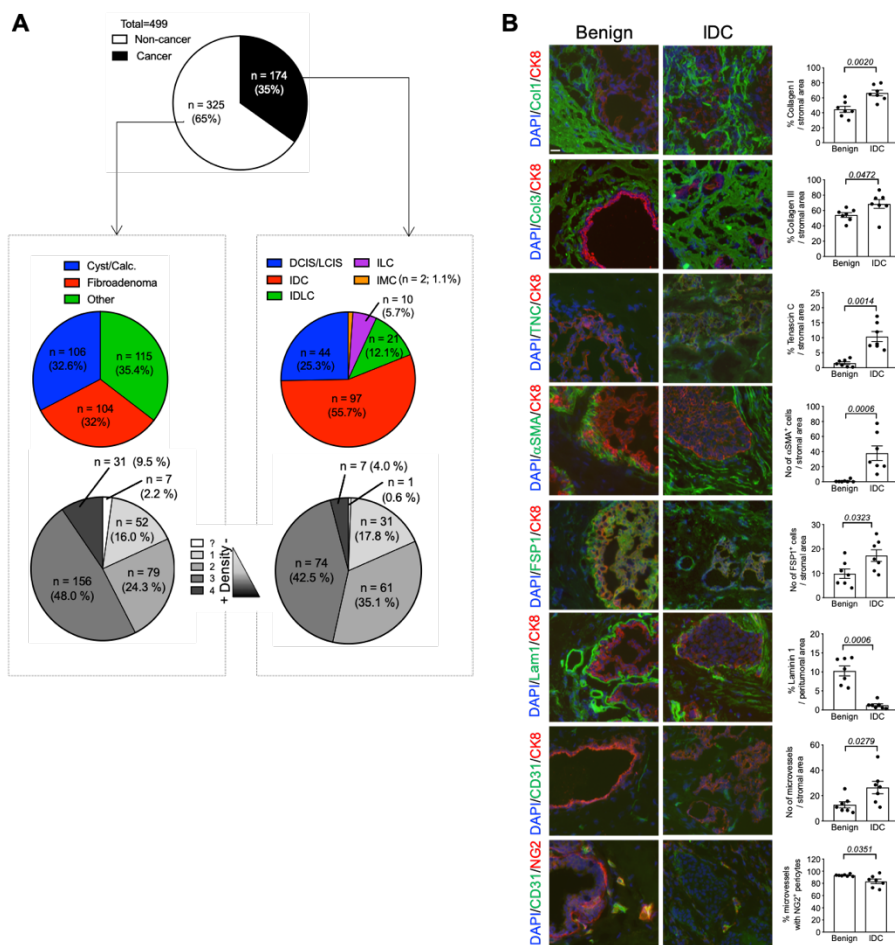


Figure 9 CAF marker expression in patient tissues of different pathologies

A. Pathology and mammographic density of patient samples collected. **B.** Immunolabeling of patient tissues with mesenchymal markers. This experiment was performed and analyzed by Hikaru Sugimoto. Scale bar: 20 μ m

Interpretation of findings

We were able to identify phenotypically distinct CAF subtypes with our multiplex immunolabeling approach in two distinct mouse models of mammary carcinoma. Unlike previous studies in which CAF subsets were identified by co-expression of several mesenchymal markers⁹¹, we found that the majority of CAFs expressed only a single marker (out of the four tested). However, we can only conclude single positivity for the markers we investigated. Any of the identified single-positive populations may co-express additional, untested mesenchymal markers. Nonetheless, the markers used in these experiments are very commonly used CAF markers. Their restrictive expression pattern suggests that none are suitable to be used as a universal CAF identifier capturing the entire CAF population. It remains to be determined whether the addition of untested markers can, in conjunction, identify the entire CAF population in a given tumor. The distinct CAF populations may play unique roles in tumorigenesis. This would explain why previous functional studies concluded varying, and sometimes contradictory roles for CAFs: Since each study used a different measure to identify CAFs, comparison among such studies may not be as meaningful.

CAF identification by flow cytometry and multiplex immunolabeling showed α SMA and FSP1 label distinct CAFs. While this observation was consistent from one method to another, absolute CAF abundance differed between the two experiments. This is not surprising due to many factors: flow cytometry analyses and immunolabeling reveal different amounts of protein expression, likely due to loss of cells during enzymatic tissue digestion. Moreover, our flow cytometry analysis solely measured GFP and RFP expression in digested tumor tissue without controlling for expression of these markers by non-fibroblast cells. When probing CAF marker expression using multiplex immunolabeling, control markers CD31 and CK8 were used to exclude CAF marker expression attributed to endothelial and epithelial cells.

In PyMT tumors, CAF marker overlaps were not tested in conjunction with additional control markers such as CD31 and CK8 because the expression of each tested markers by epithelial or endothelial cells was measured in separate experiments. Here, only two of the four CAF markers were labeled simultaneously with control markers. The experiments shown in this chapter do not allow conclusions about CAF-specific expression overlaps of all four mesenchymal markers. However, follow-up studies on these tumors (discussed in Chapter 4) included more comprehensive multiplex immunolabeling, permitting the interpretation of CAF-specific expression of the four mesenchymal markers. As discussed in Chapter 4, expression patterns remained consistent between the experiments.

4T1 and PyMT tumors represent different breast cancer subtypes, therefore, it is not surprising that CAF marker expression patterns differ between these two animal models. However, in both models, α SMA and Vimentin were the most highly expressed markers by CAFs, both individually, or together as a pair. The accumulation of α SMA CAFs in growing PyMT tumors is in agreement with a recent study^{87,88} and supports Dvorak's notion of a cancer wound.

Potential pitfalls and alternate approaches

The major limitation in this method is the limited number of markers that can be measured simultaneously. Flow cytometry allows detection of up to 18 markers simultaneously and would provide a more complex picture of overlap in expression of different markers as an alternative approach. However, tissue digestion might bias the analysis towards more viable populations that survive harsh enzymatic digestion processes⁹³. Yet, another potential future approach might be imaging mass cytometry, which allows for detection of a multitude of different markers without losing cell populations or any spatial information. In future studies we aim to analyze spatial distribution of CAF marker expression as previously shown with TSA-based multiplex immunolabeling⁸⁴ to further take advantage of this immunolabeling approach. Moreover, mammary fat pads might not present the best control tissues and future analysis will be

investigating the glandular and surrounding stromal regions of tumors of smaller volumes as additional controls for comparison.

ECM proteins are secreted proteins that are also often used as markers for CAFs and should be included in our analyses. However, staining for these would fail to identify the cells secreting the respective protein. Combining TSA with in situ hybridization may circumvent this limitation. We have tested a Collagen I in situ probe on tumor tissues from both PyMT mice as well as orthotopic 4T1 tumors with success (data not shown). Integration of in situ hybridization in TSA panels is a potential possibility⁹⁴, which would allow the detection of ECM mRNA levels together with the protein expression of additional markers.

Future directions

Now that we have identified different CAF subsets with multiplex staining, we want to investigate their spatial distribution within the tumor and in relation to each other and the other cells in the tumor microenvironment. Moreover, we are interested in probing each identified CAF population for additional markers. α SMA is a very ubiquitous CAF marker and previous studies had found α SMA expression in nearly all CAF subsets identified in the respective study^{87,88,91}. While we detected CAFs co-expressing α SMA together with other markers, the majority of α SMA⁺ CAFs were single positive in the PyMT model, and ~20% of all α SMA⁺ CAFs were single positive in the 4T1 model, suggesting a predominantly single-positive population. Future studies are needed to test how previously reported CAF subtypes fall into the α SMA⁺ populations we have discovered. Newly developed cytof or cytof imaging technologies can be used to test whether the identified CAF subsets co-express other previously reported mesenchymal markers. Moreover, human samples can be probed using single-cell RNAseq or cytof imaging in order to draw parallels between fibroblasts in human tissues and animal models.

Lastly, while it is critical to phenotypically distinguish different CAF types, it is even more important to test the functions of the identified CAF types during tumor progression. Correlative

studies, or in vitro co-culture studies as shown previously may be insufficient to decipher the biological relevance of the identified CAF types.

CHAPTER 4

DISTINCT FIBROBLAST SUBTYPES EXHIBIT DIFFERENT FUNCTIONS IN MAMMARY CARCINOMA

This work has been done with the help and collaboration of Drs. Hikaru Sugimoto, Valerie LeBleu, Sara Lovisa, Elena Rodrigues Blanco, Ehsan Ehsanipour, Pedro Correa de Sampaio, Julianne Carstens and Joyce Tse O'Connell. Some of the data shown in this chapter was generated by using tissues from previously described experiments by Joyce Tse O'Connell⁹⁵ and Sara Lovisa and is shown with their permission. Such instances are indicated in figure legends.

Parts of the work in this chapter has been published previously and is taken verbatim from the publication:

Becker, L. M.* , O'Connell, J. T.* , Vo, A. P., Cain, M. P., Tampe, D., Bizarro, L., Sugimoto, H., McGow, A. K., Asara, J. M., Lovisa, S., McAndrews, K. M., Zielinski, R., Lorenzi, P. L., Zeisberg, M., Raza, S., LeBleu, V. S., and Kalluri, R. **Epigenetic Reprogramming of Cancer Associated Fibroblasts Deregulates Glucose Metabolism and Facilitates Progression of Breast Cancer**. Cell Reports, 31(9), 107701. <https://doi.org/10.1016/j.celrep.2020.107701>

Summary

Reports of CAFs' roles in the tumor microenvironment are often inconsistent in the literature. This may be due to the paucity of well-established molecular markers that can reliably and consistently delineate CAF subpopulations, as well as the lack of mouse models that allow for definitive functional analysis of these cells. Following our identification of mesenchymal marker expression patterns in mammary tumors in Chapter 3, we probed the functions of three distinct CAF subtypes, namely α SMA⁺, FAP⁺ and PDGFR β ⁺ CAFs, using genetically engineered mouse models that enable the specific depletion of respective CAF populations in mammary carcinoma. α SMA⁺ CAF depletion led to a decrease in mammary tumor growth accompanied by several changes in the tumor microenvironment, such as reduced angiogenesis and increased hypoxia, differential mesenchymal marker expression, changes in immune cell composition, as well as downregulation of overall tumor metabolism. Depletion of FAP⁺ CAFs had no effect on mammary tumor growth or metastasis, but tumor immune response was distinctly modulated in FAP⁺ CAF-depleted tumors. While not included in the original TSA analysis in Chapter 3, PDGFR β is another commonly used CAF marker that, similar to α SMA, labels tumor pericytes. Depletion of PDGFR β ⁺ CAFs moderately decreased primary tumor growth and metastasis in one of the tumor models tested. Changes in tumor immunity in PDGFR β ⁺ CAFs depleted tumors were distinct from those in tumors deprived of α SMA⁺ or FAP⁺ CAFs. In summary, our data suggests α SMA, FAP, and PDGFR β are labeling and defining CAF subtypes that are functionally distinct.

Introduction

Numerous studies have described the interactions between CAFs and tumor cells, with most studies featuring the tumor-promoting aspect of CAF functions. In the early 2000s, research groups demonstrated breast cancer growth promoting functions of CAFs in co-culture

experiments^{96–98}. Later studies had identified signaling molecules involved in the promotion of tumor growth such as fibroblast-secreted TGF β that induces EMT-mediated migration of cancer cells⁵⁸.

CAFs have traditionally been studied in the *in vivo* setting using so-called admix experiments. These experiments showed co-injection of breast cancer cell lines with CAFs in mice result in enhanced tumor formation and growth compared to co-injection of cancer cells with normal fibroblasts or by themselves. Similar experiments, performed by several research groups in varying experimental settings, had provided different conclusions regarding the underlying mechanisms of the observed phenotypes. Orimo et al have shown CAFs promote tumor growth through enhanced angiogenesis via SDF1 secretion¹¹. Tyan et al. , on the other hand, demonstrated CAFs to enhance breast cancer growth via HGF signaling upon stimulation by cancer cells²⁹. In these admix experiments, the injection of heterogeneous fibroblast populations likely confounded the interpretation of the results.

Once the concept of heterogeneity was established, subsequent efforts were shifted towards correlating distinct CAF functions with specific identifiers of CAFs. For example, a chemo-resistant CD10⁺GPR77⁺ CAF subset was identified in breast cancers⁹⁹ via microarray analysis. These CAFs create a cancer stem-cell niche by secreting IL6 and IL8 in order to maintain quiescent and chemo-resistant cancer cells, thereby promoting a pro-tumor effect. Costa et al. identified four mammary carcinoma subsets, each with a distinct expression pattern of CD29, FAP, α SMA, FSP1, CAV1, and PDGFR β measured by flow cytometry. Two of these identified subsets have been shown to promote an immune-suppressive environment; one through attracting and activating T regulatory cells, and the other one through suppression of T effector cells⁹¹. While these studies have significantly advanced the field of CAF heterogeneity, they relied on in vitro assays to test functions of the identified CAF subsets. As CAF phenotypes and characteristics can change in 2D culture conditions, these analyses harbor inherent limitations¹⁰⁰.

One strategy to assess the functions of specific CAF subtypes in vivo is to target CAFs with specific marker expression in animal models of cancer. To this end, a DNA vaccine against FAP has been shown to reduce tumor growth and metastasis in combination with chemotherapy in the 4T1 mammary carcinoma model through the remodeling of the immune microenvironment¹⁰¹. CAR-T cells targeting FAP have also been developed. Their effects on mammary tumor growth, however, remain to be investigated as studies produced ambiguous results^{102,103}. An additional strategy is the utilization of transgenic mice that allow specific targeting of cells based on marker expression. Our laboratory has established animal models in which the viral thymidine kinase (vTK) transgene is engineered to be driven by specific promoters of fibroblast markers. In these mice, continuous administration of ganciclovir (GCV) prevents the accumulation of proliferating CAFs that express the respective marker, which would otherwise happen during tumorigenesis, and thus results in specific depletion of the respective CAFs. With this approach, we have previously tested the functions of FSP1⁺ CAFs in mammary carcinoma. We demonstrated that FSP1⁺ CAFs had no substantial effect on primary tumor progression, but facilitated metastatic growth in lungs through the secretion of VEGFA and Tenascin C⁵⁷.

Only a handful of functionally and phenotypically distinct CAF subtypes have been identified to date in breast cancer. Following our phenotypical identification of specific CAF subsets in our animal models of mammary carcinoma in Chapter 3, we aimed to characterize their specific roles in mammary tumorigenesis in this Chapter. We focused our efforts to those CAFs characterized by their expression of α SMA, FAP and PDGFR β , respectively. Upregulation of α SMA in fibroblasts is associated with their activation into myofibroblasts in wound healing and fibrosis⁶⁵. Due to close similarities between myofibroblasts in wound healing and CAFs, and the abundance of α SMA expression in tumor stroma, α SMA has been the most commonly used CAF marker in the literature encompassing all cancer types and is often used to identify CAFs in mechanistic studies^{10,104–106}. The population size and positive dynamics of α SMA⁺ CAFs

investigated in Chapter 3 suggested a functional role of these fibroblasts in tumor progression. α SMA expression in patient tissues has been shown to correlate with both detrimental and beneficial clinical outcome depending on the study design and breast cancer subtype^{90,107}, demonstrating the need to further clarify their specific functions in tumorigenesis.

FAP is a CAF marker also associated with the activation state of CAFs. In breast cancer stroma, FAP expression has been correlated with favorable prognosis^{48,108}. Functional studies of FAP⁺ CAFs have suggested immunoregulatory functions for this CAF subset^{61,109}; but targeting of these cells in breast cancer animal models led to inconclusive results^{102,103}. Even though we had only observed a very small CAF population expressing FAP in our animal models, we nevertheless sought to characterize the potential roles of this population in breast cancer progression.

Lastly, we sought to study the roles of PDGFR β -expressing CAFs. While we did not use this marker in our previous analysis described in Chapter 3, it is often used to identify CAFs^{10,65,91}. We have previously tested specific functions of pericytes during mammary tumorigenesis using NG2 and PDGFR β as putative pericyte markers. Here, mammary carcinoma animal models were utilized in which the vTK promoter drove NG2 and PDGFR β expression. Although a significant reduction of pericytes was observed when PDGFR β expressing cells were targeted, the impact of the inadvertent depletion of PDGFR β ⁺ CAFs has not been addressed directly. Since α SMA is a well-established marker for vascular smooth muscle cells and pericytes similar to PDGFR β , we hypothesized that a direct comparison of cells expressing either α SMA, or PDGFR β could help to decipher whether these markers are labeling functionally identical or distinct CAF as well as pericyte populations. While some studies have shown a substantial overlap in expression patterns between the two markers⁹², others have suggested the expression patterns of these two markers varying within different CAF subsets⁹¹. This evoked the idea that targeting cells expressing α SMA vs. PDGFR β ⁺ cells in the context of mammary carcinoma might have different effects on tumor

progression and differentially impacts the tumor microenvironment. Previous studies have suggested an involvement of α SMA⁺ CAFs as well as FAP⁺ CAFs in regulating the immune cells. α SMA and FAP showed distinct expression patterns in our animal models, suggesting that these markers label distinct CAF subsets. *Taken this knowledge into consideration, we hypothesized that different subpopulation of CAFs, as defined by the expression of either α SMA, FAP or PDGFR β , differ in their interactions with different immune cell populations in the tumor microenvironment, as well as in their ability to restrict or promote breast cancer progression.*

Functions of α SMA⁺ CAFs in mammary carcinoma

Growth kinetics and metastatic potential of orthotopically implanted 4T1 cells were evaluated in α SMA-vTK transgenic mice^{64,77}. Depletion of α SMA⁺ CAFs via GCV administration was initiated when tumors were firmly established and large (~500mm³), and pressure to limit CAFs

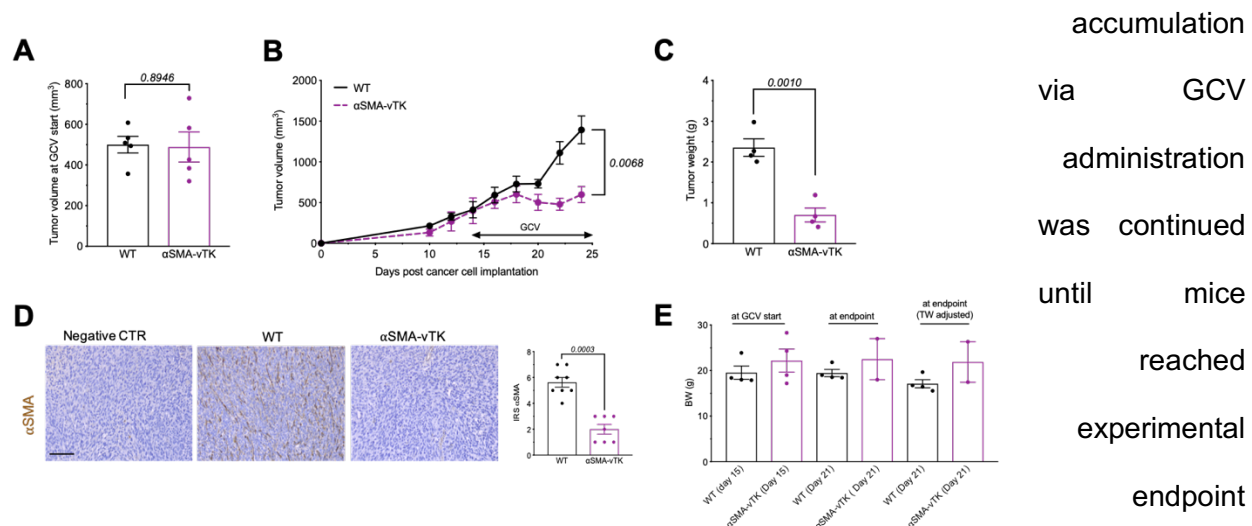


Figure 10 α SMA⁺ CAFs promote primary mammary carcinoma growth

A. Tumor volume at Day 14 after cancer cell injection (GCV start). **B.** Tumor growth kinetics of orthotopically implanted 4T1 cells in WT and α SMA-vTK mice. GCV was started at day 14 post cancer cell implantation. **C.** Tumor weight of tumors from A. at endpoint. **D.** α SMA immunolabeling of WT and α SMA-vTK tumors with quantification. Negative control was incubated with only secondary antibody. Immunolabeling was performed on tumors from an experiment previously described in ¹⁹⁴ (replicate of this experiment using the same WT and α SMA-vTK mice with the same observations on tumor growth.) Scale bar: 100 μ m. Patricia Philips performed the staining. **E.** Body weight in WT and α SMA-vTK mice at the indicated timepoints. At endpoint, body weight was adjusted by subtracting the tumor weight.

accumulation
via GCV
administration
was continued
until mice
reached
experimental
endpoint
requiring
euthanasia.
Depletion of
 α SMA⁺ CAFs
resulted in a

significant reduction in the primary tumor growth (**Figure 10A-C**), indicating an important role of α SMA⁺ CAFs in primary tumor growth. Reduction in α SMA⁺ CAFs in tumors was confirmed by immunohistochemistry (**Figure 10D**). Of note, this approach does not directly impact cancer cells, which are deprived from expressing the transgene. Body weight was not measurably impacted by the depletion of proliferating α SMA⁺ CAFs (**Figure 10E**). α SMA⁺ CAFs-depletion exacerbated primary tumor hypoxia (Carbonic anhydrase 9, CAIX, **Figure 11A**) and diminished blood (CD31) and lymphatic angiogenesis (Lyve1, **Figure 11B-C**). Pericyte coverage of blood vessels remained

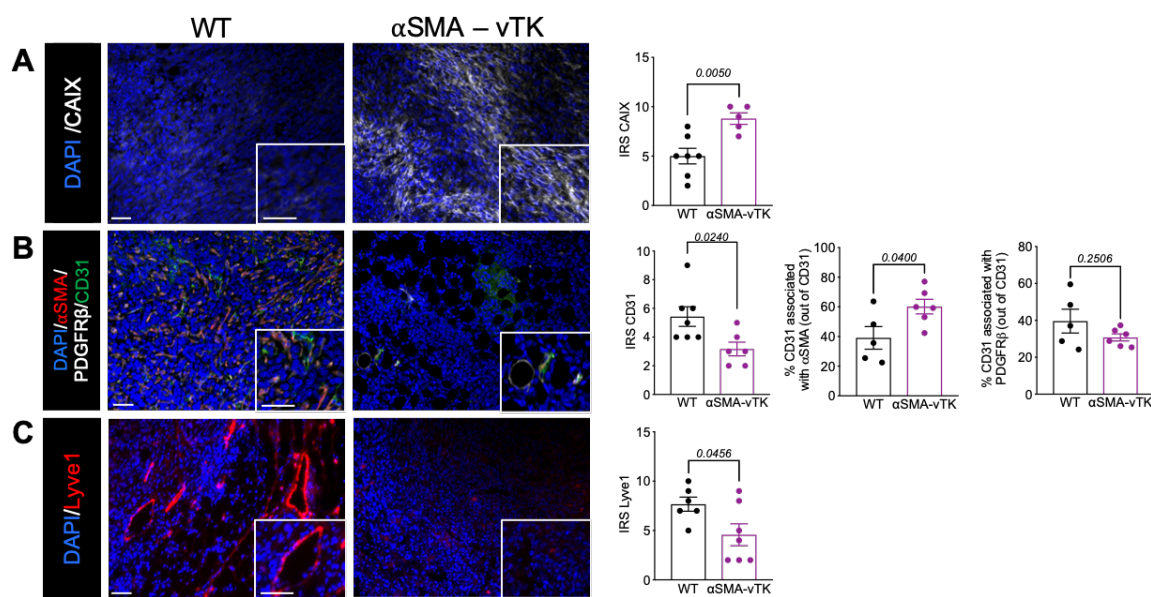


Figure 11 α SMA⁺ CAFs depleted tumors show vascular remodeling

Immunolabeling of WT and α SMA-vTK tumors with **A.** carbonic anhydrase 9 (CAIX), **B.** α SMA, PDGFR β , and CD31 and **C.** Lyve1. Representative images are shown together with quantification.

The immunolabeling experiments in this figure were performed on tumors from an experiment previously described in ⁹⁶. (This experiment is a replicate of the experiment in Figure 10 using the same WT and α SMA-vTK mice with the same observations on tumor growth). All scale bars including zoomed in images: 50 μ m

however unchanged (CD31 associated with PDGFR β , **Figure 11B**). Perivascular α SMA expression increased (**Figure 11B**), indicating that the depletion strategy primarily impacts proliferating CAFs rather than, possibly more quiescent, perivascular cells, and that the impact on tumor angiogenesis is an indirect consequence of α SMA⁺ CAFs depletion.

Despite significant decrease in primary tumor growth upon α SMA⁺ CAFs depletion, lung metastases in the invasive breast cancer models studied were similar (**Figure 12A**). Metastatic

disease was rarely seen at the time of GCV initiation in the 4T1 orthotopic model (at tumor burden of 500mm³, WT GCV start **Figure 12A**). To test whether α SMA⁺ CAFs play a role in lung colonization as previously observed for FSP1⁺ CAFs⁵⁷, 4T1 cells were intravenously (i.v.) injected into α SMA-vTK and WT control mice. α SMA depletion caused by GCV administration did not impact lung tumor growth (**Figure 12B**).

These results support that α SMA⁺ CAFs primarily play a role in suppressing primary tumor growth.

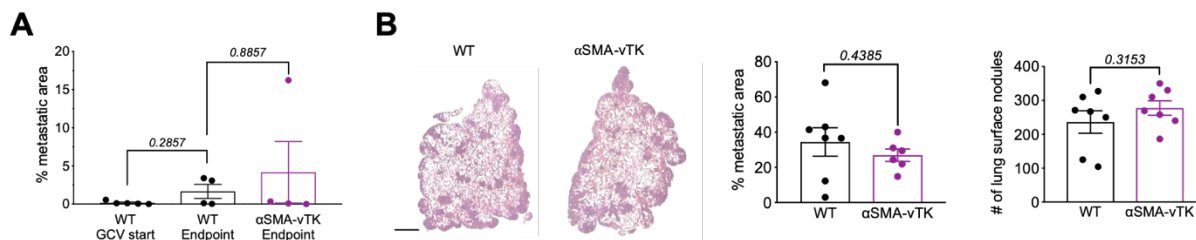


Figure 12 α SMA⁺ CAFs depletion can enhance invasion and intravasation and has no effect on lung metastatic outgrowth.

A. Quantification of metastatic area in WT mice at start of GCV, and in WT and α SMA-vTK mice at experimental endpoint. **B.** 4T1 cells were injected intravenously into WT and α SMA-vTK mice. GCV was started 2 days prior to cancer cell injection and continued until sacrifice. Representative pictures of lungs together with quantification of lung surface nodules and metastatic area are shown. Scale bar: 2mm.

Next, these findings were recapitulated in the MMTV-PyMT (PyMT) mammary carcinoma transgenic mouse model^{75,76}. PyMT mice were crossed to α SMA-vTK mice (α SMA-vTK;PyMT) and GCV treatment was initiated once the combined tumor burden reached 500mm³ to allow for the accumulation of α SMA⁺ CAFs. Depletion of α SMA⁺ cells in PyMT mice dramatically inhibited primary tumor growth (**Figure 13A**) but had no significant effect on lung metastasis (**Figure 13B**), similar to our observations in the 4T1 model. To analyze potential changes in the abundance of different CAF subsets when α SMA⁺ CAFs were depleted, we stained these tumors for α SMA, Vimentin, FAP, FSP1, Ki67, CK8, CD31 and DAPI simultaneously employing TSA-based multiplex staining (**Figure 13D**). CAFs were defined as CK8⁻CD31⁻ cells; and immune cells were excluded based on shape and size (using Inform analysis program, see methods). Interestingly, the percentage of fibroblasts (CK8⁻CD31⁻) out of all cells in the tumor was increased in α SMA-

depleted tumors (**Figure 13C**). As expected, $\alpha\text{SMA}^{\text{S}+}$ (including $\alpha\text{SMA}^+\text{Ki67}^+$) CAFs were significantly reduced in $\alpha\text{SMA-vTK}$ mice, confirming the depletion of proliferating αSMA^+ CAFs (**Figure 13E**). FSP1-expressing CAFs were unaffected (**Figure 13F**), and FAP⁺ CAFs decreased in αSMA^+ CAFs depleted tumors. Moreover, Vimentin⁺ CAFs increased in tumors of $\alpha\text{SMA-vTK}$ mice (**Figure 13D**, compare total Vimentin numbers; and **Figure 13H**). We could not observe an increase in proliferating (Ki67⁺) Vimentin⁺ CAFs (**Figure 13I**), suggesting that the Vimentin⁺ population did not increase via proliferation. The overall abundance of αSMA -expressing CAFs did not decrease (**Figure 13D**, compare αSMA total numbers) despite the dramatic reduction in $\alpha\text{SMA}^{\text{S}+}$ and $\alpha\text{SMA}^+\text{Ki67}^+$ cells. We therefore hypothesized that αSMA^+ CAFs may have begun to express additional markers in $\alpha\text{SMA-vTK}$ mice. Indeed, there was a marked increase in $\alpha\text{SMA}^+\text{Vim}^+$ CAFs in these mice (**Figure 13J**). This, in turn could contribute to the overall increase in Vimentin expression.

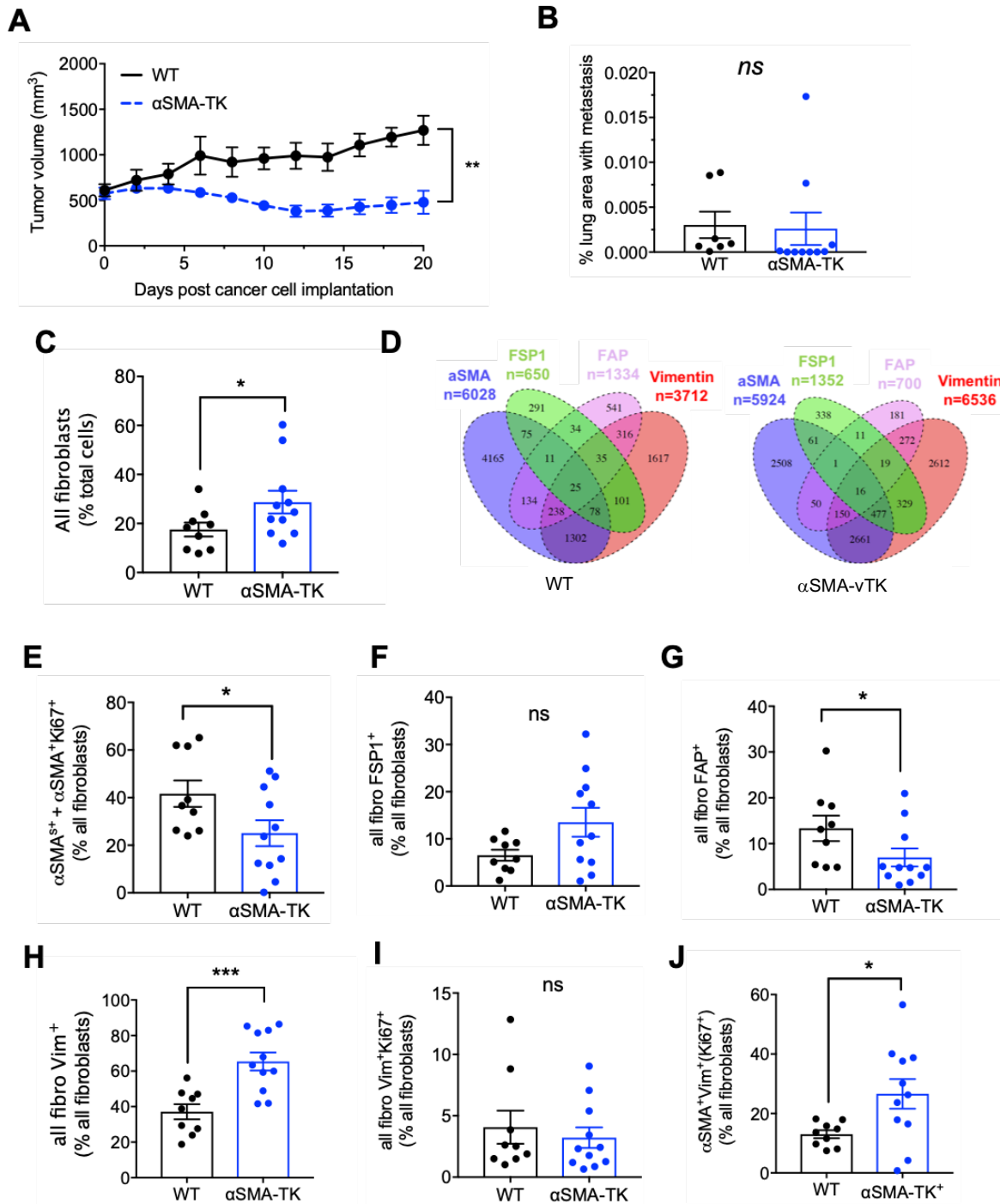


Figure 13 αSMA⁺ CAFs depletion in PyMT tumors reduce tumor growth and change CAF marker expression patterns. **A.** Tumor growth of WT;PyMT and αSMA-vTK;PyMT tumors from GCV start (~500mm³). **B.** Metastatic burden in mice from **A.** **C.** CK8-CD31⁻ cells (fibroblasts) in WT;PyMT and αSMA-vTK;PyMT tumors. **D.** Venn diagrams of expression overlaps between αSMA, Vimentin, FAP and FSP1 in WT;PyMT and αSMA-vTK;PyMT tumors (Numbers in diagram present amount of cells in any 10,000 CK8-CD31⁻ cells). **E-J.** Abundance of different CAF subsets in WT;PyMT and αSMA-vTK;PyMT tumors.

The ablation of α SMA expressing cancer cells could potentially contribute to the lack of tumor growth in α SMA-vTK; PyMT mice. To exclude this possibility, α SMA-vTK mice were implanted with fragments of tumors from parental PyMT mice (no vTK transgene, **Figure 14A**). The histology of transplanted tumors was similar to the original PyMT tumors (**Figure 14B**).

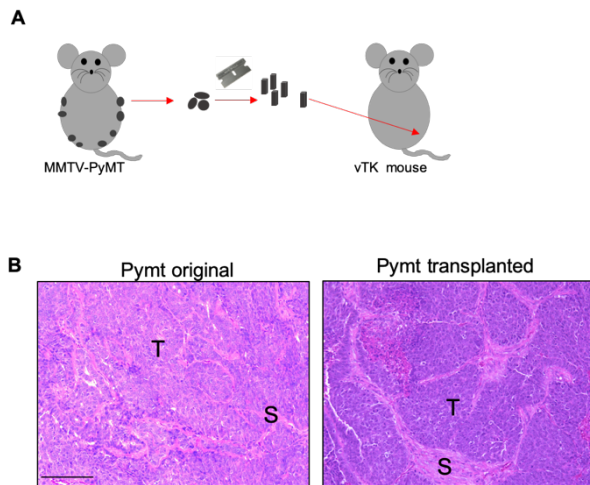


Figure 14 PyMT transplantation model

A. Schematic of PyMT transplantation model. Tumors were harvested from PyMT mice, cut in small fragments and implanted in recipient WT and vTK mice. See methods for more information. **B.** Representative picture of H&E stained original PyMT and transplanted PyMT tumors. Scale bar: 50 μ m.

The transplanted tumors displayed similar growth stagnation in the α SMA-vTK mice, suggesting that the depletion of host α SMA⁺ CAFs was the main factor in the delayed tumor growth (Error! Reference source not found.**A**). α SMA depletion was confirmed with IHC, as the tumors were too necrotic for reliable analysis of multiplex staining (Error! Reference source not found.**C**, IHC data not shown). Similar to the transgenic model, lung metastatic burden remained unchanged (Error! Reference source not found.**B**). Given the significantly smaller volume of α SMA-vTK⁺ tumors in both models, this suggests increased metastatic capability of the small

α SMA-depleted tumors. Further investigations of the consequences of α SMA⁺ CAF depletion showed that α SMA⁺ CAF-depleted tumors were extremely necrotic (Error! Reference source not found.**C**), with reduced micro-vessel (CD31) and pericyte (PDGFR β) density (Error! Reference source not found.**E, F**). In α SMA-vTK and WT tumors, 100% and 95% of vessels, respectively, were covered by pericytes (Error! Reference source not found.**G**). Thus, α SMA-depleted tumors displayed reduced angiogenesis and vascular normalization. Reduced angiogenesis may contribute to the slower primary tumor growth and necrosis, but normalized vessels become better conduits for metastasis. Assessment of hypoxia using CAIX (Error! Reference source not found.**D**) and Hypoxyprobe (not shown) revealed large areas of hypoxia in WT as well as in α SMA-depleted tumors. The proliferative activity of the tumor cells was unchanged by depletion of α SMA⁺ CAFs (Error! Reference source not found.**H**). Cancer cells are still proliferating at the same rates in the small α SMA-depleted tumors, likely because decreased angiogenesis causes death and necrosis, rather than the lack of α SMA⁺ CAFs halting proliferation.

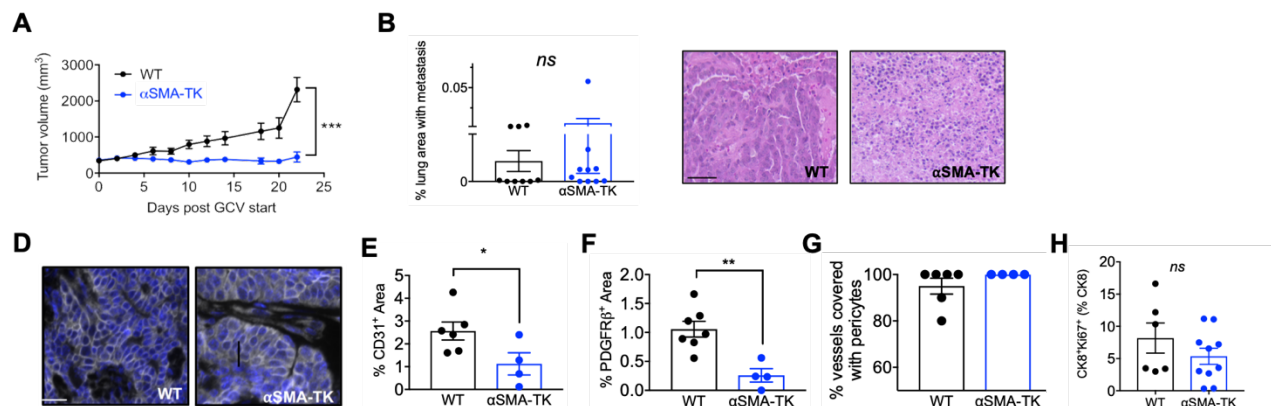


Figure 15 α SMA⁺ CAF depletion in transplanted PyMT tumors leads to growth stagnation and vascular remodeling.

A. Tumor growth in WT and α SMA-vTK mice implanted with PyMT tumors from GCV start. **B.** Metastatic burden in mice from **(A)**. Representative images of H&E staining **(C)** and CAIX immunolabeling **(D)** in tumors from **(A)**. CD31 **(E)** and PDGFR β **(F)** expression, as well as quantification of pericyte coverage of vessels (CD31⁺PDGFR β ⁺, **G**) in tumors from **(A)**. **H.** Quantification of CK8⁺Ki67⁺ proliferating cancer cells in tumors from **(A)**. Data presented as mean \pm s.e.m., individual dots in graphs indicate individual mice. Unpaired t test (with Welch correction when appropriate) or Mann-Whitney test were used, depending on normality distribution of data. * $p < 0.05$, ** $p < 0.01$, *** $p < 0.001$. ns, not significant. Scale bars: 50 μ m.

CAFs have been reported to interact with different immune cell populations and thereby shaping the immune microenvironment in order to either facilitate or suppress tumorigenesis^{60,61,91}. In order to measure the impact of α SMA⁺ CAFs depletion on immune cells, tumors were dissociated after harvest and the single cell suspensions were probed with different panels of immune cell markers (see methods). We observed downregulation of myeloid cells, and increase of B-cells, with no changes in T-cells and NK cells (**Figure 16A**). When investigating further subsets of those immune cells, the most interesting changes were observed within myeloid cells. In α SMA⁺ CAFs-depleted tumors, relative abundance within the myeloid cell department of Gr1⁻ cells was increased, which present monocytes or macrophages¹¹⁰ (**Figure 16B**). PD-L1 expression on neutrophils (CD11b⁺Ly6G⁺) and on CD11b⁺Gr1⁻ macrophages was significantly upregulated. The increase in PDL1 expression on CD11b⁺Gr1⁻ macrophages suggests M2 conversion¹¹¹ (**Figure 16D**). Increased infiltrates of PD-L1⁺ tumor associated M2 macrophages (or tumor-associated macrophages, TAMs) could explain persistent metastasis in α SMA-vTK mice despite the drastically reduced primary tumors¹¹². PD-L1/PD1 signaling supports macrophages' proliferation and immunosuppressive functions. Both can be reversed by anti-PD-L1/PD1 therapy¹¹². PD1 is also a marker of immunosuppressive, tumor-promoting macrophages¹¹². In α SMA⁺ CAFs-depleted tumors, PD1 was increased in all myeloid cells, including macrophages (**Figure 16E**). We therefore hypothesized that PDL1⁺ and PD1⁺ TAMs promote metastasis upon α SMA⁺ CAFs depletion. To test this hypothesis, we treated α SMA-vTK and WT mice transplanted with PyMT tumors with GCV + anti-PDL1 (or control IgG) antibody (200ug / mouse, **Figure 16F**). Analysis of this experiment is still ongoing. As expected, we could not observe any impact on primary tumor growth in WT or α SMA-vTK mice that received anti-

PDL1 (**Figure 16G**). However, we are currently evaluating the metastatic burden in the lungs of mice in different treatment groups.

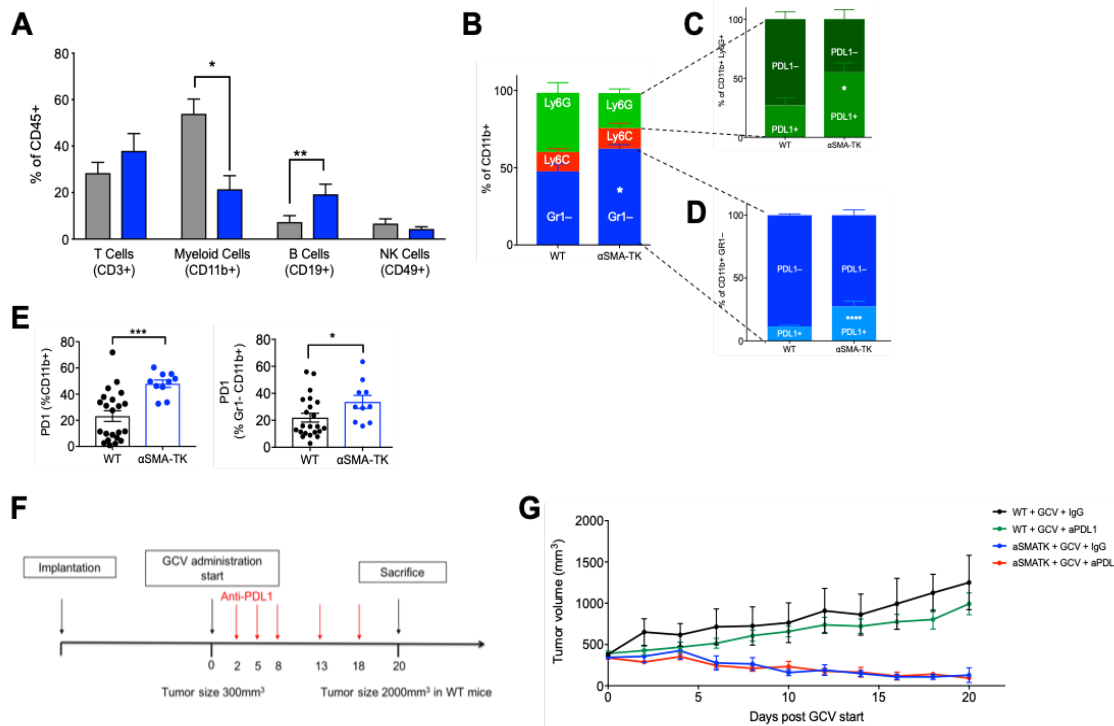


Figure 16 α SMA⁺ CAFs depleted tumors show increased tumor associated macrophage infiltration.

A. % of CD3⁺, CD11b⁺, CD19⁺ and CD49b⁺ cells out of all CD45⁺ lymphocytes in WT (grey) and α SMA-vTK (blue) tumors. **B.** relative expression of Ly6G and Ly6C in CD11b⁺ cells in WT and α SMA-vTK tumors. **C.** relative expression of PDL1 in CD11b⁺Ly6G cells. **D.** relative expression of PDL1 in CD11b⁺Gr1⁻ cells. **E.** relative expression of PD1 in CD11b⁺ cells and CD11b⁺Gr1⁻ cells. **F.** Experimental setup for PDL1 and GCV treatment in WT and α SMA-vTK mice implanted with PyMT tumors. **G.** Tumor growth from GCV start in PDL1/GCV treated WT and α SMA-vTK mice implanted with PyMT tumors. Data presented as mean \pm s.e.m., individual dots in graphs indicate individual mice. Unpaired t test (with Welch correction when appropriate) or Mann-Whitney test were used, depending on normality distribution of data. *p < 0.05, **p < 0.01, ***p < 0.001, ****p < 0.0001.

In summary, we showed that α SMA⁺ CAFs are facilitating primary tumor growth, but do not impact metastasis significantly using three independent animal models of mammary carcinoma. Depletion of α SMA⁺ CAFs led to remodeling of the tumor microenvironment as demonstrated by decreased angiogenesis, changes in different immune cells and new distribution of CAF marker expression patterns. Moreover, α SMA⁺ CAFs seem to metabolically support tumor growth, as overall tumor metabolism was downregulated upon depletion of this CAF subset.

Functions of FAP⁺ CAFs in mammary carcinoma

Although FAP⁺ CAFs represented one of the least abundant CAF subsets in our model,

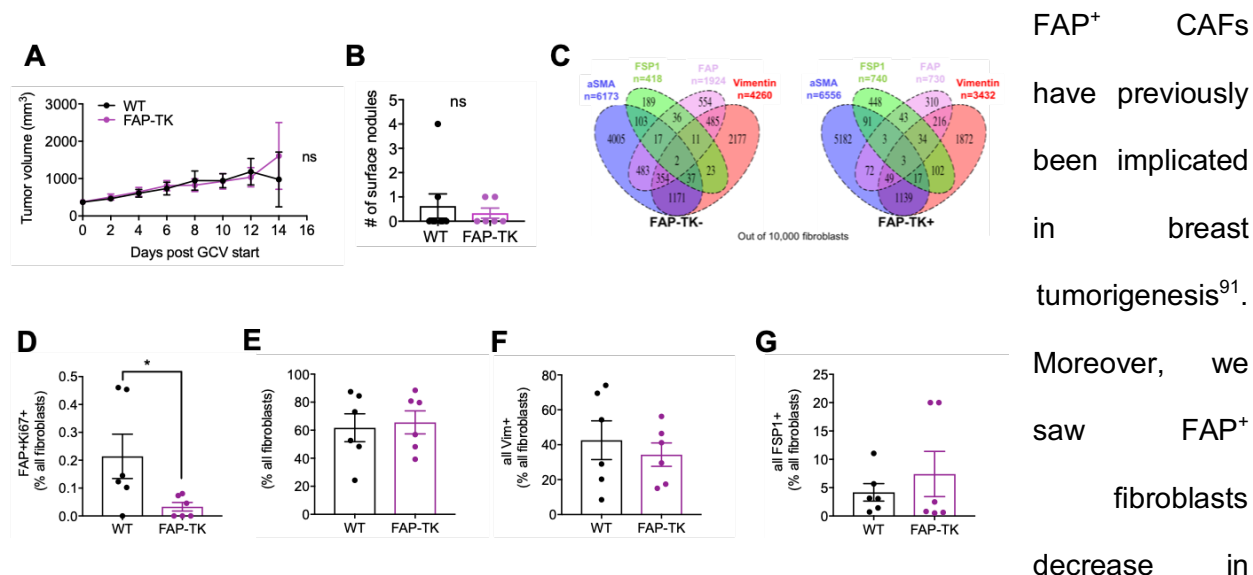


Figure 17 Depletion of FAP⁺ CAFs does not impact primary tumor growth

A. Tumor growth from GCV treatment start in WT and FAP-vTK mice implanted with PyMT tumors. **B.** Lung surface nodules in mice from **(A)**. **C.** Venn diagrams of expression overlaps between α SMA, Vimentin, FAP and FSP1 in implanted tumors of WT and FAP-vTK mice (Numbers in diagram present amount of cells in any 10,000 CK8⁺CD31⁻ cells). **D-G** Abundance of different CAF subsets in implanted tumors of WT and FAP-vTK mice.

whether α SMA⁺FAP⁺ CAFs were targeted in α SMA-vTK mice, we postulated that FAP⁺ CAFs depletion should result in decrease in α SMA⁺ CAFs with possible similar phenotypes. We therefore implanted tumor fragments from PyMT mice into the right mammary fat pad of recipient FAP-vTK mice (generated in our laboratory). Tumor growth was comparable between FAP-vTK⁺ and WT mice upon GCV treatment (**Figure 17A**). Moreover, we did not observe any changes in the number of lung surface nodules (**Figure 17B**). To confirm the depletion of FAP⁺ CAFs and to investigate the expression of the remaining CAF markers, we performed TSA multiplex staining as described before. Although overall FAP-expression did not decrease amongst all CAFs (**Figure 17C**), the proliferating (Ki67⁺) FAP⁺ CAFs decreased significantly as expected in this model (**Figure 17D**). We did not detect any changes in any of other CAF subset (**Figure 17C, E-G**). α SMA⁺ CAFs were thus not affected by depletion of FAP⁺ CAFs.

FAP⁺ CAFs have previously been implicated in breast tumorigenesis⁹¹. Moreover, we saw FAP⁺ fibroblasts decrease in α SMA-vTK;PyMT mice. To investigate

Previous studies suggested FAP⁺ CAFs modulate tumor immune response^{91,113}. We therefore sought to analyze changes in immune cell populations in FAP⁺ CAFs-depleted tumors. Depletion of FAP⁺ CAFs did not change abundance of T-cells, B-cells, myeloid cells or NK cells in the tumors (**Figure 18A**). However, when we tested the abundance of subsets of these immune cell types, we detected a decrease in Ly6C expression, accompanied by an increase in the Gr1⁻ myeloid cell population, similar to α SMA-depleted tumors (**Figure 18B-C**).

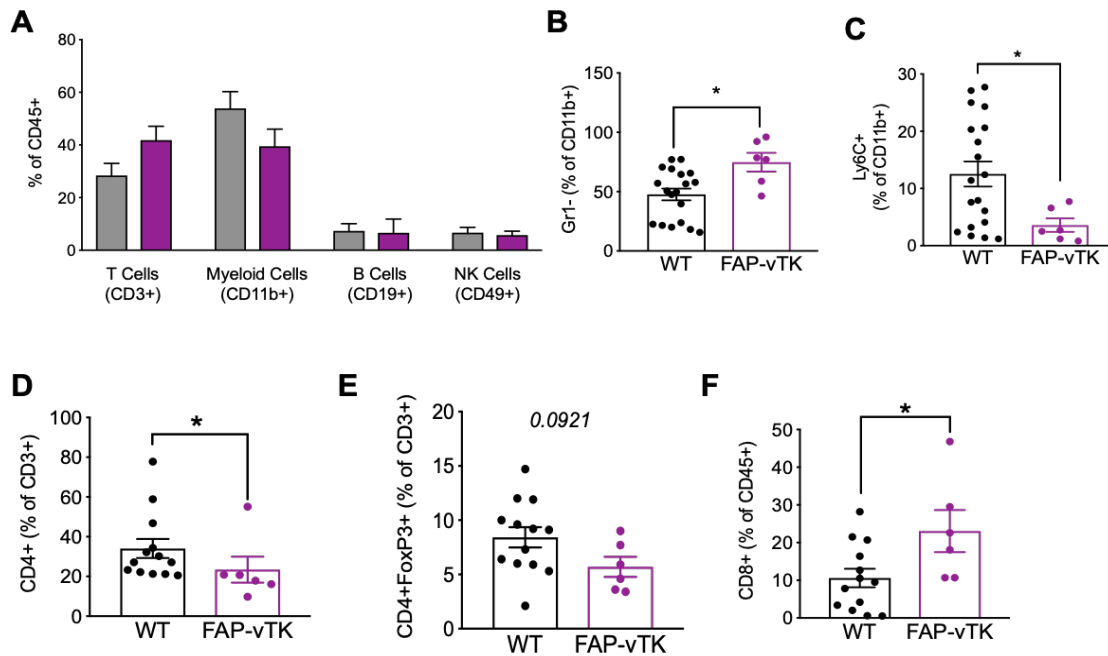


Figure 18 FAP⁺ CAFs depleted tumors exhibit different immune cell composition.

A. % of CD3⁺, CD11b⁺, CD19⁺ and CD49b⁺ cells out of all CD45⁺ lymphocytes in WT (grey) and FAP-vTK (purple) tumors. **B-F.** Relative abundance the indicated immune cell subsets in WT and FAP-vTK tumors.

In addition to changes in the myeloid department, CD4⁺ T cells decreased in FAP-TK⁺ tumors compared to wildtype tumors (**Figure 18D**). Within the CD4 T cells, regulatory T cells (Foxp3⁺) were slightly downregulated. While we could not detect any significant change in CD8 T cells when comparing CD8 expression in the CD3⁺ T-cell population, we did detect a significant increase in CD3⁺CD8⁺ cells out of total lymphocytes in the tumor (CD45⁺). Therefore, while not

effecting tumor growth and metastasis significantly, FAP⁺ CAF depletion caused changes in immune cell populations.

Functions of PDGFR β ⁺ CAFs in mammary carcinoma

The observed reduction in PDGFR β ⁺ cells in α SMA-TK tumors, prompted us to investigate their functional role. Similar to α SMA, PDGFR β is expressed by CAFs, as well as intratumoral pericytes¹¹⁴. Interestingly, overall PDGFR β expression was reduced in stroma of α SMA-vTK tumors, alongside CD31 reduction. However, CD31-associated PDGFR β expression (pericyte PDGFR β expression) remained unchanged, which might suggest that PDGFR β ⁺ CAFs were reduced rather than PDGFR β ⁺ pericytes in the α SMA⁺ CAFs-depleted tumors. Studies from our lab and others have shown the important prognostic and functional roles of PDGFR β ⁺ cells in the breast tumor microenvironment^{78,114–116}. To directly compare PDGFR β ⁺ cells to α SMA⁺ cells in the breast tumor microenvironment, we tested their functions in the same experimental setting and utilized PDGFR β -vTK (P β -vTK) mice; either crossed to PyMT mice, or implanted with PyMT tumors. Depletion of PDGFR β ⁺ cells moderately reduced primary tumor growth and metastasis in the transgenic tumor model (**Figure 19A-C**), but did not impact tumor growth of implanted tumors (**Figure 19D-E**). Furthermore, no changes in microvessel coverage were detected (**Figure 19F-G**). α SMA, as well as PDGFR β expression in the stroma was moderately reduced (**Figure 19F, H-I**). Necrotic tissue within these tumors potentially caused autofluorescence. We therefore probed for PDGFR β expression using immunohistochemistry and observed a strong reduction of PDGFR β expression in PDGFR β -vTK tumors (**Figure 19J**, staining was not quantified). Tumors in the transplanted model showed changes in the immune cell compartment, which were distinct from those described in α SMA⁺ CAFs-depleted tumors.

NK cells were significantly reduced compared to WT controls (**Figure 19K**). In addition, although overall numbers of T cells were similar (data not shown), more T effector cells pertained in tumors from PDGFR β -vTK mice, and T regulatory cells were decreased (**Figure 19L-M**).

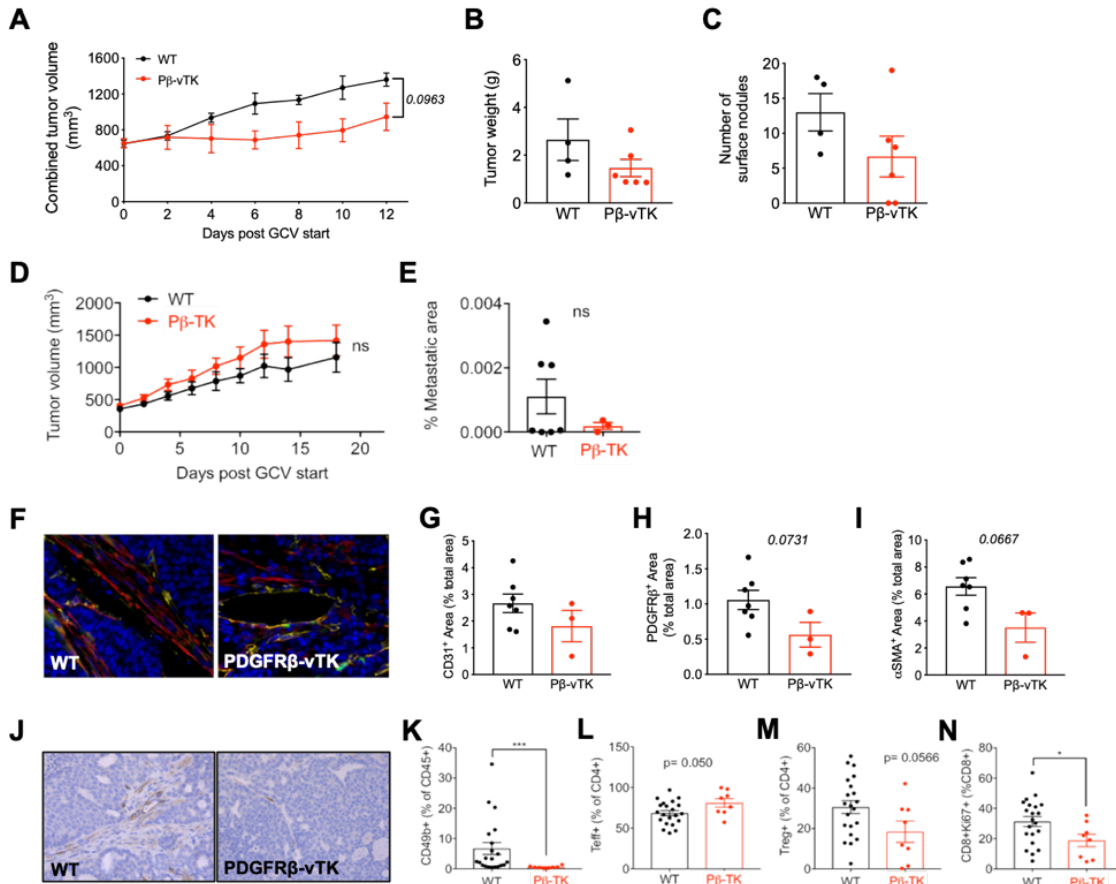


Figure 19 Depletion of PDGFR β ⁺ CAFs impacted tumor immunity

A. Tumor growth from GCV treatment start in WT,PyMT and PDGFR β -vTK, PyMT mice. **B.** Tumor weight of tumors from **(A)**. **C.** Lung surface nodules in mice from **(A)**. **D.** Tumor growth from GCV treatment start in WT and PDGFR β -vTK mice implanted with PyMT tumors. **E.** Metastatic burden in lungs of mice from **(D)**. **F-I.** Immunolabeling for CD31, α SMA and PDGFR β in tumors from **(D)**. Representative image and quantification of individual stains. **J.** Representative images of PDGFR β immunolabeling in tumors from **(D)**. **K-N.** Changes in immune cell subsets in tumors from **(D)**.

Further analysis will determine the activation state of these cells and reveal what additional stimuli are needed to coerce an immunosuppressive tumor microenvironment towards cancer immune surveillance. Of note, we found activated (Ki67⁺) cytotoxic T cells (CD8⁺, **Figure 19N**)

to be decreased in tumors from PDGFR β -vTK mice, which might cause the continued tumor growth in these mice despite increase in T effector cells.

Interpretation of findings

While further analyses will be required to assess the mechanistic roles of α SMA⁺, PDGFR β ⁺, and FAP⁺ CAFs, it is evident that α SMA, FAP and PDGFR β each label functionally distinct CAF subsets in the breast tumor microenvironment. CAFs identified by these markers differentially modify primary tumor growth and the immune microenvironment.

We report a robust reduction in primary tumor growth when α SMA⁺ CAFs were selectively depleted, yet metastasis was unchanged in three distinct mouse models of mammary carcinoma. The similar metastatic burden in α SMA⁺ CAFs-depleted tumor bearing mice compared to the control mice is significant because despite ~50% reduction in primary tumor, metastases were still able to develop unabated, suggesting that cancer cells likely gained metastatic potential or the remaining cancer cells were able to seed the lung at the same rate as the control tumors. We also showed in a lung colonization assay (i.v. injection of cancer cells) that the depletion of α SMA⁺ CAFs did not affect metastatic outgrowth, suggesting a more dominant role for these cells in the primary tumor. This was manifested principally by increased intratumoral hypoxia and suppressed angiogenesis when α SMA⁺ CAFs were depleted.

We can conclude that α SMA⁺ CAFs promote the growth of the primary tumor, potentially through increasing angiogenesis. While a decrease in microvessel coverage was observed upon α SMA⁺ CAFs depletion in all tumor models (data for transgenic tumor model not shown), intratumoral hypoxia was only impacted in the 4T1 mammary carcinoma model. These differences are likely due to the inherent differences between the two tumor models, which represent different breast cancer subtypes, and exhibit different baseline levels of necrosis and hypoxia (see Chapter 3). Interestingly, despite the observed vascular remodeling, α SMA⁺ pericytes were not targeted

in our animal models, which stands in contrast to previous studies targeting PDGFR β ⁺ pericytes using the vTK system. This might indicate PDGFR β ⁺ labels more proliferative pericytes and is either expressed at higher levels in pericytes than α SMA, or labels a separate pericyte population. Our lab previously reported significant overlap between α SMA and PDGFR β expression by CAFs in 4T1 mammary carcinomas. This is in line with our findings of reduction in PDGFR β expression upon α SMA⁺ CAFs depletion. Similarly, α SMA expression was reduced in PDGFR β -vTK mice in our hands. Nevertheless, targeting α SMA⁺ CAFs and PDGFR β ⁺ CAFs had distinct effects on primary tumor growth, metastasis and the immune cell response in tumors, demonstrating that despite expression overlaps, distinct subsets were targeted.

Out of all immune cell populations that were analyzed (see methods for list of markers used in different flow cytometry panels), only a few changes in myeloid cell populations alongside reduction in B cells were observed upon α SMA⁺ CAFs depletion. This was surprising considering several studies had suggested that CAFs can impact immune system functions. As α SMA was identifying such large fibroblast populations in breast tumors, we expected to see an effect on T cell populations as previously reported⁹¹. However, most functional studies investigating CAF-immune cell interactions have been in vitro co-culture studies that do not capture the complexity of interactions between all cells in the tumor microenvironment entirely. On the other hand, α SMA⁺ CAF depletion reshaped the tumor microenvironment by inducing vascular remodeling. Such changes could potentially also impact the immune cells in the tumors, possibly counteracting or masking effects of α SMA⁺ CAFs depletion on immune cell populations. Hypoxia can lead to the accumulation of immunosuppressive cells in tumors¹¹⁷. Although we observed increased intratumoral hypoxia in the 4T1 mammary cancer model when α SMA⁺ CAFs were depleted, this was not the case in the transplantation model, in which we assessed immune cell composition. Whether the significant increase in CD11b⁺Gr1⁺PDL1⁺ cells was caused by a decrease in angiogenesis, or if a direct crosstalk exists between α SMA⁺ CAFs and these immune cells or

other immune populations that influence CD11b⁺Gr1⁺PDL1⁺ cells, remains to be further evaluated. Nevertheless, the increase in CD11b⁺Gr1⁺PDL1⁺ cells was intriguing. We interpreted CD11b⁺Gr1⁺PDL1⁺ cells as M2-like macrophages^{112,118}. At first glance, it seems counterintuitive for immunosuppressive cells to accumulate in shrinking tumors. However, these cells could potentially be the cause for metastasis to persist¹¹² and therefore we hypothesized that targeting α SMA⁺ CAFs together with inhibiting TAMs via anti-PDL1 treatment might lead to the reduction of tumor growth and metastatic disease. Evaluation of the metastatic burden in mice from this experiment is still ongoing and it is premature to draw any conclusions from this study at this point. Of note, when investigating the immune cell composition in the 4T1 mammary carcinoma model depleted of α SMA⁺ CAFs, TAMs were moderately, but not significantly increased (data not shown). We did not include these data here, as only tumors from 4 mice in each group were tested for changes in immune cells, a sample size too small to yield reliable results in our experience.

Of note, when we investigated CAF marker composition in the WT and α SMA⁺ CAFs-depleted tumors, mesenchymal marker expression was tested in the context of the control markers CK8 and CD31. The WT tumors in the experiment serve as a control for our experiments in Chapter 3, where the TSA panel for PyMT tumors lacked CD31 and CK8. When comparing **Figure 7A to Figure 13D**, one can appreciate that expression overlaps between mesenchymal markers were very similar, confirming that CAF marker expression patterns shown in Chapter 3 were representative of expression specifically by CAFs.

Depletion of FAP⁺ CAFs did not have any effect on tumor growth or metastasis. Metastasis analysis was only based on the number of lung surface nodules, conclusions about the metastatic phenotype might therefore have to be confirmed with a more thorough metastasis analysis as described in other animal experiments (see methods). FAP⁺ CAFs depleted tumors contained less CD4 T-cells and T regulatory cells (moderate decrease) when compared to WT control tumors. While no change in CD8 T-cells was detected within all T-cells (CD3⁺), CD8 T-cells out

of total lymphocytes (CD45⁺) were increased in FAP⁺ CAF depleted tumors. Activation markers Ki67 as well as Granzyme B were used in the immune panels as described in methods. An increase in activated T-cells (based on Ki67 or Granzyme B) was not detected, which might explain the unchanged primary tumor burden despite fewer T regulatory cells and more cytotoxic (CD8⁺) T-cells within tumors. Immunoregulatory functions of FAP⁺ CAFs have also been suggested when using a DNA vaccine against FAP. Here, in a 4T1 model, specific targeting of FAP⁺ CAFs in combination with doxorubicin treatment significantly reduced tumor growth and metastasis when compared to doxorubicin treatment alone. Disease reduction was attributed to a Th2 to Th1 cytokine shift in the tumor microenvironment that is accompanied by a decrease of immunosuppressive cells and an increase in cytotoxic T-cells¹⁰¹. Of note, tumor growth and metastasis were not affected when mice were treated with only the FAP-targeting vaccine in the absence of chemotherapy, in line with our findings from FAP⁺ CAF depletion experiment without any further therapy. Studies using CAR-T cells targeting FAP reported opposing results in the 4T1 model^{102,103}. Strategies such as vaccines or CAR T-cells affect all cells expressing the target regardless of the proliferation status of the cells. As the viral thymidine kinase model relies on proliferation to be effective, one can argue this approach is more specific to CAFs, which are by definition activated and proliferating. Nevertheless, in all such approaches, targeting of non-CAFs cannot be ruled out, as FAP has also been shown to be expressed in the immune cells^{119–122}. This raises the possibility that the effects on tumor immunity could stem from direct targeting of immune cells. It remains to be determined whether in these studies, as well as in our model immune cells were directly targeted.

Depletion of PDGFR β ⁺ CAFs in our previous studies using the 4T1 mammary carcinoma model has shown more dramatic effects on tumor growth and metastasis as shown here in the PyMT models. This might be due to the inherent differences between these two animal models. One should note that when we depleted α SMA⁺ CAFs in these two different models as shown in

this Chapter, the impact on tumor growth, metastasis and microenvironment was greater in the 4T1 model. We observed a moderate, but not significant reduction in primary tumor growth and metastasis, a trend similar to the results reported when PDGFR β ⁺ cells were depleted in small, non-hypoxic 4T1 tumors. GCV treatment was started in the PyMT tumors when the combined tumor burden reached 500mm³, at which stage all tumors are relatively small with generally lower hypoxia (hypoxia levels in PyMT tumors of different sizes is demonstrated in the following Chapter). In the transplantation model, no changes in primary tumor growth was observed. Possible explanations why we cannot observe an effect in this additional tumor model might be the inherent differences in the composition of the microenvironment between the two models. Implantation of the tumors is accompanied by an inflammatory response, which might remodel the microenvironment, so that the effect of PDGFR β ⁺ CAFs depletion was masked. PDGFR β expression was downregulated, confirming successful depletion. The observed changes in immune cell populations could be partly responsible for the lack of tumor growth reduction. Even though more T effector cells were present in the tumor, activated (Ki67⁺) cytotoxic T-cells number was reduced. Preliminary investigation showed α SMA expression reduced, while microvasculature (CD31) was unchanged. Further investigations are necessary in order to test for vessel leakage and investigate the contributions of PDGFR β ⁺ CAFs vs. PDGFR β ⁺ pericytes depletion.

While further investigations are needed in order to draw more definitive conclusions, we can conclude that α SMA, PDGFR β and FAP label functionally distinct CAF subsets in mammary carcinoma. **Table 2** summarizes the different changes that were observed upon depletion of each subset. In our previous studies we have demonstrated FSP1⁺ CAF's involvement in facilitating metastatic outgrowth in the lungs. When comparing these results to our results in this thesis, we can conclude that FSP1⁺ CAFs represent a forth, additional CAF subset.

Lastly, the vTK model is depleting CAFs only based on expression of one particular marker. Using TSA-based multiplex staining we determined the expression overlaps between the mesenchymal markers tested were minimal and therefore the depletion approach was appropriate. However, this does not take into consideration the potential expression of additional, untested CAF markers that may further delineate CAF subsets. Here, we have characterized four CAF subsets based on expression of α SMA, PDGFR, FAP and FSP1. Further studies will investigate the expression of additional markers within these groups to further delineate the cell subpopulations.

Table 2 Effects of CAF subtype depletion in mammary carcinoma

	α SMA-vTK			PDGFR β -vTK			FAP-vTK	FSP1-vTK
Animal model	4T1	PyMT	PyMT Transpl.	4T1 (previous ¹¹⁵)	PyMT	PyMT Transpl.	PyMT Transpl.	4T1 (previous ^{194, 57})
Tumor growth	↓	↓	↓	↓	↓	No change	No change	No change
Metastasis	No change	No change	No change	↓/↑	↓	↓	No change	↓
T-cell changes	n/a	n/a	No change	n/a	n/a	FoxP3 ⁺ (of CD4 ⁺)↓ FoxP3 ⁻ (of CD4 ⁺)↑ CD8 ⁺ Ki67 ⁺ (of CD8 ⁺)↓	CD4 ⁺ (of CD3 ⁺) ↓ FoxP3 ⁺ (of CD3 ⁺)↓ CD8 ⁺ (of CD45 ⁺) ↑	n/a
B-cell changes	n/a	n/a	↑	n/a	n/a	No change	No change	n/a
Myeloid cell changes	Similar trends than Transpl.	n/a	CD11b ⁺ ↓ CD11b ⁺ PDL1 ⁺ ↑ CD11b ⁺ PD1 ⁺ ↑	n/a	n/a	No change	No change	n/a
Other changes	Vascular remodeling, hypoxia, tumor metabolism	Change in mesenchymal marker expression patterns	Vascular remodeling	Vascular remodeling, EMT induction, hypoxia, ANG2 ↑	n/a	NK cells↓	n/a	VEGF ↓ Tenascin A ↓ (in lung)

Potential pitfalls and alternate approaches

Our previous experience with these models has indicated no enhanced immune infiltration due to cell death caused by targeting of fibroblasts (unpublished data), neither have we observed a bystander effect in this model. We have previously shown that the tumor stage at the onset of GCV-induced depletion can be very critical to the outcome¹¹⁵. In the setting of α SMA⁺ CAFs depletion we tested many different approaches using three distinct animal models. In the 4T1 model we repeated the experiment four times; in each setting tumors had progressed to a different

stage at start of GCV administration (here only data shown for one experiment; the other experiments were performed by another graduate student in the lab). Robust reduction in primary tumor growth was observed in all scenarios, but in one of the tested settings, metastasis increased upon α SMA⁺ CAFs depletion (data not shown in this thesis). Therefore, our studies do not fully elucidate α SMA⁺ CAFs' contribution to metastasis and this aspect remains to be further assessed. Here, 4T1 tumors of different volumes (different stages) in α SMA-vTK and WT mice could be treated with GCV to probe whether GCV onset is critical in contributing to metastasis. Moreover, when 4T1 cells were intravenously injected in the context of α SMA⁺ CAFs depletion, we did not assay the lung tissue for reduction in α SMA. This critical immunolabeling in the lungs remains to be performed in order to draw definitive conclusions from this i.v. experiment.

Since CAFs are by definition activated, proliferating fibroblasts, we expect the vTK system to differentially target those cells. However, these models may miss any CAF population potentially having important functions but remained quiescent. Depending on which subset one wishes to target, alternative strategies, such as antibodies, vaccines, or other animal models (such as diphtheria toxin-mediated depletion) could be used. On the other hand, non-CAF cells expressing the respective markers might have been targeted inadvertently with our approach. Here, a thorough analysis of expression of α SMA, FAP and PDGFR β by other cell types in the context of the vTK models should be undertaken.

We observed changes in the immune cell composition in the considerably smaller, and less vascularized α SMA⁺ CAFs depleted tumors. Interpretation of these results are limited and it is unclear whether observed changes were caused by the lack of α SMA⁺ CAFs in the stroma or rather due to smaller and/or less vascularized tumors displaying different immune landscapes. Tumors from WT mice of comparable size could be used for comparison, and vasculature remodeling drugs such as anti-VEGF (Avastin) could be used as controls. The same holds true for the metabolomic analysis of the tumors.

Future Directions

Studies focus on the functions of α SMA⁺ CAFs and PDGFR β ⁺ CAFs, especially with respect to immune modulation are ongoing. Most importantly, due to the known roles of PD-L1⁺ TAMs in metastasis¹¹², we are now testing whether α SMA⁺ CAFs depletion together with PD-L1 inhibition can reduce metastasis. Single-cell RNAseq will identify growth factors and cytokines potentially involved in the interactions between α SMA⁺ and PDGFR β ⁺ CAFs and different immune cells.

A new TSA panel will also include PDGFR β , to determine the expression overlaps between all CAF markers that were functionally characterized. Importantly, this panel will also enable us to distinguish α SMA and PDGFR β expression by CAFs or pericytes in WT and tumors in which α SMA⁺ cells or PDGFR β ⁺ cells were depleted. This will therefore enable the deciphering of the pericytes and CAFs' respective contribution to tumorigenesis.

The expression dynamics of mesenchymal markers also demands more investigation. We observed a gain of Vimentin expression in α SMA⁺ CAFs in vTK models. It would be interesting to see if these cells acquire Vimentin expression and thereby become more quiescent to evade targeting pressure. To test these dynamic expression patterns, transgenic animals that allow lineage tracing of specific markers can be utilized.

We have established four functionally distinct CAF subsets via independent expression of four mesenchymal markers. Future efforts should be directed towards probing expression of additional mesenchymal markers within these subsets to further delineate functional CAF subpopulations.

CHAPTER 5

CANCER-ASSOCIATED FIBROBLASTS ARE REPROGRAMMED BY HYPOXIA TOWARD INCREASED GLYCOLYSIS AND FACILITATE MAMMARY CARCINOMA PROGRESSION

The work in this chapter has been accomplished with the help and in collaboration with Drs. Joyce Tse O'Connell, Annie Vo, Margo Cain, Valerie LeBleu, Desiree Tampe, Lauren Bizarro, Hikaru Sugimoto, Anna McGow, Sughra Raza, John Asara, Kathleen McAndrews, Rafal Zielinski, Philip Lorenzi, and Michael Zeisberg. Some of the data shown in this chapter was generated by Joyce Tse O'Connell, Margo Cain and Hikaru Sugimoto (indicated in figure legends) and is shown with their permission.

This chapter is based on findings in previous studies (In some instances, previously described experiments were repeated or reproduced with permission, as indicated in figure legends):

Vo, A. P. Glucose Metabolism in Cancer-Associated Fibroblasts. *Harvard Univ.* (2013). doi:10.1029/91JD03139

Tse, J. C. Functional Heterogeneity of Fibroblasts in Cancer Progression and Metastasis. *Harvard Univ.* (2011). doi:10.16194/j.cnki.31-1059/g4.2011.07.016

Parts of the work in this chapter has been published previously and is taken verbatim from the publication:

Becker, L. M.*, O'Connell, J. T.*, Vo, A. P., Cain, M. P., Tampe, D., Bizarro, L., Sugimoto, H., McGow, A. K., Asara, J. M., Lovisa, S., McAndrews, K. M., Zielinski, R., Lorenzi, P. L., Zeisberg, M., Raza, S., LeBleu, V. S., and Kalluri, R. **Epigenetic Reprogramming of Cancer Associated Fibroblasts Deregulates Glucose Metabolism and Facilitates Progression of Breast Cancer.** *Cell Reports*, 31(9), 107701. <https://doi.org/10.1016/j.celrep.2020.107701>

Summary

A specific mechanism, of how CAFs may contribute to tumor growth and progression is providing metabolic support for cancer cells. CAFs exhibit an altered metabolism toward increased glycolysis, which may help fuel cancer cells' growth through increasing lactate availability in the tumor microenvironment. While studies suggest such a lactate shuttle, how the metabolic reprogramming in CAFs emerges and is sustained remains unknown. Studying fibroblasts isolated from a large cohort of patients with benign breast tissues and breast cancer, in conjunction with animal models, we demonstrate that CAFs exhibit a metabolic shift towards lactate and pyruvate production and fuel biosynthetic pathways of cancer cells. In vitro studies using patient derived benign and cancer associated fibroblasts demonstrated that the CAFs' glycolytic phenotype can be induced in normal fibroblasts by altered oxygen availability. Hypoxia leads benign fibroblasts to adopt a pro-glycolytic, CAF-like transcriptome. Our findings suggest that glucose metabolism in CAFs evolves during tumor progression and their functional phenotype is mediated, at least in part, by oxygen-dependent metabolic changes that favor a breast cancer promoting function.

Introduction

CAFs are a heterogeneous cell populations with several functionally distinct subtypes. We have tested the functions of three different CAF subsets in chapter 4 and observed different impacts of these cells on tumor growth and metastasis and on different components of the tumor microenvironment. In this chapter, we sought to further probe one particular aspect of α SMA⁺ CAFs: their metabolic crosstalk with cancer cells. Previous studies from our lab show that depletion of α SMA⁺ CAFs results in decrease in whole tumor metabolites, which suggested that

these CAFs contribute to tumor metabolism and are possibly fueling cancer cell growth¹³⁵ (data not shown in this thesis).

CAFs have been proposed to undergo metabolic reprogramming toward aerobic glycolysis, a phenomenon known as the reverse Warburg effect. It has first been observed in the context of cancer by studying activated myofibroblasts. The absence of Caveolin1 (CAV1) has been associated with fibroblast activation and a myofibroblast-like phenotype^{123,124}. CAV1^{-/-} fibroblasts have been shown to upregulate expression of several enzymes involved in glycolysis. Subsequent studies showed that in vitro co-culturing of breast cancer cells and fibroblasts caused upregulation of the lactate exporter monocarboxylate transporter 4 (MCT4) in fibroblasts along with expression of the lactate importer monocarboxylate transporter 1 (MCT1) in cancer cells. Immunostaining of patient breast cancer tissue confirmed compartmentalized expression of the two monocarboxylate transporters, suggesting that fibroblasts secrete and cancer cells take up lactate¹²⁵. Other in vitro studies showed co-culture of fibroblasts and breast cancer cells results in increased mitochondrial mass in breast and decreased mitochondrial mass in fibroblasts. The increase in mitochondrial mass in the cancer cells when in co-culture with fibroblasts could be mimicked by feeding them lactate¹²⁶. Further in vitro studies showed metabolic cooperation between CAFs and cancer cells suggesting additional CAF-derived metabolites to fuel cancer cells' growth¹²⁷⁻¹²⁹. In vivo evidence for the metabolic liaison between cancer cells and CAFs is limited. The most relevant study demonstrating a lactate shuttle has used a prostate cancer model, in which knockdown of MCT1 in prostate cancer cells limited their growth potential in vivo⁷⁰.

In the center of all studies investigating the mechanism of metabolic reprogramming of CAFs is the master regulator of glycolysis, HIF-1 α ¹³⁰, but CAFs may also be metabolically reprogrammed by paracrine signaling from cancer cells. Co-culture with cancer cells has shown to induce loss of CAV1, increase in oxidative stress and reactive oxygen species production, associated with HIF-1 α upregulation^{66,125}. The glycolytic phenotype of CAFs can be triggered by

TGF β and PDGF treatment, which cause downregulation of IDH3a and HIF-1 α stabilization¹³¹. While these few studies offer possible explanations how CAFs may acquire a glycolytic phenotype, the exact molecular underpinnings of such regulation remain to be discovered. Interestingly, studies investigating the metabolic phenotypes detect distinct changes in CAFs when compared to normal tissue fibroblasts, although normal fibroblasts have been shown to gain a CAF-like phenotype in 2D cultures¹⁰⁰. This intriguing observation points to irreversible epigenetic changes in CAFs responsible for the glycolytic phenotype. In fact, CAFs present altered DNA methylation patterns, but such have not been linked yet with specific functions and characteristics of those cells^{132,133}. Lastly, hypoxia has been reported to induce loss of global methylation in human dermal fibroblasts¹³⁴. In this chapter, we aimed to characterize the metabolic relationship between cancer cells and CAFs and investigated CAFs' metabolic regulation. *We hypothesize that CAFs' altered metabolism is caused by specific changes in DNA methylation, which might be induced by the hypoxic tumor microenvironment.*

CAFs display a glycolytic phenotype

Our lab has previous shown that depletion of α SMA⁺ CAFs in 4T1 tumors led to reduction in overall tumor metabolites¹³⁵. To identify whether α SMA⁺ CAFs depletion impacted glycolysis in cancer cells, WT and α SMA-vTK 4T1 tumor tissues were probed for CK8 (to label cancer cells) together with pyruvate kinase M2 (PKM2), hexokinase 2 (HK2) and glucose transporter 1 (GLUT1). While PKM2 expression in cancer cells was decreased, CK8-specific GLUT1 and HK2 expression remained unchanged (**Figure 20A-C**).

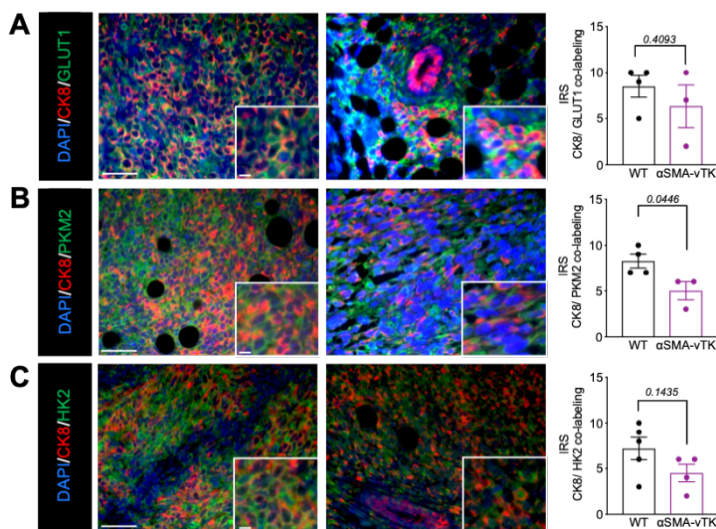


Figure 20 Glycolytic changes in cancer cells in α SMA⁺ CAFs depleted tumors

A. Immunolabeling of CK8 and GLUT1 in WT and α SMA-vTK tumors. Representative images with quantification. **B.** Immunolabeling of CK8 and PKM2 in WT and α SMA-vTK tumors. Representative images with quantification. **C.** Immunolabeling of CK8 and HK2 in WT and α SMA-vTK tumors. Representative images with quantification. Data presented as mean \pm s.e.m., individual dots in graphs indicate individual mice. Unpaired t test (with Welch correction when appropriate) or Mann-Whitney test were used, depending on normality distribution of data. p values are indicate above graphs. Scale bars in all images including inserts: 50 μ m

The immunolabeling experiments in this figure were performed on tumors from an experiment previously described in ¹⁹⁴ (replicate of experiment in Figure 10 using the same WT and α SMA-vTK mice with the same observations on tumor growth).

In order to directly determine the metabolic shifts in CAFs, we purified and cultured CAFs (murine CAFs or mCAFs) from PyMT tumors and fibroblasts derived from healthy murine mammary tissue (hereafter referred to as murine normal fibroblasts or mNFs). Gene expression analyses revealed elevated transcript levels for metabolic enzymes in mCAFs compared to mNFs. The elevated enzymes included monocarboxylate transporter 4 (MCT4, encoded by *Slc16a3*), hexokinase 2 (*Hk2*), and pyruvate kinase M1/2 (*Pkm*). (**Figure 21A**).

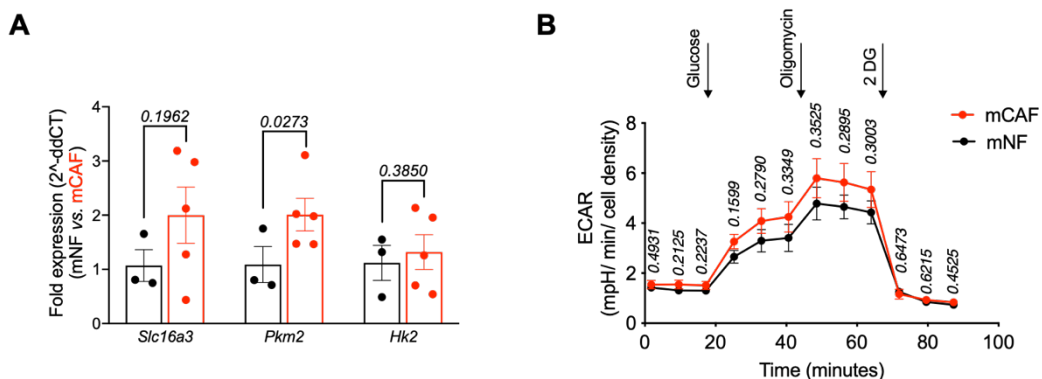


Figure 21 mCAFs are highly glycolytic compared to mNFs

A. Gene expression of key glycolytic enzymes and transporters in mCAFs compared to mNFs. mCAFs were derived from mammary carcinomas in MMTV-PyMT mice. **B.** Glycolysis stress test comparing mCAFs to mNFs. mCAFs were isolated from PyMT tumors. p values are indicated above graphs.

Next, extracellular acidification was measured in mCAFs and mBFs via Seahorse Glycolysis Stress Test. mCAFs demonstrated enhanced glycolysis compared to mNFs (**Figure 21B**, increase in extracellular acidification rate (ECAR, $p = 0.15 - 0.3$) upon addition of glucose, as well as oligomycin, which maximizes glycolysis by inhibition of mitochondrial respiration).

A lactate shuttle has been proposed in the literature between CAFs and cancer cells in the tumor microenvironment^{70,126,136}. We have previously investigated the impact of a potential lactate shuttle between CAFs and cancer cells. In these experiments, 4T1 cells were orthotopically injected and tumor growth was measured. 4T1 cells were either modulated for reduced monocarboxylate transporter-1 (MCT1) expression, or implanted together with fibroblasts with impaired lactate secretion achieved by Pdk4 knockdown. When cancer cells were unable to take up lactate, tumor growth was impaired. Moreover, we found that lack of lactate expression in fibroblasts (via Pdk4 knockdown) when injected together with 4T1 cancer cells, resulted in tumor growth retardation¹³⁵. Here, we tested whether any changes in tumor vasculature or fibroblasts proliferation might have caused the reduction in tumor growth in these experiments; as we saw with α SMA⁺ CAFs depletion.

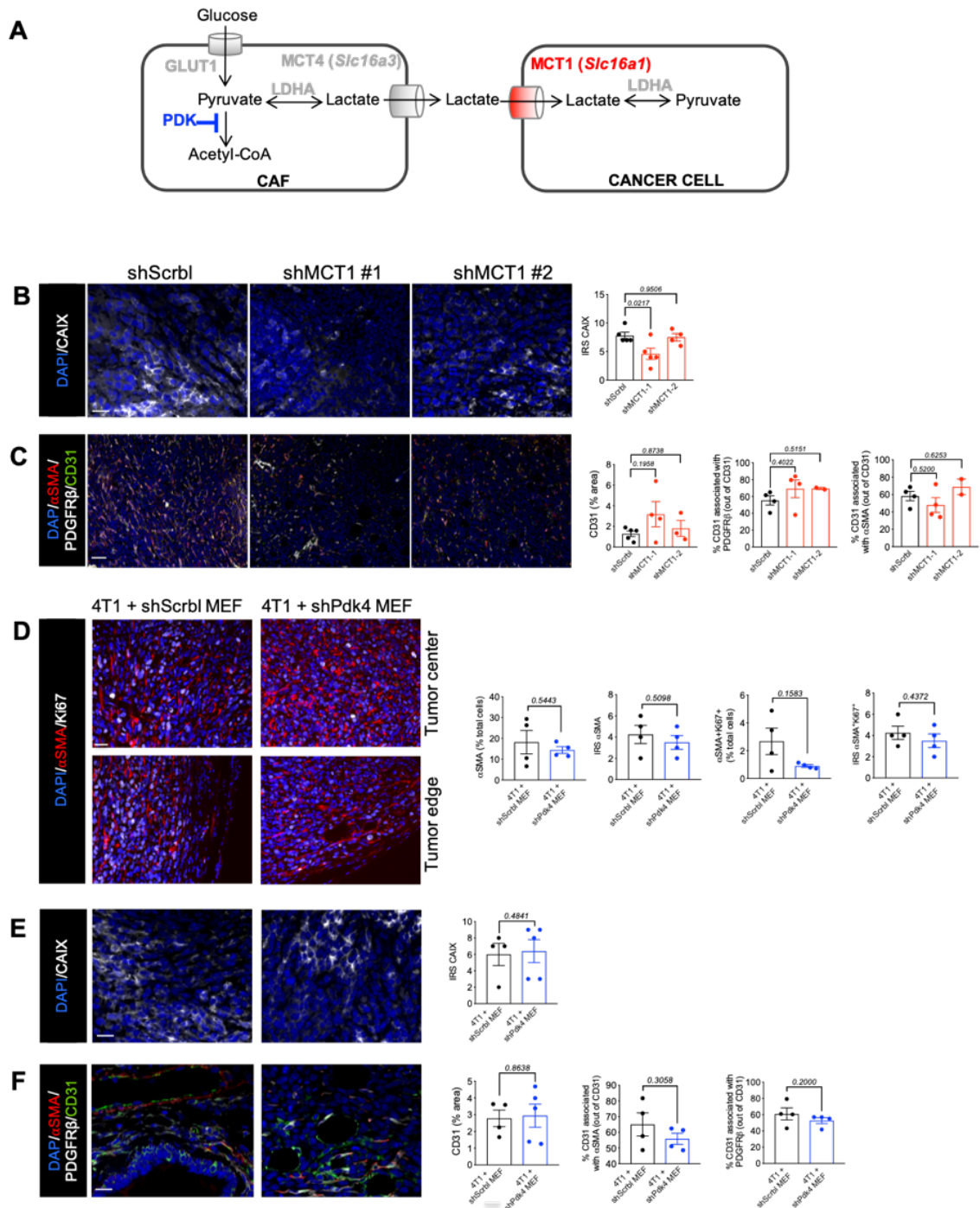


Figure 22 Abrogation of lactate intake by cancer cells results causes no changes in tumor vasculature

A. Schematic presentation of proposed lactate shuttle. **B.** Slc16a1 (MCT1) expression in control 4T1 cells (shScrbl) and 4T1 cells with MCT1 knockdown (shMCT1 #1/2). **C.** Tumor growth of control 4T1 cells and shMCT1 4T1 cells. **D.** Tumor weight in tumors from **(C)**. **E.** Lung metastatic area in mice from **(C)**. **F.** α SMA expression in tumors from **(C)** with quantification. **G.** Hypoxia levels measured by CAIX in tumors from **(C)**. Representative pictures with quantification. **H.** Immunolabeling for α SMA, PDGFR β and CD31 in tumors from **(C)**. Representative pictures with quantification. Data presented as mean \pm s.e.m., individual dots in graphs indicate individual mice. Unpaired t test (with Welch correction when appropriate) or Mann-Whitney test were used, depending on normality distribution of data. p values are shown above the graphs.

The immunolabeling experiments in this figure were performed on tumors from experiments previously described in ¹²⁴. Scale bars: A-B: 50 μ m, C: 12.5 μ m, D: 20 μ m, E: 50 μ m

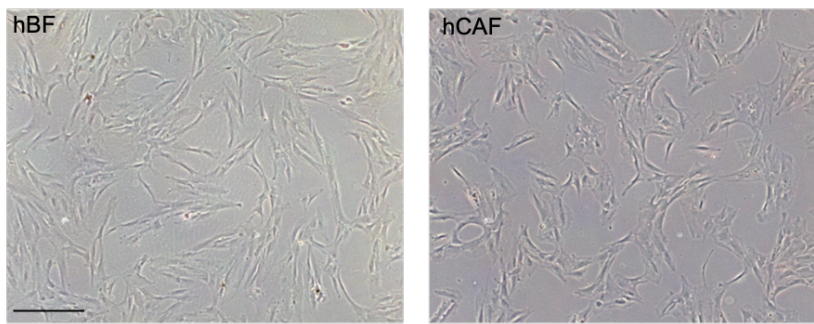
Loss of *Slc16a1* (MCT1) in 4T1 cancer cells did not significantly change tumor vasculature (**Error! Reference source not found.B-C**). These results support that limiting lactate uptake in cancer cells inhibits tumor growth without affecting CAF recruitment. In tumors with fibroblasts with Pdk4 knockdown, α SMA⁺ CAF numbers and their proliferative index, hypoxia, angiogenesis, and pericyte coverage remained unchanged (**Error! Reference source not found.D-F**) supporting that the enhanced glycolytic activity of mammary CAFs promote tumor growth via lactate transfer to cancer cells.

Breast cancer-derived human CAFs display enhanced glycolytic activity

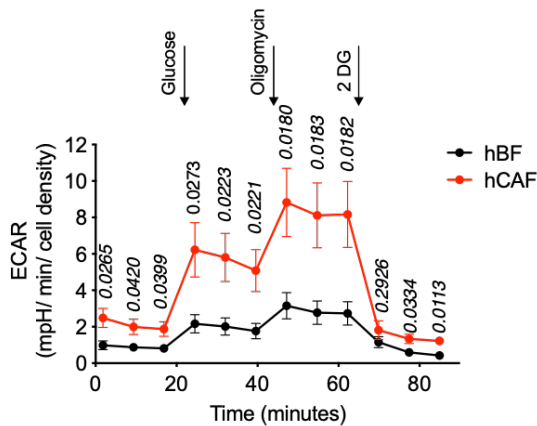
We evaluated the metabolic rewiring of human breast cancer-associated fibroblasts (hCAFs). We used the established catalog of human breast fibroblasts, from both benign, as well as cancerous breast biopsies as shown in Chapter 3. Fibroblasts were isolated from these samples and in ~39% of all culture was successful; and ease of establishing cultures and their propagation did not indicate any bias with respect to pathology or mammographic density parameters. All subsequent analyses were performed on low passage fibroblasts cultures (< 20 passages, see methods), and a selected number of lines were used for in-depth analyses. The biopsy-derived fibroblasts were thereafter referred to as CAFs if derived from breast neoplasms (human CAFs, hCAFs) and benign fibroblasts if derived from non-cancerous breast tissue (human benign fibroblasts, hBFs), respectively (**Figure 23A**).

Extracellular acidification rate (ECAR) measured by Seahorse Glycolysis Stress Test was significantly increased in hCAFs compared to hBFs (**Figure 23B**). hCAFs exhibited increased glycolysis, glycolytic capacity and glycolytic reserve when compared to hBFs (**Figure 23C**), supporting a pronounced pro-glycolytic phenotype of hCAFs. The results support that cultured human and murine CAFs demonstrate a pro-glycolytic phenotype compared to BF, and such acquired features are maintained even after in vitro passages of the cells.

A



B



C

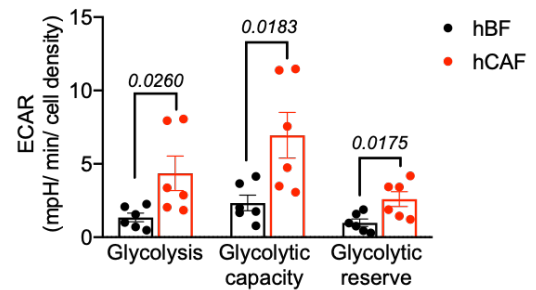


Figure 23 hCAFs are highly glycolytic compared to hBFs

A. Representative pictures of isolated hBFs and hCAFs. Scale bar: 200 μ m **B.** Glycolysis stress test in hCAFs and hBFs. Extracellular acidification rate was measured and arrows indication injection of glucose, oligomycin and 2-deoxy glucose (2DG). **C.** Glycolysis, Glycolytic capacity and glycolytic reserve was measured in hCAFs and hBFs. Data presented as mean \pm s.e.m., individual dots in graphs indicate individual mice. Unpaired t test (with Welch correction when appropriate) or Mann-Whitney test were used, depending on normality distribution of data. p values are shown in graphs.

Cancer cells uptake and utilize CAF-secreted metabolites to fuel their metabolism

To define the metabolic exchange between CAFs and cancer cells, we evaluated the fate of labeled metabolites in cancer cells fed with CAFs metabolic products. Uniformly labeled ^{13}C glucose ($[\text{U-}^{13}\text{C}]$ glucose) was fed to hCAFs (48 hours), and utilization of glucose by hCAFs was evidenced by labeled metabolites implicated in glycolysis, TCA cycle, PPP, nucleotide synthesis, AA biosynthesis, and urea cycle (**Figure 24A**).

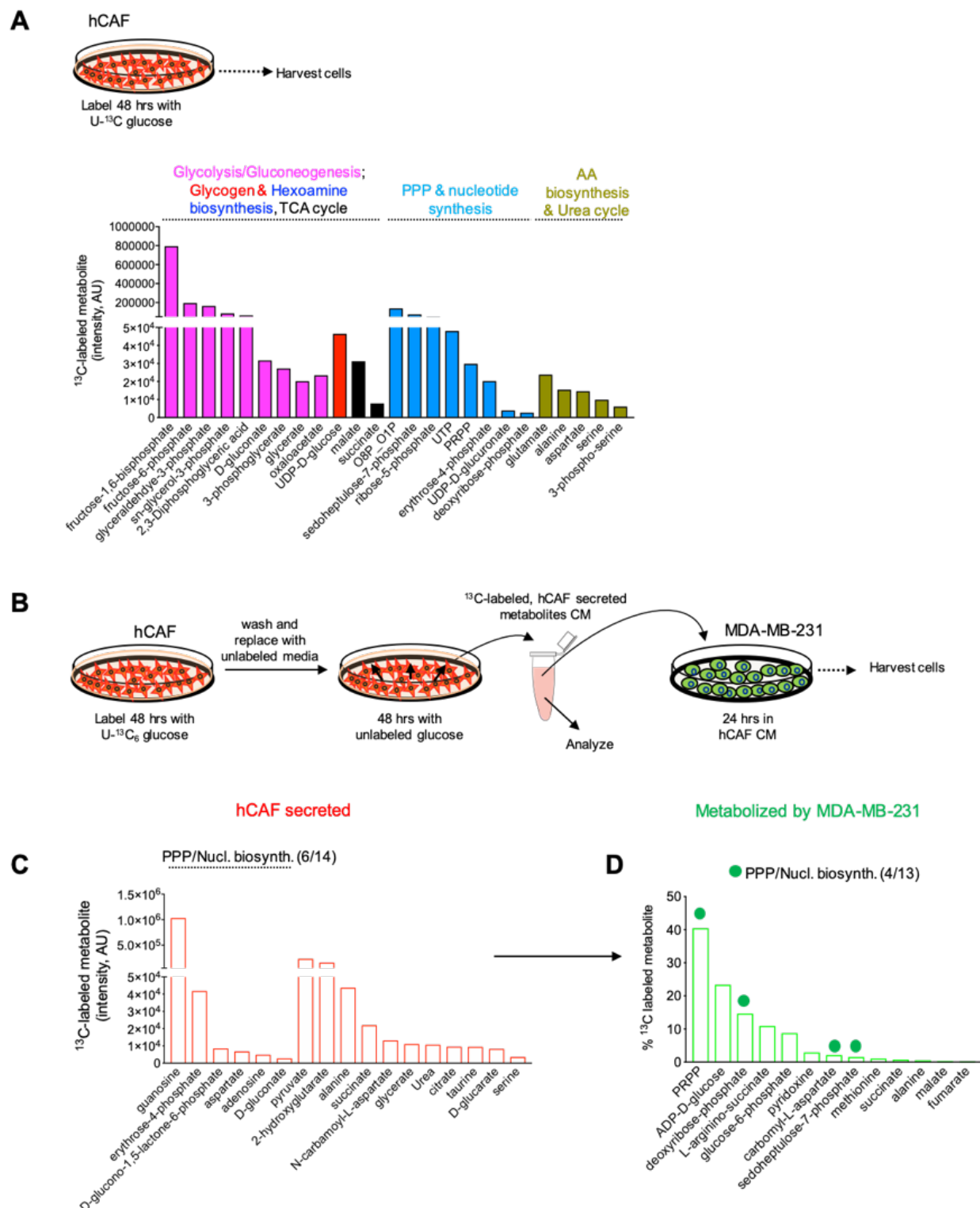


Figure 24 Cancer cells incorporate CAFs-derived metabolites in their metabolism

A. ^{13}C -glucose was fed to CAFs and labeled metabolites were measured in CAFs. **B.** CAFs were fed ^{13}C -labeled glucose. Subsequently CAFs were cultured in medium with no label to allow for labeled metabolites to be secreted in medium (conditioned medium, CM). This CM was fed to a culture of MDA-MB-231 cells and metabolites were probed for ^{13}C label in cancer cells. **C.** ^{13}C -labeled metabolites in CAF CM. **D.** ^{13}C -labeled metabolites in MDA-MB-231 cells fed with CAF CM. This experiment was performed by Margo Cain and I analyzed the data.

Next, the secreted, ^{13}C -labeled hCAFs metabolites were captured: hCAFs were fed [U- ^{13}C] glucose for 48 hours to label all glucose-derived hCAF metabolites; the cells were then washed and cultured for 48 hours in unlabeled glucose media (**Figure 24B**). The hCAF-secreted labeled metabolome revealed metabolites involved in PPP, TCA cycle and nucleotide synthesis (**Figure 24C**). The CM containing hCAF-labeled metabolites was also used to feed triple negative human breast cancer cells, MDA-MB-231, for 24 hours (**Figure 24B**). MDA-MB-231 cells were harvested and ^{13}C labeled metabolites derived from these cells were measured (**Figure 24D**). The analysis indicated that hCAFs-derived metabolites were used by cancer cells to fuel PPP and nucleotide biosynthesis (**Figure 24D**). Controls for the metabolite transfer experiment included unlabeled hCAFs, as well as unlabeled MDA-MB-231. These experiments indicate that human cancer cells utilize hCAF-derived metabolites to fuel their metabolic needs, which includes nucleic acid metabolism.

Oscillating oxygen tension results in reprogramming of hBFs to attain CAF-like metabolic profiles

The pro-glycolytic metabolism of hCAFs was maintained despite repeated in vitro passages in atmospheric oxygen conditions (21% O_2). Metabolomic analyses revealed consistent upregulation of glycolytic enzymes and accumulation of representative metabolites along with elevated ECAR (**Figure 23**, **Figure 24B**). We have previously shown differential methylation patterns of rate limiting glycolytic genes, namely fructose-1,6-bisphosphatase (*FBP1*), *PKM*, *LDHA*, and *HIF1A* in hBFs and hCAFs from the same patient cohort¹³⁵. Such epigenetic reprogramming can at least in part contribute to the hCAFs glycolytic phenotype. To test this hypothesis, we treated hBFs with the demethylating agent 5-Azacytidine (5-Aza). Upon exposure to 5-Aza, hBFs showed an increase in *LDHA*, *HIF1 α* , and *PKM2* transcript levels, suggesting an epigenetic regulation of pro-glycolytic genes in fibroblasts (**Figure 25A**). Previously, we found HIF-1 protein and transcript levels elevated in hCAFs when compared to hBFs¹³⁵. Chronic hypoxia

is a feature of growing tumors, leading to the stabilization of HIF-1 α protein. We hypothesized that chronic hypoxia may initiate HIF-1 α -mediated metabolic reprogramming of CAFs due to promoter hypomethylation, resulting in sustained elevation of HIF-1 α levels in hCAF_s compared

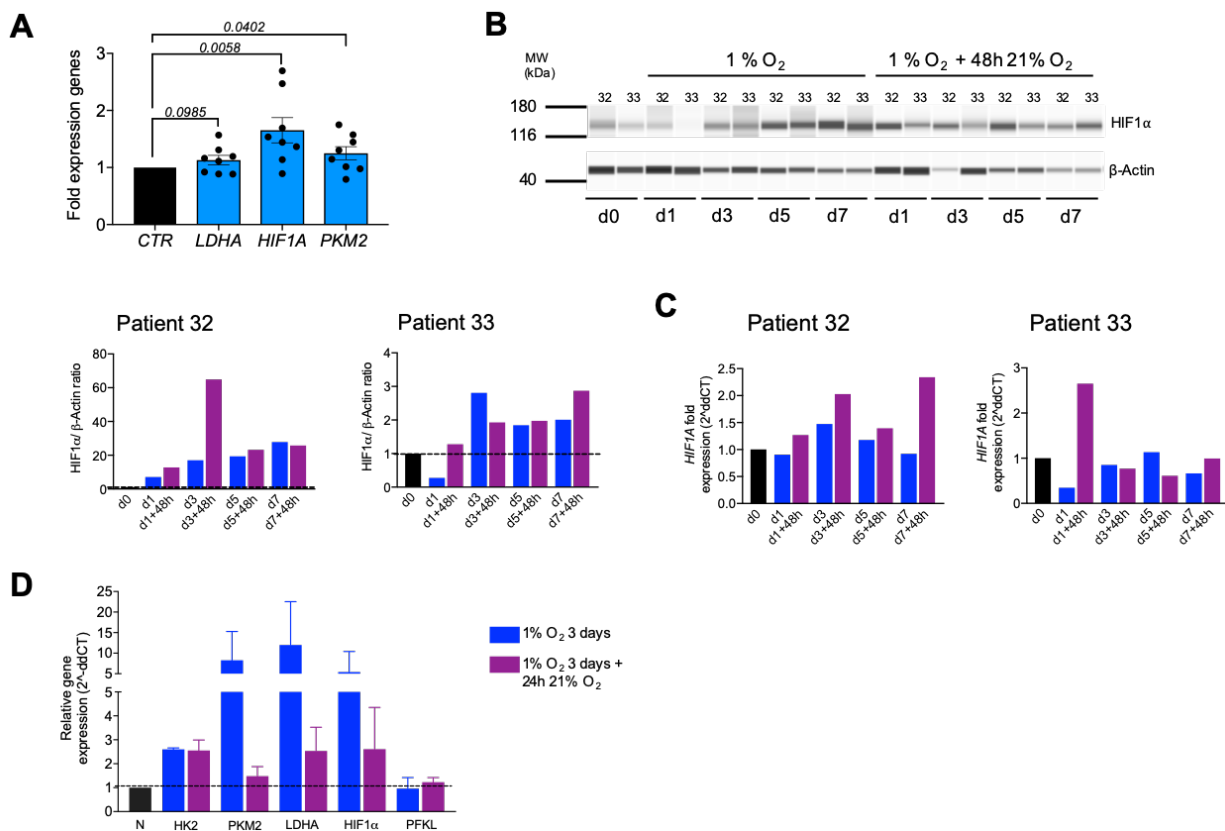


Figure 25 Chronic hypoxia induces stable expression of HIF-1 α and glycolytic enzymes in hBFs.

A. Expression of indicated genes in hBFs when treated with 5Aza and untreated (CTR) assessed by qPCR. This experiment was performed by Joyce Tse O'Connell and reproduced with permission. A similar experiment using fibroblasts from different patients has previously been described in doctoral dissertation of Annie Vo¹²⁴. **B.** HIF1- α protein levels in hBFs from two distinct patients in the indicated conditions of normoxia, hypoxia and hypoxia followed by reoxygenation. **C.** Transcript levels of HIF1- α in experiment from (B). **D.** Gene expression for indicated genes in hBFs from three patients at normoxia, 3 days of hypoxia, or 3 days of hypoxia followed by 24hr reoxygenation. The experiments in panels B-D are repetitions of experiments previously performed by Annie Vo¹²⁴.

to hBFs¹³⁵. To test this hypothesis, hBFs from two distinct patients were subjected to increasing intervals of hypoxia (1% O₂) for 1, 3, 5 and 7 days, followed by 48 hours of reoxygenation (21% O₂) for each timepoint. When hBFs were subjected to a prolonged exposure of hypoxia (5 and 7 days), HIF-1 α protein expression was elevated despite re-oxygenation (**Figure 25B**).

HIF-1 α transcripts were elevated in one out of the two tested hBFs lines upon hypoxia exposure and remained increased upon re-oxygenation (**Figure 25B**). Further, alternating exposures of hBFs to hypoxia/re-oxygenation cycles elevated the normoxic baseline transcript levels of *HIF-1 α* and glycolytic enzymes *SLC2A1*, *HK2*, *PFKL*, *PKM*, and *LDHA* (**Figure 25D**). Of note, we have previously performed similar experiments as shown in **Figure 25** with similar observations¹³⁵. To determine if changes in intratumoral hypoxia in growing tumors contribute to the accumulation of glycolytic CAFs in vivo, we evaluated the glycolytic profiles of CAFs in hypoxic and normoxic tumor regions. Glycolytic CAFs, defined by co-expression of α SMA and PKM2 or HK2 (α SMA/PKM2 and α SMA/HK2 CAFs) were more abundant in hypoxic (CAIX high) rather than normoxic (CAIX low) areas of MMTV-PyMT tumors (**Figure 26A**). The inverse relationship was observed for α SMA⁺ CAFs expressing FBP1 (presumed less glycolytic), with α SMA/FBP1 CAFs more abundant in normoxic rather than hypoxic areas (**Figure 26A**). In both MMTV-PyMT and 4T1 tumors, larger tumor volumes were partly associated with increased intratumoral hypoxia, and significant accumulation of glycolytic fibroblasts (α SMA/PKM2) (**Figure 26B-C**). In 4T1 tumors, α SMA/HK2 fibroblasts also significantly expanded with tumor growth. While non-glycolytic fibroblasts (α SMA/FBP1) remained unchanged in 4T1 tumors, in MMTV-PyMT tumors this population significantly decreased as tumor volumes increased. Lastly, patient tissues were probed for fibroblasts presenting with hypoxia. In tumors (IDC), there was a significant increase in hypoxia-associated fibroblasts (α SMA⁺CAIX⁺ out of total α SMA), when compared to benign tissues (**Figure 26D**).

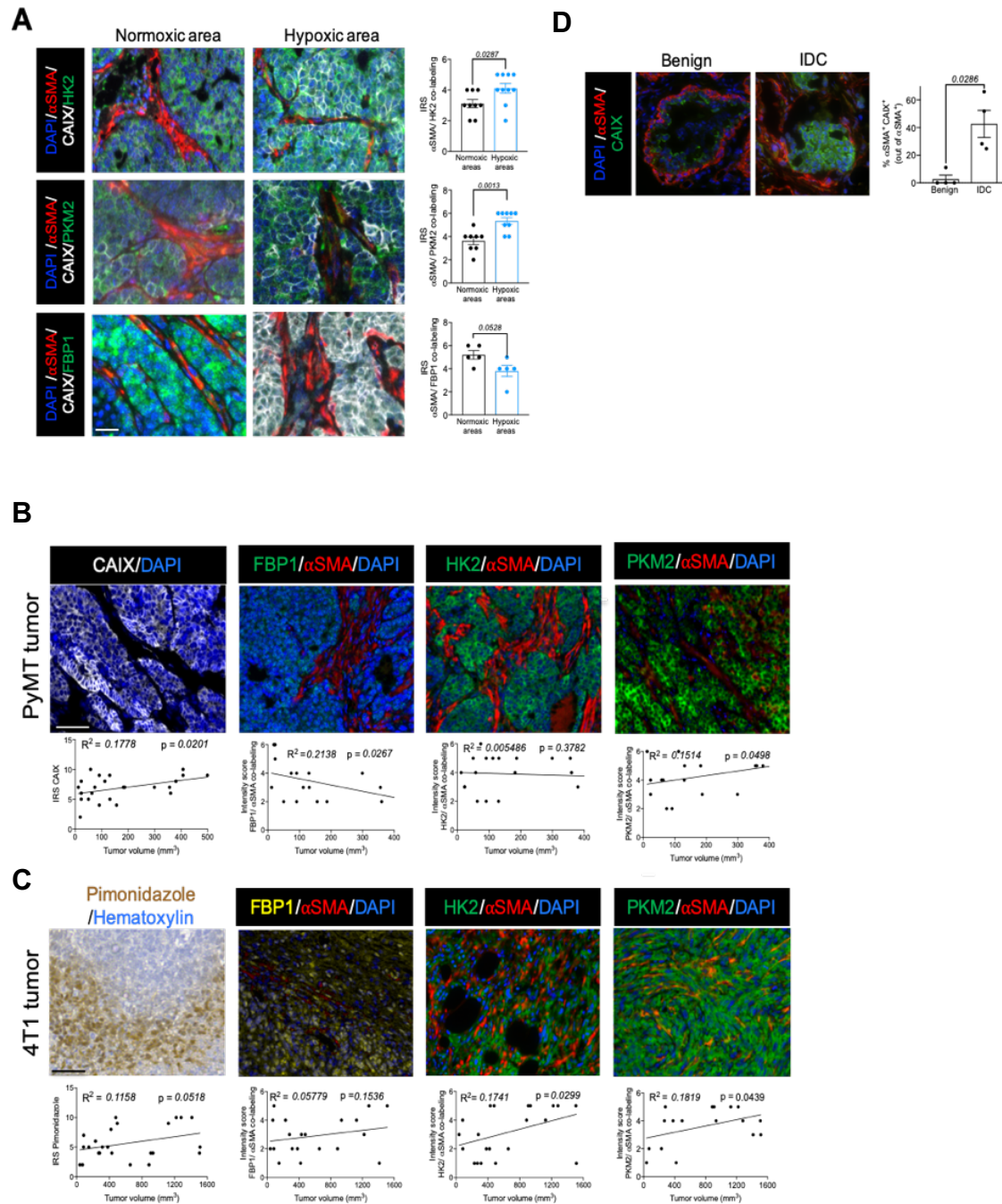


Figure 26 Glycolytic CAFs accumulate in hypoxic areas of tumors

A. Expression of HK2 (top panel), PKM2 (middle panel) and FBP1 (bottom panel) in hypoxic (CAIX high) and normoxic (CAIX low) areas in PyMT tumors. Representative image from each immunolabeling with quantification. **B.** Immunolabeling for Carbonic anhydrase 9 (CAIX, panel 1), α SMA/FBP1 (panel 2), α SMA/HK2 (panel 3), α SMA/PKM2 (panel 4) in MMTV-PyMT tumors of different volumes. Pearson correlations between tumor volume and expression of respective markers are shown together with representative pictures of each immunofluorescence labeling. **C.** Immunolabeling for Pimonidazole (panel 1), α SMA/FBP1 (panel 2), α SMA/HK2 (panel 3), α SMA/PKM2 (panel 4) in 4T1 tumors of different volumes. Pearson correlations between tumor volume and expression of respective markers are shown as well as representative pictures of each immunofluorescence/ immunohistochemistry labeling. Scale bars: 50 μm . **D.** Immunolabeling of α SMA and CAIX in patients with benign breast biopsies or breast cancer. This experiment was performed by Hikaru Sugimoto and is shown with his permission. One-tailed unpaired t test or Mann-Whitney test, Pearson Correlation, P and R^2 values are indicated in all graphs

Together, our data suggests a model in which normal benign fibroblasts that are not tumor promoting and not very glycolytic can convert into CAFs through tumor progression in which oxygen tension changes and increased levels of hypoxia are observed. This causes the epigenetic changes in HIF-1 α and glycolytic enzymes we showed, which makes the CAFs highly glycolytic and tumor promoting (**Figure 27**).

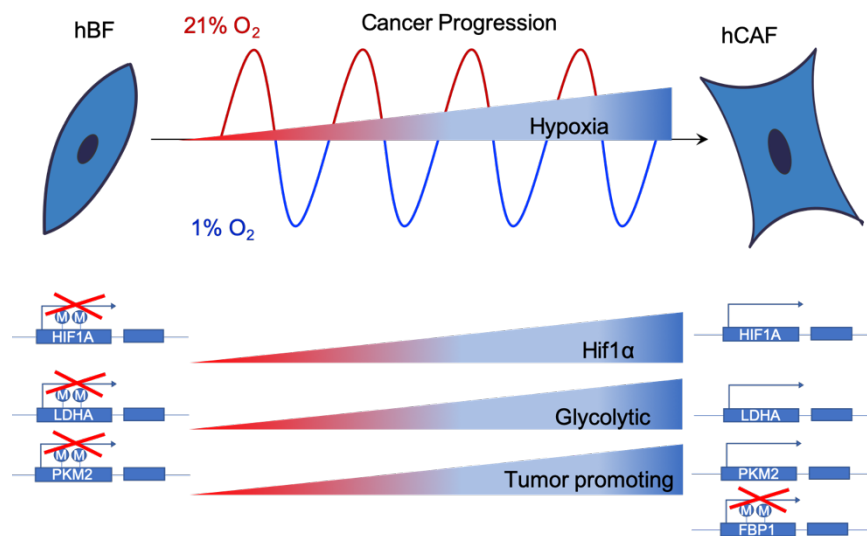


Figure 27 Proposed model of fibroblast reprogramming

Interpretation of findings

We have shown that murine as well as human CAFs present with a highly glycolytic phenotype, compared to their benign or healthy counterparts, as it had been previously suggested^{72,137,138}. mCAFs derived from PyMT transgenic mice show a less pronounced glycolytic phenotype than what we have observed previously in mCAFs derived from 4T1 orthotopic tumors¹³⁵, demonstrating the heterogeneity between different animal models. The differences are likely due to higher hypoxia levels in 4T1 tumors when compared to PyMT tumors of similar

volume (as shown in chapter 3), in agreement with our observations of hypoxia-induced metabolic reprogramming of CAFs.

In the previous chapter, we demonstrated that α SMA⁺ CAFs' tumor promoting role in mammary carcinomas is associated with remodeling of the tumor microenvironment, with CAFs depletion impeding tumor angiogenesis and enhancing intratumoral hypoxia. In this chapter we used tissues from a previous study¹³⁵ that shows disruption of the lactate shuttle between cancer cells and CAFs results in reduced tumor growth, and probed these tissues for changes in tumor vasculature. Here, we could not detect changes we observed with α SMA⁺ CAFs depletion, demonstrating that CAFs' metabolic support for cancer cells is an independent tumor-promoting mechanism of these cells. In α SMA⁺ CAFs depleted tumors, expression of glycolytic enzymes by cancer cells upon was moderately decreased. High intratumoral hypoxia in CAFs-depleted tumors is expected to elevate cancer cell glycolysis, thereby possibly masking greater effects of CAFs depletion on cancer cells' metabolism^{70,130,131}.

In addition to a CAFs-cancer cell lactate shuttle, our metabolite transfer experiment employing human breast carcinoma-derived CAFs indicates that CAFs-secreted metabolites fuel biosynthetic processes of cancer cells, specifically pentose phosphate pathway and nucleotide synthesis. While it remains unknown whether the uptake of CAFs-derived metabolites by cancer cells could be influenced when nutrients are scarce, our experiments inform on the basal metabolic relationship between CAFs and cancer cells. Here we carried out metabolite exchange experiments in conditions wherein cancer cells were not deprived from critical nutrients or oxygen, and despite the relatively short exposure time of cancer cells to the CAFs-derived metabolites, the uptake was principally noted in biosynthetic pathways. For instance, erythrose-4-phosphate was found in the CAF secretome, which can be taken up by cancer cells and fuel pentose phosphate pathway by conversion into sedoheptulose-7-phosphate and PRPP¹³⁹, and both of these metabolites were found in MDA-MB-231 cancer cells when fed the ¹³C labeled CAF

conditioned media. These results support the notion that cancer cells likely present with scavenging properties that enable efficient uptake of metabolites secreted by other cells, including CAFs, thus effectively hijacking metabolites in the tumor microenvironment to support their growth and survival¹⁴⁰.

In our experimental setting, lactate was not amongst the top metabolites secreted by CAFs. Although lactate was noted in the CAF secretome, the high false positive detection rate of labeled lactate in the control unlabeled CAFs (> 5%) rendered its detection as CAFs-secreted metabolite inconclusive. Increased lactate secretion was however confirmed by a glycolytic stress test. In the metabolite transfer experiment, pyruvate was the second most abundant CAF-secreted metabolite. Previous studies suggest growth stimulatory effects of pyruvate on cancer cells by fueling their mitochondrial respiration¹⁴¹. Moreover, pyruvate uptake by cancer cells has been shown to render them resistant to metformin treatment. Gui et al. demonstrated that the pyruvate taken up by cancer cells is converted to lactate to increase the intracellular NAD⁺ level, which is lowered by metformin treatment. NAD⁺ is then utilized for aspartate biosynthesis¹⁴². Since lactate as well as pyruvate can be transferred via MCT1, these reports are also in agreement with our previous findings associated with *Slc16a1* (MCT1) knockdown, and both a lactate and pyruvate shuttle between CAFs and cancer cells may fuel cancer cell metabolism¹³⁵.

Our study identified a hypoxia-induced re-wiring of fibroblasts towards a pro-glycolytic phenotype and results in a sustained elevation of *HIF1- α* , *PKM2*, and *LDHA*, and suppression of *FBP1* gene expression. The acquired baseline pro-glycolytic phenotype, persistent in murine and human breast carcinoma-derived CAFs was likely facilitated by changes in the DNA methylation status of specific metabolic gene promoters¹³⁵. Fibroblasts, along with cancer cells in growing tumors, are exposed to chronic hypoxia, creating an opportunity for metabolic coupling, coordinated by epigenetic events that favor the accumulation of pro-glycolytic CAFs with pro-tumorigenic properties. The accumulation of pro-glycolytic CAFs in regions of increased intratumoral hypoxia in our analyses of multiple breast tumor models supports this notion.

Oxygen availability can drive metabolic adaptation of tissues¹⁴³. Although not studied here, it is possible that the increase in intratumoral hypoxia associated with α SMA⁺ CAF depletion influenced the dissemination of cancer cells by impacting their metabolism, as reviewed by Rankin and Giaccia¹⁴⁴. In contrast to the increase in intratumoral hypoxia from genetically controlled depletion of CAFs, the increase in intratumoral hypoxia in growing tumors, imposed by inadequate angiogenesis promotes the emergence of pro-glycolytic CAFs which may, at least in part, fuel cancer cell biosynthetic needs. Here we show that the chronic exposure to hypoxia and reoxygenation of normal fibroblasts was sufficient to induce a transcriptome characteristic of CAFs (pro-glycolytic). These findings suggest CAFs are cells with the capacity for hyper-responsiveness to hypoxia.

In summary, we identify that patient-derived breast CAFs exhibit an activated metabolism with enhanced glycolytic activity. This feature of CAFs' metabolism fuels cancer cells and promotes tumor growth. Therapeutic agents targeting glycolysis that are currently undergoing clinical evaluation might also function by concomitantly affecting the metabolism of pro-tumorigenic CAFs in breast cancer.

Potential pitfalls and alternate approaches

The study was initiated to further investigate a phenotype of α SMA⁺ CAFs. While we started the study based on our α SMA⁺ CAF depletion model, fibroblast heterogeneity was not taken into consideration in later studies. Future experiments need to address this point and investigate whether our observations were specific to α SMA⁺ CAFs.

In the metabolite transfer experiment, only unfed CAFs or unfed cancer cells were used as controls. We can confidently conclude, that CAF-derived metabolites feed into cancer cells' metabolism. However, this does not exclude the possibility of benign fibroblasts also metabolically fueling cancer cells. In order to test whether normal benign fibroblasts are also able to provide

cancer cells with metabolites, and if so, how those differ from CAF-derived metabolites, the experiment needs to be repeated using benign fibroblasts or normal fibroblasts derived from healthy breast tissue.

Future directions

Future directions of this study involve the unraveling of the exact mechanisms of epigenetic modifications. We propose that hypoxia induced not only the observed stable hypomethylation of HIF-1 α ¹³⁵, but also the differential DNA methylation of PKM2, LDHA and FBP1 promoter in fibroblasts, as previously described¹³⁵. However, future experiments will confirm or disprove this suggestion. Intriguingly, hypoxia induced a glycolytic, CAF-like phenotype in benign fibroblasts. Our study indicates that such fibroblasts could have acquired the tumor growth promoting functions by providing metabolic fuel for cancer cells. Future studies will address this question and test additional characteristics of hypoxia-activated fibroblasts, in order to test to what extent those are comparable to CAFs.

TET hydroxylases are known regulators of DNA methylation, which are interestingly dependent on binding to TCA cycle intermediate oxoglutarate^{145,146}. It would be of interest to further investigate potential feed forward loops between metabolism and DNA methylation, particular in CAFs. Such questions should be addressed in future studies.

Loss of CAV1 has been associated with the glycolytic phenotypes of CAFs. Future analyses will be focused on measuring CAV1 expression in human CAFs compared to benign fibroblasts. In line with this, whole transcriptome analysis on these human-derived fibroblasts could be performed to further decipher distinct CAF metabolic phenotypes in patient-derived fibroblasts.

Lastly, we found several different metabolic pathways upregulated in hCAFs compared to hBFs in previous investigations¹³⁵. Future studies should be aimed to investigate the contributions of additional differentially regulated metabolic pathways in CAFs to cancer progression.

CHAPTER 6

DEREGULATED SIGNALING IN FIBROBLASTS CAN INITIATE EPITHELIAL TUMORIGENESIS

This work is based on the previously published study:

Eikesdal, H. P.*, Becker, L. M.*, Teng, Y.*, Kizu, A., Carstens, J. L., Kanasaki, K., Sugimoto, H, LeBleu, V. S., Kalluri, R. (2018). **BMP7 Signaling in TGFB β 2-Deficient Stromal Cells Provokes Epithelial Carcinogenesis**. Molecular Cancer Research, 16(10), 1568-1578.
<https://doi.org/10.1158/1541-7786.mcr-18-0120>

* Co-first authors

Data presented was generated by all authors on this publication and is shown with their permission. Parts of this chapter are taken verbatim from the publication.

Summary

Fibroblasts can elicit their heterogeneous effects on tumor development and progression indirectly, via matrix remodeling, and directly by secreting metabolites, cytokines and growth factors (such as TGF β , FGF, HGF) that enhance or inhibit cancer cell proliferation, survival (resistance to apoptosis) and migration. We have shown how different CAF subsets have distinct roles in mammary carcinoma progression. Moreover, we have demonstrated how fibroblasts can be epigenetically reprogrammed towards increased glycolysis with a CAF-like phenotype. This glycolytic rewiring presumably happens during tumor progression due to limited oxygen availability in the tumor microenvironment. In the last part of this thesis, we focused our investigations on an additional aspect of CAF biology: CAFs or fibroblasts' role in tumor initiation.

Deregulated TGF β signaling in the stromal fibroblasts has been shown sufficient to induce tumors of epithelial origin³⁶. Specifically, knockdown of *TGFB RECEPTOR 2* (*TGFB R2*) in FSP1⁺ fibroblasts (*TGFB R2*^{CKO} animals) led to development of forestomach carcinoma with 100% penetrance. In order to better understand cancer initiation in this intriguing mouse model, we aimed to decipher the roles of downstream elements of the TGF β signaling cascade. We chose to deplete the common Smad protein, *SMAD4*, in order to target both canonical arms of the TGF β superfamily signaling pathway. Surprisingly, mice lacking both *TGFB R2* and *SMAD4* in FSP1⁺ fibroblasts (*TGFB R2*/*SMAD4*^{CKO} mice) no longer developed forestomach cancer. We found that in the *TGFB R2*^{CKO} animals, BMP7 signaling caused increased HGF secretion by fibroblasts, which in turn induced proliferation of epithelial cells via Met phosphorylation. This was supported by upregulation of BMP7 receptor ALK6 in these fibroblasts. Taken together, our data suggests a model of a complex feed forward loop, in which the loss of *TGFB R2* specifically in FSP1⁺ fibroblasts allows BMP-dependent signaling due to upregulation of ALK6 receptor on the *TGFB R2* deficient fibroblasts. This then leads to increased HGF production, which, in turn, results in Met phosphorylation in the epithelial cells causing them to proliferate at an increased rate. The

hyperproliferative epithelial cells are producing BMP7, which then binds to ALK6 on the fibroblasts to further induce Smad4-dependent HGF production. Of note, in order to address the specificity of TGFRB loss in FSP⁺ fibroblasts, we showed that the knockout of the receptor in α SMA⁺ fibroblasts caused no phenotype in mice. This underlines the distinction between α SMA⁺ and FSP1⁺ CAFs, both in tumor initiation and progression.

Introduction

During all stages of tumorigenesis, cancer cells are continuously engaged in crosstalk with cells of the surrounding stroma. Fibroblasts, which are abundant in the tumor microenvironment (TME), have emerged as critical for development and progression of many solid cancers. However, their exact roles are not fully understood. Published studies indicate that fibroblasts can either promote or suppress tumor progression, suggesting bimodal functions and heterogeneity amongst this cell type⁶⁵. Apart from their intensely-researched involvement in tumorigenesis, several studies indicate that fibroblasts play a causative role in tumor development whereby mutational events in the fibroblasts can result in hyperproliferation and subsequent malignancy in epithelial cells^{147,148}. Such observations are exceptionally rare and need further investigation, but they add another layer of complexity to an already intricate crosstalk between fibroblasts and cancer cells. Fibroblasts can elicit their heterogeneous effects on tumor development and progression indirectly, via matrix remodeling, and directly by secreting factors (such as TGF β , FGF, HGF) that enhance or inhibit cancer cell proliferation, survival (resistance to apoptosis) and migration⁶⁵.

Transforming growth factor beta (TGF β) signaling is heavily involved in multiple aspects of cancer-stroma interactions. TGF β binds to the TGF β receptor 2 (TGFR2), causing recruitment of TGF β receptor 1 (TGFR1) and subsequently results in downstream signaling through multiple Smad family proteins. These Smad proteins can also be activated by other ligands, such as

activins, nodal proteins and bone morphogenetic proteins (BMPs), and their receptors, which are all part of the TGF superfamily¹⁴⁹. Canonically, TGF β elicits downstream signaling through Smad2/3, while BMP signals through Smad1/5/8. However, both canonical signaling pathways complex with Smad4 to initialize transcription¹⁴⁹. TGF β signaling has been implicated to play significant roles in most cancers. TGF β secretion by tumor cells and immune cells leads to recruitment and activation of fibroblasts in the tumor microenvironment⁶⁵. CAFs can in turn secrete TGF β , which triggers tumor-promoting events¹⁵⁰ and programs in cancer cells, such as epithelial-to-mesenchymal transition (EMT)¹⁵¹. Therefore, in advanced stages of cancer progression, TGF β critically contributes towards tumor growth and metastasis. However, TGF β is also known to have quite opposing effects, as studies demonstrate its function as tumor suppressor in earlier stages of tumorigenesis¹⁴⁹. In most solid tumors, deregulation of the balance between TGF β /BMP signaling is a common feature. In line with these observations, many cancers present with mutations in genes linked to TGF β signaling pathways, such as TGFBR2 and SMAD4¹⁵². However, studies using genetically engineered mouse models have shown insufficiency of such mutations in epithelial cells alone to elicit carcinogenesis. For instance, depletion of TGFBR2 specifically in the epithelium of head and neck tissues, such as oral cavity, esophagus and forestomach only resulted in tumorigenesis when combined with an additional KRAS mutation in the epithelium, but not by itself¹⁵³. In contrast, deregulated TGF β signaling in the stroma was sufficient to induce tumors of epithelial origin. Specifically, Bhowmick et al. showed that mice with conditional TGFBR2 knockdown in FSP1⁺ fibroblasts develop squamous cell carcinoma (SSC) of the forestomach and neoplastic changes in the prostate³⁶. All of these pieces of data suggest a complex regulatory network involving many signaling molecules across and within various cell types for tumor initiation and progression.

In an attempt to better understand this complexity with regard to the crosstalk between cancer cells and fibroblasts that could lead to tumor initiation, we focused on the FSP1⁺ fibroblast

loss of *TGFBR2* model of forestomach cancer originally published by Bhowmick et al. In order to better understand forestomach cancer initiation in this intriguing mouse model, we aimed to decipher the roles of downstream elements of the TGF β signaling cascade. We chose to deplete the common Smad protein, SMAD4, in order to target both canonical arms of the TGF β superfamily signaling pathway and show the obligate Smad4-mediated signaling in FSP1⁺ fibroblasts lacking *TGFBR2* to give rise to epithelial carcinogenesis in the forestomach.

Loss of Smad4-mediated signaling in FSP1⁺ stromal cells lacking *TGFBR2* abrogates forestomach cancer development

We faithfully replicated the findings by Bhowmick *et al.*, wherein conditional loss of *TGFBR2* in FSP1⁺ stromal cells (*Tgfb2*^{flloxE2}; FSP1-Cre mice, entitled *TGFBR2* conditional knockout, *TGFBR2*^{cKO} mice) resulted in squamous cell carcinomas of the forestomach, with 100% penetrance at 1.5 months of age, and moribundity between 1 to 2 months of age³⁶ (**Figure 28A-C**) Strikingly however, when these mice were further crossed onto the *Smad4*^{flloxE8-9} background to generate mice with FSP1⁺ stromal cells lacking both *TGFBR2* and *SMAD4* (*Tgfb2*^{flloxE2}; *Smad4*^{flloxE8-9}; FSP1-Cre, hereafter referred to as *TGFBR2/SMAD4*^{cKO}), they no longer presented with cancer, and had a normal life span, similar to control (wt) mice (**Figure 28A-C**).

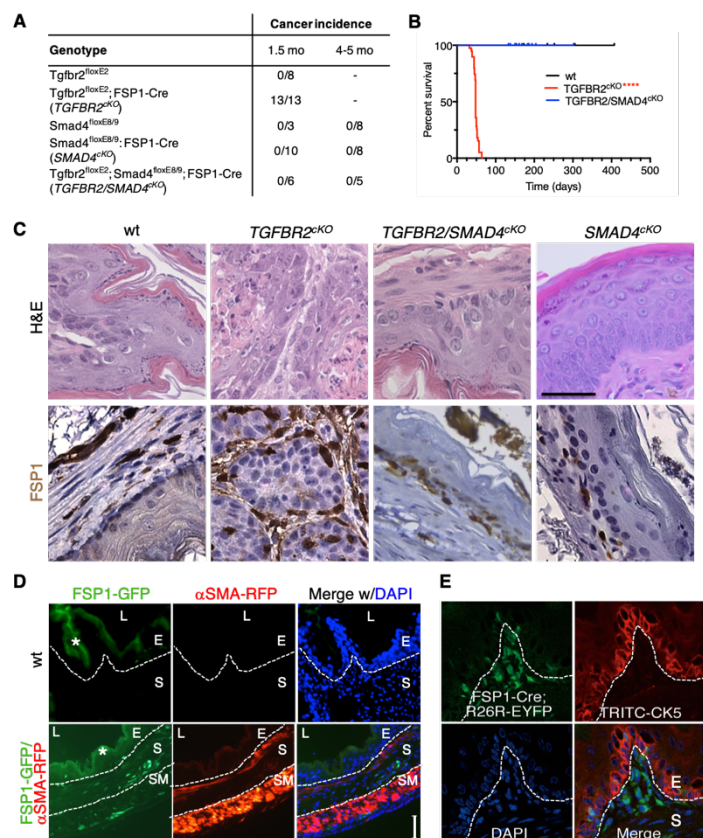


Figure 28 Loss of SMAD4 together with TGFRB2 in FSP1⁺ fibroblasts does not result in forestomach cancer development.

A. Forestomach squamous cell carcinoma incidence rate and **B.** survival of mice with the indicated genotypes. Log-rank (Mantel-Cox) test. **** $p < 0.001$. wt, $n = 7$; *TGFR2^{CKO}*, $n = 38$; *TGFR2/SMAD4^{CKO}*, $n = 14$ mice. **C.** Hematoxylin-eosin (H&E) staining and FSP1 immunolabeling of forestomach tissue of mice with the indicated genotypes. Scale bar: 50 μ m. **D.** Visualization of FSP1-GFP and α SMA-RFP fluorescent gene product in sections of the forestomach of FSP1-GFP; α SMA-RFP double transgenic mice. L: lumen, E: epithelium, S: stroma, SM: smooth muscle, *: green autofluorescence in the epithelial keratin layer. DAPI (blue): nuclei. Scale bar: 50 μ m. **E.** EYFP visualization (green) and immunolabeling for Cytokeratin 5 (CK5) detected with TRITC-conjugated secondary immunolabeling in sections of the forestomach tissue from R26-EYFP; FSP1-Cre⁺ mice. DAPI (blue): nuclei. E: epithelium, S: stroma.

In contrast to the *TGFR2^{CKO}* mice, *TGFR2/SMAD4^{CKO}* mice showed no evidence of forestomach carcinogenesis and presented with normal forestomach histology (**Figure 28C**). *SMAD4* conditional loss in FSP1⁺ stromal cells (*Smad4^{loxE8&9}; FSP1-Cre: SMAD4^{CKO}*) did not result in forestomach cancer (**Figure 28A, C**), and these mice presented with mild cartilage developmental defects as previously described¹⁵⁴. Cre-negative controls (*Tgfr2^{loxE2}* and *Smad4^{loxE8-9}*) were phenotypically normal (**Figure 28A**).

Notably, FSP1⁺ stromal cells appeared equally abundant in the forestomach of wild-type (wt) and *TGFR2/SMAD4^{CKO}* mice (**Figure 28C**). These results indicated that the loss of *Smad4* in FSP1⁺ stromal cells lacking *Tgfr2* did not result in loss of FSP1⁺ cells in the

forestomach, but rather changed their downstream signaling, leading to a phenotypic, fully penetrant, reversal of the oncogenic potential of FSP1⁺ stromal cells acting on the epithelium.

Mesenchymal FSP1⁺ stromal cells specifically induce forestomach cancer

In the forestomach tumors of *TGFBR2^{ckKO}* mice, the squamous cell carcinoma cells were characterized by cytokeratin 5 and phosphorylated p63 positive staining (**Figure 29A**), whereas the FSP1 immunolabeling was localized to the stroma (**Figure 28C**). Systematic analysis of the healthy gastrointestinal tract of double transgenic α SMA-RFP; FSP1-GFP mice demonstrated that FSP1⁺ stroma cells were abundantly found immediately below the epithelium, whereas α SMA⁺ stromal cells were mostly located in the deeper smooth muscle layers (**Figure 28C**, **Figure 29B**).

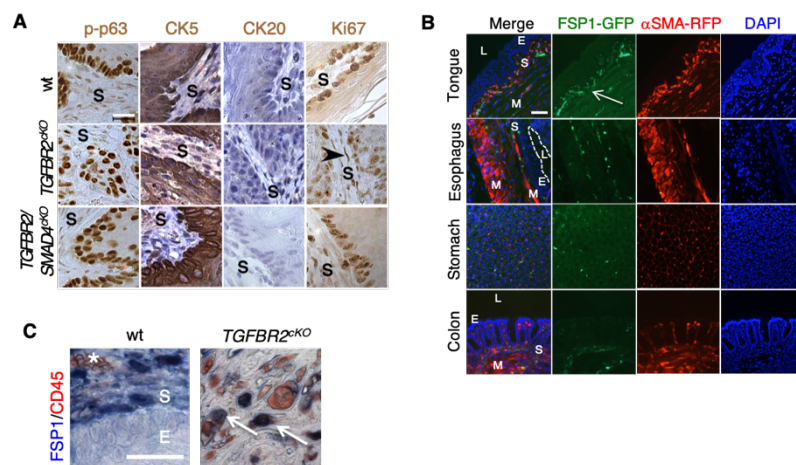


Figure 29 Tumor initiation by conditional loss of TGFBR2 is specific to FSP1 fibroblasts

A. Immunolabeling for p64, CK5, CK20 and Ki67 in forestomachs of wt, *TGFBR2^{ckKO}*, and *TGFBR2/SMAD4^{ckKO}* mice. S: stroma. Arrowhead points to a Ki67⁺ stromal cell. Scale bar: 20 μm. **B.** α SMA-RFP, FSP1-GFP mice were used to probe for mesenchymal marker expression in different tissues. L: lumen, E: epithelium, S: stroma, M: smooth muscle, dotted line: outlines the boundaries of the esophageal lumen. DAPI (blue): nuclei. Scale bar: 100 μm. Arrows point to FSP1-GFP⁺ stroma. **C.** Immunolabeling for CD45 and FSP1 in forestomachs of wt and *TGFBR2^{ckKO}* mice. White arrow: co-localization of FSP1 and CD45. * depicts CD45⁺ cells within a vessel. S: stroma. E: epithelium. Scale bar: 50 μm.

Lineage tracing of FSP1⁺ cells in normal forestomach of adult mice, employing FSP1-Cre; R26R-LSL-EYFP mice, indicated that FSP1 was largely

expressed in the stroma and not the epithelium of the forestomach (**Figure 28E**). Combined

immunolabeling for

FSP1 and the pan-leucocyte marker CD45 indicated that a subset of the FSP1⁺ stromal cells were leukocytes (**Figure 29C**), in agreement with previous reports^{155,156}. While inflammation could affect forestomach cancer progression¹⁵⁷ leukocyte infiltration in the forestomach of *TGFBR2^{ckKO}* mice was not a dominant feature of the histopathological findings. These results support that

deregulated TGF β signaling specifically in the mesenchymal FSP1⁺ stroma most proximal to the forestomach epithelium leads to forestomach carcinoma.

Loss of TGFB2 in FSP1⁺ stromal cells induces epithelial proliferation via HGF/Met signaling

Analysis of forestomachs from *TGFB2*^{ckO} mice prior to the emergence of carcinoma (mice 2 and 4 weeks old) indicated a progressive, robust induction of FSP1⁺ stromal cell

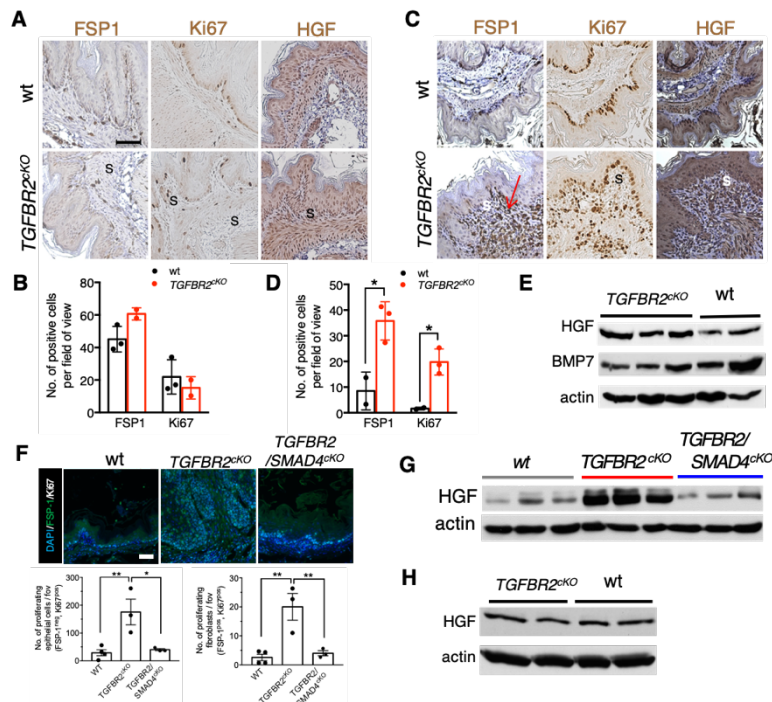


Figure 30 HGF signaling is elevated in forestomachs of *TGFB2*^{ckO} mice

A-B. Immunolabeling (**A**) and quantification (**B**) for FSP1, HGF and Ki67 expression in the forestomachs of 2-week-old wt and *TGFB2*^{ckO} mice. n=2-3 distinct mice per group, unpaired two-tailed t test. **C-D.** Immunolabeling (**C**) and quantification (**D**) for FSP1, HGF and Ki67 expression in the forestomachs of 4-week-old wt and *TGFB2*^{ckO} mice. n=2-3 distinct mice per group, unpaired two-tailed t test. Red arrow points to FSP1⁺ fibroblasts in the pre-cancerous forestomach stroma of *TGFB2*^{ckO} mice. In **A** and **C**, DAB (brown) was used as the color substrate for the immunohistochemistry, and nuclear hematoxylin counterstaining was omitted for the Ki67 immunolabeling. S: stroma. Scale bar: 100 μ m. **E.** Western blots analyses for HGF and BMP7 protein levels in 4-week-old wt and *TGFB2*^{ckO} forestomach whole tissue lysates, 30 μ g of protein loaded per lane, each lane represents a distinct mouse. **F.** Immunolabeling for FSP1 and Ki67 and quantification of Ki67 positive epithelial and stromal cells in the forestomachs of 6-week-old wt, *TGFB2*^{ckO} and *TGFB2*/*SMAD4*^{ckO} mice. (for *TGFB2*^{ckO}: squamous cell carcinoma). Scale bar: 60 μ m. The quantification of Ki67 positive cells was based on three distinct mice per group, and the groups were compared by one-way ANOVA. **G.** Western blot analysis for HGF in the forestomach lysate of 6-week-old mice with the listed genotypes, 30 μ g of protein loaded per lane, each lane represents a distinct mouse. **H.** HGF expression in forestomach lysates of 2 weeks old wt and *TGFB2*^{ckO} mice. *p<0.05, **p<0.01.

proliferation beneath the forestomach epithelium (**Figure 30A-D, F**). Elevated HGF was noted in *TGFBR2^{ckO}* forestomach tumor lysates when carcinomas had developed and this was not seen in *TGFBR2/SMAD4^{ckO}* forestomachs or in forestomachs of 2-week-old *TGFBR2^{ck}* mice (**Figure 30E and G-H**).

These data suggested that HGF production by *TGFBR2*-deficient fibroblasts participated in neoplasia of the forestomach. RT-PCR was used to assess gene expression of known growth factors secreted by fibroblasts to directly affect epithelial cells, such as EGF, IL6, CTGF, and others (see references ^{158–168}).

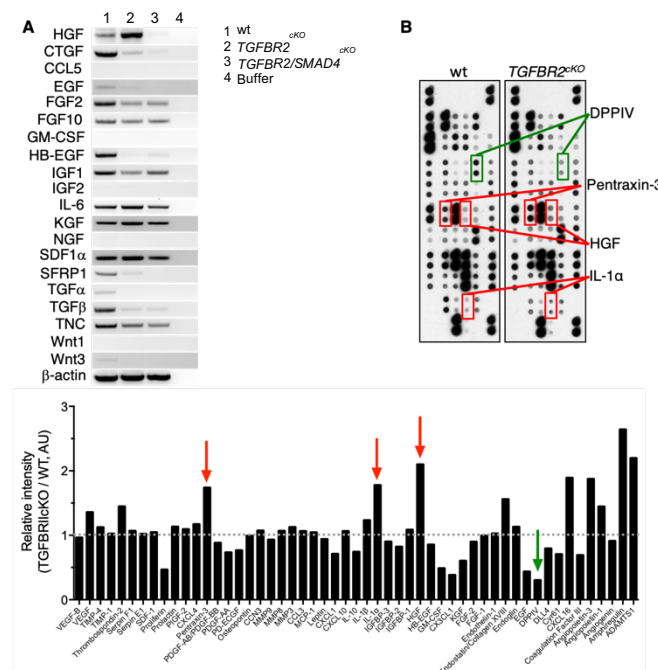


Figure 31 HGF signaling is elevated in *TGFBR2^{ckO}* mice
A. RT-PCR electrophoretic product for the listed genes in the forestomach fibroblasts from approximately 6-week-old mice with the listed genotypes. Buffer: no template control. **B.** Cytokine array using forestomach lysates from wt and *TGFBR2^{ckO}* mice. Bar graph below is the quantification of the array.

Out of all tested growth factors, HGF was found specifically upregulated in *TGFBR2^{ckO}* forestomach fibroblasts (**Figure 31A**). Increased secreted HGF levels by *TGFBR2^{ckO}* forestomach-derived fibroblasts expanded *in vitro*, compared to wt control forestomach fibroblasts, was validated using a mouse angiogenesis cytokine array (**Figure 31B-C**). Immunolabeling analysis showed that *TGFBR2^{ckO}* forestomach fibroblasts, in contrast to wt and *TGFBR2/SMAD4^{ckO}* forestomach fibroblasts, had upregulated HGF expression (**Figure 32A**). Notably, all

fibroblasts expressed FSP1, and a specific loss of *Tgfr2* expression in *TGFBR2/SMAD4^{ckO}* and *TGFBR2^{ckO}* forestomach fibroblasts was confirmed (**Figure 32A**).

The impact of elevated HGF production by *TGFBR2^{ckO}* forestomach fibroblasts was evaluated in the E10 normal mouse lung epithelial cell line (**Figure 32B-C**). Conditioned media

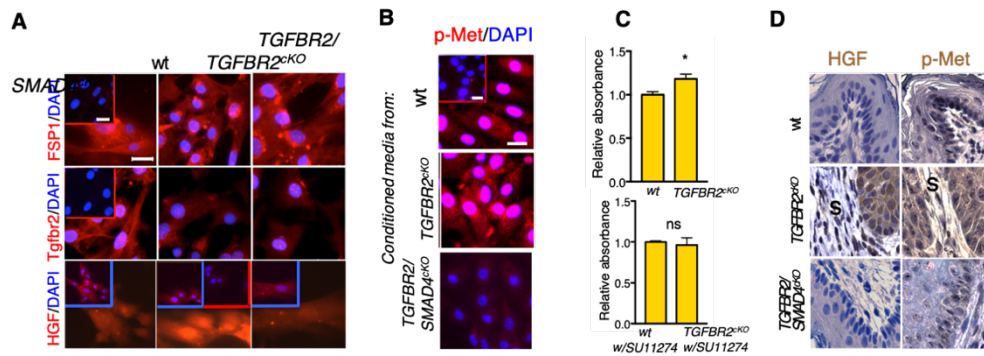


Figure 32 Elevated HGF signaling in *TGFR2^{cKO}* fibroblasts causes Met phosphorylation in neighboring epithelial cells **A.** Immunolabeling for FSP1, HGF and Tgfr2 in cultured forestomach fibroblasts isolated from mice with the listed genotypes. DAPI (blue): nuclei; omitted in HGF panel. Red insets: negative control (Secondary antibody alone). Blue insets: display the merged image while the larger image omits the DAPI signal to clearly show the nuclear localization. Scale bars: 50 μ m. **B.** Immunolabeling for phosphorylated Met (p-Met) in E10 lung epithelial cell incubated with conditioned media from cultured forestomach fibroblasts isolated from mice with the listed genotypes. DAPI (blue): nuclei. Red inset: negative control (Secondary antibody alone). Scale bars: 50 μ m. **C.** E10 lung epithelial cell proliferation (methylene blue absorbance) after exposure to conditioned media of the forestomach fibroblasts isolated from mice with the listed genotypes, with and without the Met inhibitor, SU11274 (10 μ M). Unpaired two-tailed t test. The data is presented as the mean \pm SEM. *p<0.05, **p<0.01, ns: not significant. See accompanying source data. **D.** Immunolabeling for HGF and p-Met. Color substrate: 3, 3'-diaminobenzidine (DAB, brown). Scale bar: 20 μ m. S: stroma.

TGFR2/SMAD4^{cKO} forestomach fibroblasts failed to induce Met phosphorylation (**Figure 32C**). Critically, *TGFR2^{cKO}* forestomach fibroblasts conditioned media induced E10 cell proliferation in a Met signaling dependent manner, with SU11274 Met inhibitor abrogating these effects (**Figure 32C**). While our transcriptomic analysis and cytokine array analysis of conditioned media from purified forestomach fibroblasts indicate that additional cytokines and growth factors could play a role in the induction of forestomach epithelial cell proliferation and emergence of forestomach carcinoma (**Figure 31A-C**), HGF emerged as a critical player in forestomach carcinogenesis since rescuing the malignant phenotype by additional *SMAD4* deletion normalized HGF production and Met phosphorylation (**Figure 30G**, **Figure 32D**).

from *TGFR2^{cKO}*
forestomach
fibroblasts
induced E10 cell
Met
phosphorylation,
whereas
conditioned
media of

BMP7/HGF imbalance in forestomach and epithelium paracrine signaling aggravates forestomach carcinogenic response

Given that stromal *SMAD4* deletion led to a complete rescue of the *TGFBR2*^{ckO} forestomach cancer (**Figure 28A-C**), Smad4-dependent signaling, implicating (bone morphogenic protein) BMP and Activin receptor mediated signaling, thus emerged as critical for

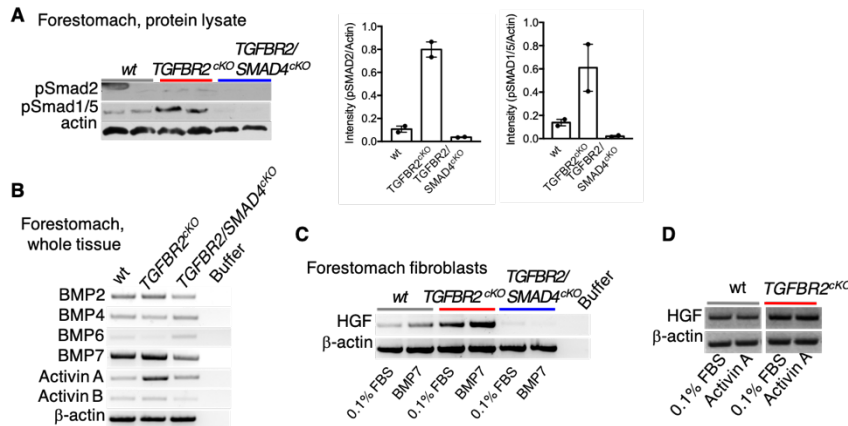


Figure 33 BMP7 signaling is disrupted in *TGFBR2/SMAD4*^{ckO} mice. A. Western blots analyses for Smad2 and Smad1/5 phosphorylation levels in forestomach tissue lysate from approximately 6-week-old mice with the listed genotypes, 30 µg of protein loaded per lane, each lane represents a distinct mouse. **B.** RT-PCR electrophoretic product for the listed genes in the forestomach of approximately 6-week-old mice with the listed genotypes. Buffer: no template control. **C-D.** RT-PCR electrophoretic product for HGF in the forestomach fibroblasts from approximately 6-week-old mice with the listed genotypes with or without (0.1% FBS) stimulation with BMP7 (**C**) or Activin A(**D**).

carcinogenesis of the forestomach epithelium. Within the TGFβ superfamily, bone morphogenic proteins (BMPs) and activins signal via BMP and activin receptors, respectively, to activate regulatory Smads, which use Smad4 to translocate to the

nucleus¹⁵². Forestomach lysates from *TGFBR2*^{ckO} mice showed increased levels of phosphorylated Smad1/5 and Smad2 (normalized to actin), while this was not observed in forestomach lysates from wt and *TGFBR2/SMAD4*^{ckO} mice (**Figure 33A**). We also assessed the expression levels of alternative ligands of the TGFβ superfamily (BMP2, BMP4, BMP6, BMP7, Activin A and Activin B) in the forestomach that could activate Smad4 signaling (**Figure 33B**). Activin A and BMP7 were both upregulated in *TGFBR2*^{ckO} forestomachs in contrast to *TGFBR2/SMAD4*^{ckO} forestomachs (**Figure 33B**). BMP7 exposure robustly induced HGF expression in *TGFBR2*^{ckO} fibroblasts in vitro (**Figure 33C**), whereas Activin A failed to induce HGF expression in *TGFBR2*^{ckO} forestomach fibroblasts (**Figure 33D**).

Transcriptomic analysis as well as BMP7-dependent HGF induction thus implicated BMP7 as a

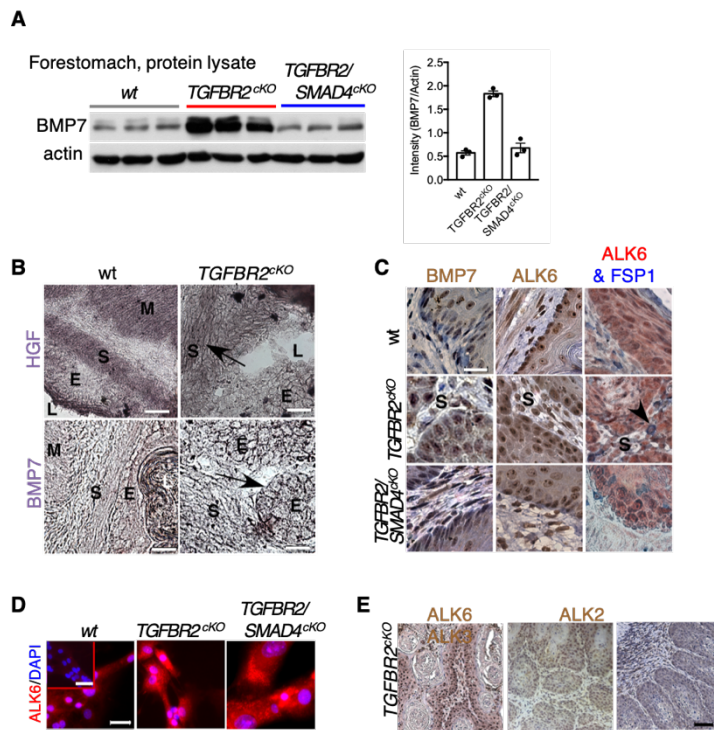


Figure 34 BMP7 is expressed by epithelial cells and FSP1 fibroblasts express the receptor ALK6.

A. Western blot analysis for BMP7 in forestomach tissue lysate from approximately 6-week-old mice with the listed genotypes, 30 μ g of protein loaded per lane, each lane represents a distinct mouse. The actin blot is the same as depicted in **Figure 32G B**. In situ hybridization for HGF and BMP7 mRNA (NBT/BCTP substrate, purple) in sections of the forestomach of the listed mice. L: lumen, S: stroma, E: epithelium/cancer cells, M: smooth muscle. Arrows point to stromal HGF and cancer cell BMP7 expression, respectively. Scale bars: upper panel (HGF): 50 μ m, lower panel (BMP7): 20 μ m. **C.** Immunolabeling for BMP7, ALK6, ALK6 & FSP1. Color substrate: 3, 3'-diaminobenzidine (DAB, brown); for ALK6 & FSP1: 3-amino-9-ethylcarbazole (AEC, red) and Vector Blue. Scale bar: 20 μ m. S: stroma. Arrowhead points to FSP1⁺ fibroblast with ALK6 immunoreactivity. **D.** Immunofluorescence for ALK6 in cultured forestomach fibroblasts from approximately 6-week-old mice with the listed genotypes. Scale bars: 50 μ m. Red inset: negative control, scale bar: 20 μ m. **E.** Immunolabeling for ALK6, ALK2, and ALK3 in forestomachs of TGFB2^{ckO} mice. Scale bar: 50 μ m.

key signaling molecule able to induce HGF in fibroblasts lacking Tgfr2 but with intact Smad4. BMP7 protein level was markedly elevated in forestomachs of TGFB2^{ckO} mice, concomitant with increased HGF expression, during forestomach cancer progression (**Figure 34A**). In situ hybridization demonstrated that HGF expression localized to forestomach stromal cells, while

BMP7 was produced in the epithelium (**Figure 34B**). BMP ligands are known to signal via ALK2, ALK3 or ALK6 to activate Smad1/5/8, bind Smad4 and translocate to the nucleus^{152,169}.

BMP7 preferentially signals via ALK2 and ALK6 and is known to stimulate mesenchymal cell growth^{166,170}. BMP receptor IB

(ALK6) was expressed on stroma

cells, as well as on the tumor epithelium, and double-staining demonstrated that the ALK6 receptor was present on FSP1⁺ cells (**Figure 34C**). Moreover, the ALK6 receptor was strongly

expressed on the *in vitro* fibroblasts (**Figure 34D**). The two alternative BMP-specific co-receptors, ALK2 and ALK3, exhibited weaker immunolabeling (**Figure 34E**).

BMP7 can also signal via non-Smad dependent pathways, including FAK, ERK1/2, JNK and p38 MAPK-mediated signaling, depending on BMP7 concentration^{171,172}. Phosphorylated Akt and Erk1/2 levels were elevated in *TGFBR2/SMAD4*^{ckO} fibroblasts, possibly as a compensatory mechanism for lack of Smad4 (**Figure 35A**).

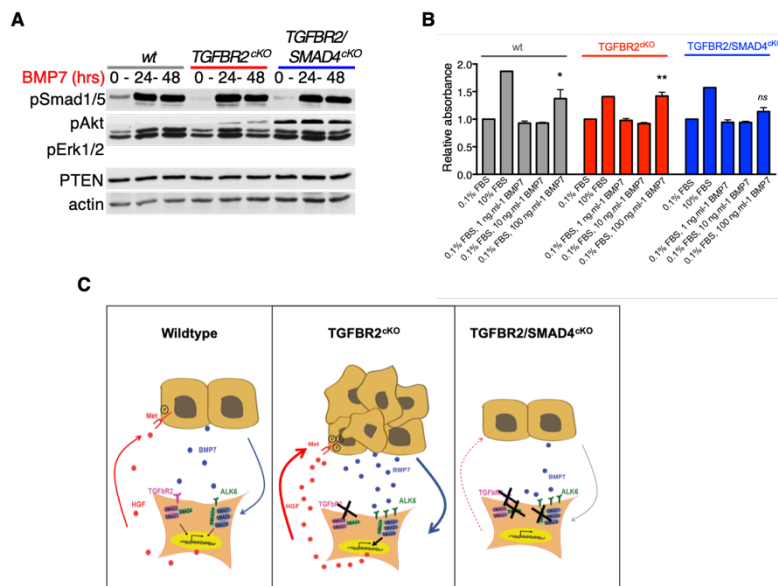


Figure 35 Forestomach cancer can be initiated through a feed forward loop HGF/BMP7 signaling between fibroblasts and cancer cells

A. Western blot analyses of forestomach lysates of mice in the indicates phenotypes. **B.** Cell proliferation (methylene blue absorbance) of wt (gray), *TGFBR2*^{ckO} (red) or *TGFBR2/SMAD4*^{ckO} (blue) forestomach fibroblasts cultured *in vitro* with the indicated treatments. The data is normalized by setting the 0.1% FBS control at 1. Unpaired one-tailed t test compared to 0.1% FBS control, statistical analyses carried out on untransformed data. The data is presented as the mean ± SEM. **p*<0.05, ***p*<0.01, ns: not significant. See accompanying source data. **C.** Diagram of the proposed crosstalk between the *Tgfbr2*-deficient FSP1⁺ fibroblasts (blue) and the overlying epithelium (black). FSP1⁺ fibroblasts produce HGF to activate Met receptors on overlying epithelial cells, causing epithelial cells to produce BMP7, which stimulates ALK6 receptors on FSP1⁺ fibroblasts to produce HGF.

production by FSP1⁺ fibroblasts lacking *Tgfbr2*. HGF stimulates epithelial Met signaling and induces epithelial cell proliferation (**Figure 35C**). HGF production is in part promoted by epithelial-derived BMP7/ALK6 signaling via Smad4 in fibroblasts (**Figure 35C**). The deregulated BMP7/HGF signaling between fibroblasts and epithelial cells enables carcinogenesis of the

Critically however, the activity of high levels of BMP7 on forestomach fibroblasts indicated enhanced proliferation in wt and *TGFBR2*^{ckO} fibroblasts, in contrast to *TGFBR2/SMAD4*^{ckO} fibroblasts (**Figure 35B**), supporting Smad4 signaling is required for BMP7 to stimulate fibroblast proliferation (**Figure 35B**) and HGF production (**Figure 33C**). Altogether our studies support a model wherein carcinogenesis of the forestomach epithelium may ensue from perpetual HGF

forestomach epithelium, wherein loss of *Tgfr2* in *FSP1*⁺ stromal cells promotes HGF production due to increased dependence on epithelial cell-derived BMP7 signaling via ALK6 and Smad4 (Figure 35).

HGF mediated induction of epithelial carcinogenesis is specific to *FSP1* stromal cells

After we observed this intriguing signaling crosstalk between fibroblasts and cancer cells, we wondered whether this is specific to *FSP1*⁺ fibroblasts. We had previously crossed α SMA-Cre mice to *Tgfr2*^{flloxE2} mice in order to knockout TGF β in α SMA⁺ fibroblasts. These *Tgfr2*^{flloxE2}; α SMA-Cre mice did not develop any pathologies and presented with normal forestomach development

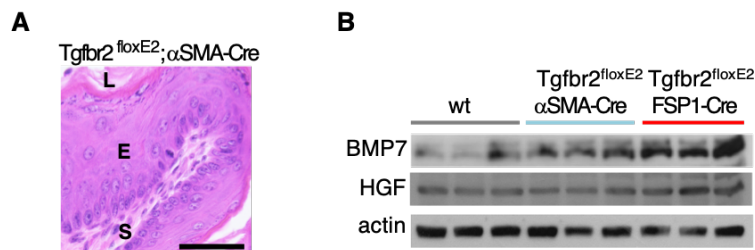


Figure 36 Epithelial cancer cells- fibroblast crosstalk via BMP7/HGF signaling is specific to *FSP1*⁺ fibroblasts.

A. Forestomach histology of *TGF β R2*^{flloxE2}; α SMA-Cre mice. Scale bar: 50 μ m. S: stroma. E: epithelium. L: lumen in the forestomach.

B. Comparison of BMP7 and HGF protein levels in forestomach whole tissue lysates of wt, *TGF β R2*^{flloxE2}; α SMA-Cre and *TGF β R2*^{flloxE2}; *FSP1*-Cre (*TGFBR2*^{cKO}) mice. Western blots, 30 μ g of protein loaded per lane. BMP7 and HGF are highly upregulated in the *TGFBR2*^{cKO} forestomach cancer tissue.

(Figure 36A,⁷⁷). We probed whole tissue lysates from forestomachs of *Tgfr2*^{flloxE2}; α SMA-Cre mice for BMP7 and HGF expression. Both proteins were expressed at levels comparable to those in forestomachs of WT mice, and less than in *Tgfr2*^{flloxE2}; *FSP1*-Cre mice (Figure 36B).

We can therefore conclude that observed BMP7/HGF crosstalk is specific to *FSP1*⁺ fibroblasts.

Interpretation of results

The crosstalk between epithelial cells and the stroma is extensive, and while loss of *TGFBR2* in epithelial cells is not sufficient to elicit carcinogenesis^{149,153}, deletion of *TGFBR2* in *FSP1*⁺ stromal cells mediates epithelial carcinogenesis³⁶ pointing at the regulatory role of stromal *Tgfr2*

signaling towards the epithelium. We investigated more deeply the reported fibroblasts driven forestomach carcinogenesis and found that Smad4 is required to elicit cancer. Furthermore, our data demonstrate that BMP7 signaling via Smad1/5/8 up-regulates HGF production from forestomach stromal cells to promote epithelial cell proliferation via Met activation.

Here we propose that a crosstalk circuit exists in *TGFBR2^{ckO}* forestomachs consisting of BMP7 secreted by the cancer cells and HGF secreted by the stroma, which is a known signaling circuit in prostate cancer¹⁷³.

Crosstalk between the cancer epithelial cells and the stroma is important for tumor progression, and apart from HGF and BMP7, numerous other growth factors are known to be secreted by these two cell compartments^{65,164,174,175}. Importantly, the predominant source of HGF production in epithelial cancers is the tumor stroma¹⁷⁴ which was confirmed by *in situ* hybridization shown in this chapter. Our collective analyses indicated a dominant role for HGF deregulated signaling in *TGFBR2*-deficient forestomach fibroblasts, leading to the activation of epithelial Met receptors, thereby stimulating epithelial proliferation. Furthermore, we report that BMP7 is produced by the epithelial cells to activate BMP receptor signaling in the fibroblasts, and requiring Smad4 to promote HGF production. In contrast, *Tgfr2* binds the TGF β ligand and mediates signaling via Smad2/3 & Smad4 to inhibit cell proliferation in normal tissues, by up-regulating *p21* and down-regulating *c-Myc* transcription^{176,177}. Accordingly, our data demonstrate that stromal *SMAD4* is indispensable for epithelial carcinogenesis when *TGFBR2* is deleted in FSP1⁺ fibroblasts.

Potential pitfalls and alternative approaches

Although we clearly show the BMP7-dependent upregulation of HGF expression in *TGFBR2^{ckO}* fibroblasts, the rescue experiment was not performed, in which TGF β signaling should be restored in fibroblasts and effects on epithelial cell-fibroblasts cross-talk would be

tested. In vitro co-culture experiments using isolated TGFB R2^{cKO} fibroblasts could be used in order to address this point.

Westernblot analyses for phosphorylated Smad1/5 and phosphorylated Smad2 compare levels of phosphorylated proteins to beta actin. Instead, total Smad1/5 and Smad2 should be measured to get a more accurate readout for phosphorylated proteins.

Future directions

The most important question that was not answered by our study is the reason for the organ specificity to develop cancer. Whether the acidic environment of the forestomach pre-conditions epithelial cells for cancer development remains to be tested. Here, injury could be induced in other organs, similar to early wounding studies²⁰, and test if TGFB R2 knockout in FSP1⁺ fibroblasts could have similar effect in wounded organs than in the forestomach. Of particular interest would be mammary carcinoma, as here deregulated BMP signaling in the stroma has already been shown to promote tumor progression^{148,178}.

Moreover, it is most intriguing that despite similar abundance of αSMA and FSP1 in the forestomach, TGFB R2 knockout in αSMA fibroblasts did not cause any abnormalities in mice. Therefore, future studies should be directed towards investigating differences between αSMA^+ fibroblasts and FSP1⁺ fibroblasts in the forestomach.

CHAPTER 7

DISCUSSION

Discussion

CAF heterogeneity

Over the past decade, it has become increasingly clear that successful cancer therapy calls for targeting cancer cells as well as the tumor microenvironment simultaneously. Recent successes in immunotherapy are evidence for this proposition. Here, immune cells are modulated to increase their anti-tumor activity or decrease their immune-suppressive functions. While extremely successful in hematopoietic cancers and melanoma, immunotherapy is only modestly effective against solid cancers, in particular breast cancer^{179–181}, and alternative approaches are needed. Owing to their critical involvement in cancer progression, CAFs represent an attractive therapy target in the tumor microenvironment⁶⁵. However, multiple clinical studies^{182–185} proved targeting CAFs a challenging task. For instance, Pegvorhyaluronidase alfa (PEGPH20) is a recombinant enzyme degrading the ECM component hyaluronan. This has shown moderate effects in a phase II clinical trial for pancreatic cancer¹⁸³. Talabostat, an inhibitor against FAP has failed to show efficacy in non-small cell lung cancer, colorectal cancer and melanoma^{182,184,185}. In addition to directly targeting tumor microenvironment components, CAF-specific signaling, such as Hedgehog signaling has been targeted with several different drugs in many different cancer types, with disappointing results¹⁸⁶. These clinical studies demonstrate the urgency to understand CAF biology at a deeper level, so that future targeting approaches can be more successful. CAF targeting might be such a great challenge due to their extreme heterogeneity with tumor-promoting or tumor-suppressive CAF subtypes, that to date are not clearly distinguishable. Therefore, it appears critical to catalogue CAFs into distinct subtypes with defined functions in tumorigenesis. Similar classification performed for myeloid cells in the past decades led to identification of tumor-reactive and tumor-suppressive cell subsets. Such subsets can now be modulated with specific therapies with the goal to suppress tumor progression, with great success. It stands

to reason that a comprehensive classification of CAFs could promote new strategies to target the most detrimental CAF subtypes while sparing tumor-restrictive cell populations in solid tumors, in particular those which are less amendable to immunotherapy.

In this work, we have attempted to unravel CAF heterogeneity and identify new functions of CAFs. We chose to focus on breast cancer, because of the large stromal content of those tumors. Moreover, immunotherapy has not been very successful for breast cancer patients and therefore additional tumor microenvironment targeting strategies could be of great use. We first identified phenotypically distinct CAF subsets based on expression of α SMA, FAP, FSP1 and Vimentin in two distinct murine models of mammary carcinoma. Of course, many additional mesenchymal markers are used to identify CAFs and our approach presents only a first step in order to delineate CAF subtypes. Moreover, spatial relationships between different cell types should be taken into consideration in future analyses of our data. While RNA sequencing, flow cytometry or CyTOF allow detection of many more markers simultaneously, the necessary tissue digestion causes loss of cells and can therefore add bias to the analysis⁹³. Future experiments should consider newly developed CyTOF imaging methods, which allow utilization of a multitude of markers on a tissue section. More importantly, phenotypical analyses should go hand in hand with functional characterization of the identified cells.

We identified functionally distinct CAF subtypes in our mammary carcinoma animal models based on expression of α SMA, FAP and PDGFR β . FAP has been reported in the literature to be critically involved in tumorigenesis, mainly in pancreatic cancer, as well as in lung cancer and melanoma^{187,188}. We observed no significant effect of FAP⁺ CAFs depletion in our model of mammary carcinoma, in line with previous observations in mammary carcinoma models^{101,102}. One explanation why we could not detect any significant impact on tumor growth or metastasis when FAP⁺ CAFs were targeted might merely be the relatively

low abundance of these cells in the breast tumor microenvironment when compared to other CAF subsets we detected. This might also explain the differences of the impact of FAP targeting between different cancer types^{102,103,109}. Interestingly, when FAP targeting therapy was combined with chemotherapy, it improved the effectiveness of chemotherapy, despite showing no effect on its own¹⁰¹. This suggests to test the functions of FAP⁺ CAFs in the context of cancer therapies. Here, it would be of particular interest to assess FAP⁺ CAFs roles in immunotherapy-treated tumors, due to FAP⁺ CAFs immunomodulatory effects we and others observed.

PDGFR β , as well as α SMA label pericytes as well as CAFs in the tumor microenvironment. All proteins used to identify CAFs are expressed by other cell types in the tumor microenvironment. We found it therefore important to directly compare such markers that label the same CAF and non-CAF cells in the tumor microenvironment. In the past, we have shown that targeting PDGFR β ⁺ pericytes resulted in tumor growth regression. Metastatic burden was decreased when ablation was started when tumors were small and non-hypoxic. However, when PDGFR β ⁺ cells were depleted from larger, hypoxic tumors, increase in lung metastatic burden was observed. Our results of PDGFR β ⁺ CAFs/pericyte depletion in the PyMT model mimic the observations when these cells were depleted from small, non-hypoxic tumors in the 4T1 model. Intriguingly, when we depleted α SMA⁺ CAFs, metastatic burden was unchanged; however, in studies not shown in this thesis revealed that impact of α SMA CAFs depletion depends on the specific experimental setting (unpublished data from the lab). We indeed could see an increase in metastasis when α SMA depletion was started at larger tumor volumes⁹⁵, therefore mimicking the previously observed effects of PDGFR β targeting¹⁸⁹. We showed in this thesis that our strategy to deplete α SMA⁺ CAFs did not impact perivascular α SMA⁺ cells. In our previous publication overall PDGFR β expression was measured in tumors from PDGFR β -vTK animals. One might speculate that

when targeting PDGFR β ⁺ cells in our previous publication, CAFs were targeted as well. A thorough analysis of expression of these two markers in tumors from α SMA-vTK and PDGFR β -vTK is required in order to decipher distinct distribution from different cell types. In the greater picture of cancer therapy, such distinction only matters if those cells are functionally different. PDGFR β -expressing cells can directly be targeted using antibodies¹⁹⁰ or other PDGFR β targeting drugs¹⁹¹. In this case all cells expressing the protein would be targeted regardless of other cell characteristics. α SMA as a cytoskeletal protein cannot be directly targeted with an antibody, or CAR-T cell based on surface recognition. However, one can aim to disrupt tumor promoting signaling pathways between α SMA⁺ CAFs and cancer cells; for instance treatment with antibodies targeting CXCL12 reduced breast cancer growth after CXCL12 was identified as CAF-derived promoter of angiogenesis¹¹.

We have identified several different roles of α SMA⁺ CAFs in the breast tumor microenvironment. α SMA⁺ CAFs seem to impact tumor immunity, angiogenesis and tumor metabolism. CAFs have been shown to induce angiogenesis; however, this has not yet been attributed to a specific CAF type identified by a particular marker¹¹. It remains to be determined how α SMA⁺ CAFs induces angiogenesis in our model. We found an increase in α SMA⁺Vimentin⁺ CAFs accompanied depletion of α SMA^{s+} CAFs. One could speculate whether Vimentin expression in CAFs renders those more quiescent. Therefore, acquisition of Vimentin expression might present a mechanism to escape GCV treatment. Such speculations can only be tested in sophisticated lineage tracing animal models. Most intriguingly, α SMA⁺ CAFs have been shown to recruit tumor-associated macrophages in pancreatic and colorectal cancer^{192,193}. These studies stand in contrast to our findings. Whether interactions between CAFs and immune cells are dependent on cancer type, or whether different experimental settings (in vivo vs. in vitro experiments) are reason for these opposing observations, remains to be addressed in future studies. When compared to

depletion of PDGFR β ⁺ or FAP⁺ CAFs, targeting α SMA⁺ CAFs in the tumor microenvironment of mammary tumors had a variety of different effects. While such effects could be consequential of tumor environment remodeling, this could also suggest multifaceted roles of α SMA⁺ CAFs. We therefore propose that α SMA labels a large subset of CAFs, that can be further delineated using additional markers. One can then hypothesize that one subset might be responsible to induce angiogenesis, while another subset is involved in direct signaling crosstalk with immune cells, and a third subset supplies cancer cells with necessary metabolites to fuel their growth.

CAFs' altered metabolism

We observed downregulation of whole tumor metabolites when we depleted α SMA⁺ CAFs in mammary tumors in previous studies¹³⁵, which prompted us to further investigate the metabolic liaison between cancer cells and CAFs. We showed transfer of CAF-derived metabolites to cancer cells and direct incorporation of these metabolites in cancer cells' metabolism. Moreover, we uncovered how normal fibroblasts can be reprogrammed by hypoxia towards a CAF-like phenotype with increased glycolysis as we previously already indicated¹³⁵.

While we initially observed downregulation of tumor metabolites in α SMA⁺ CAFs depleted tumors and went on to further investigate CAFs metabolic function in mammary carcinoma, we did not probe these functions particularly in α SMA⁺ CAFs, but used heterogeneous CAF populations isolated from patient tissues for the majority of our experiments. The main reason was the nature of the experiments, which encompassed majorly experiments in 2D cultures of fibroblasts grown out of patient tissues. In our experience, once fibroblasts are cultured on plastic, expression of markers are not comparable to expression patterns in vivo (data not shown). Therefore, we did not carefully

characterize the CAFs and benign fibroblasts in culture. However, in light of the current findings, one could now further test population-specific metabolic phenotypes by utilizing conditional knockout mouse models, such as LDHA^{fl/fl} or PKM2^{fl/fl}^{194,195} and cross to mice that harbor Cre driven by a mesenchymal promoter, such as α SMA-Cre⁷⁷, or FSP1-Cre¹⁹⁶.

In our previous studies we have also shown that limiting the metabolic support of CAFs can result in tumor growth reduction¹³⁵ independent of tumor microenvironment remodeling. The effectiveness of the MCT1 inhibitor AZD3965 has been shown in preclinical models, and is currently tested in early phase clinical trials^{197–199}. Our results indicate that MCT1 inhibition would also be effective in breast cancer. Indeed, recently a study demonstrated its effectiveness in inhibiting 4T1 mammary carcinoma cell growth²⁰⁰. Moreover, an inhibitor of MCT4 has shown promising results in pre-clinical studies^{201,202}. We therefore hypothesize that combination therapy using MCT1 as well as MCT4 inhibition in breast cancer might have beneficial effects. Moreover, Dichloroacetate is an FDA approved drug used for inherited mitochondrial disorders. Preclinical studies indicate its effect in breast cancer treatment^{203–205}, in agreement with our findings. However, while these studies focus on the effects of the drug directly on cancer cells, our work also suggests that Dichloroacetate could potentially also inhibit CAF-derived lactate secretion and thereby provide an additional beneficial effect in cancer treatment.

Fibroblasts' roles in tumor initiation

We have discovered how chronic hypoxia can induce epigenetic reprogramming in normal fibroblasts and render those more CAF-like. This is thought to occur throughout tumorigenesis when oxygen availability within the tumor microenvironment is limited. To assess how changes in fibroblasts can not only contribute to tumor progression, but also cause cancer initiation, we focused our attention to a known model, in which deregulated TGF β signaling in FSP1⁺ fibroblasts

has been shown to initiate carcinomas of the forestomach. We have discovered that Smad4 is obligatory to elicit the hyperactivated HGF/BMP7 signaling crosstalk between fibroblasts and epithelial cells leading to epithelial carcinogenesis. Murine forestomach cancer presents squamous cell carcinoma of the esophagus in humans²⁰⁶. C-Met inhibitors are on the market for treatment of non-small cell lung cancer and kidney cancer^{207–209}. As fibroblast-derived HGF signaling is not only involved in cancer initiation, but also in progression of esophageal cancer²¹⁰, this cancer type could be a potential additional application for such inhibitors. Bhowmick et al. suggested elevated HGF signaling in fibroblasts to be responsible for epithelial carcinogenesis. We identified Smad4 dependency of this signaling circuit in order to initiate epithelial carcinogenesis.

The occurrence of carcinomas exclusively in the forestomach is most intriguing and further studies are needed to explain the tissue specificity. One possibility is the importance of stroma for tissue maintenance, specifically for the hyperproliferative squamous epithelium in the upper part of the stomach. In this part of the stomach, high acidity level and continuous mechanical erosion may cause damage to epithelial cells more and pre-condition them for cancer development. Stromal BMP signaling is an important contributor to cancer progression in other cancers. It was previously reported that conditional deletion of *BMP receptor 2 (BMPR2)* in FSP⁺ fibroblasts or disruption of *BMPR2* in breast epithelial cells promotes breast cancer metastasis in mice expressing the PyMT oncogene^{148,211}. In contrast, when *BMPR2* was deleted in nestin-positive stromal cells intestinal polyps developed¹⁴⁷ and inhibition of BMP signaling in all cell compartments with the BMP antagonist DMH1 suppressed breast cancer metastasis¹⁷⁸. BMP signaling in cancer is thus highly context dependent. The importance of BMP signaling in breast cancer evokes the question whether breast carcinogenesis could also be initiated by deregulated stromal TGF β /HGF signaling under highly proliferative circumstances such as pregnancy.

Interestingly, we found that the HGF/BMP7 signaling axis does not exist between α SMA⁺ fibroblasts and epithelial cells, highlighting the heterogeneity in fibroblasts even in normal tissue homeostasis. This opens up questions of the evolvement of heterogenous cancer-associated fibroblasts from heterogenous fibroblasts in healthy host tissues. We have shown one mechanism of how fibroblasts can be activated and reprogrammed. Future studies will test whether this reprogramming is specific to a particular fibroblast population and gives rise to one particular CAF subtype, or whether this is a universal mechanism for all fibroblast types in hypoxic tumor areas.

Lastly, it remains to be seen how relevant these findings are with respect to human disease. Genetic mutations as well as epigenetic alterations have been detected in CAFs. In fact, in breast cancer associated fibroblasts such alterations indicated changes in HGF and Tgf β signaling²¹². Although, it is impossible to conclude whether mutations in fibroblasts preceded cancer, or whether those arose throughout tumor progression. One could imagine designing long term patient studies that probe for stromal mutations, e.g. in routine breast biopsies, and then correlate them to later-on cancer development. However, the feasibility of such studies might not be very high considering that in a cancer therapy setting it is irrelevant how the tumor arose.

Future directions

The biggest challenge in the field of CAF biology is currently the unraveling of heterogenous CAF subtypes. Future and ongoing studies are focused on identifying new CAF subsets and their functions in tumorigenesis. With this work we have identified functionally distinct CAF subsets in breast tumorigenesis and simultaneously introduced new questions. We have shown the multitude of potential functions exhibited by α SMA⁺ CAFs and postulate that further subtyping of this population is necessary to delineate further subtypes of this large CAF population. Similar to the cells in the hematopoietic system, CAFs need careful cataloguing into distinct cell populations. With respect to CAF marker expression

future lineage tracing studies will unravel how different CAFs evolve throughout tumorigenesis. Here, not only CAFs in the tumor microenvironment, but also fibroblasts in healthy tissues should be investigated. We saw distinct differences between α SMA⁺ fibroblasts and FSP1⁺ fibroblasts with respect to induction of forestomach carcinogenesis. In breast cancer, we have discovered distinct expression of α SMA and FSP1 by CAFs, as well as demonstrated that such α SMA⁺ and FSP⁺ CAFs have distinct functions in breast tumorigenesis. Future studies might address whether these CAFs stem from the distinct α SMA⁺ and FSP1⁺ fibroblasts in normal tissue, or whether they might stem from one progenitor cell.

Finally, we have discovered a mechanism of how fibroblasts can be activated and become highly glycolytic like CAFs. Future studies are aimed to investigate these reprogrammed fibroblasts carefully and investigate their CAF-like characteristics, such as primary tumor growth promotion via metabolic fueling of cancer cells.

Conclusion

Collectively, our studies have offered an insight into the multifaceted functions of CAFs in the context of a highly complex tumor microenvironment. Depletion of CAFs resulted in a multitude of changes within this signaling network of cells, which all are interdependent. It is therefore important – as far as it is possible – to conduct research to decipher CAF functions in model systems that take these intricate interactions into consideration. We are just at the beginning of unraveling CAF biology and the future will bring many more exiting insights into the diverse functions of this important cell type in cancer biology. In the hematopoietic system, research over the past 25 years has resulted in a hierarchal layout of distinct immune cell types, which have later been attributed specific functions in tumor biology. The successful cataloguing of the cells of the hematopoietic system has allowed to develop therapies that specifically target

and modulate tumor immune cell responses, with great success. It therefore stands to reason that similarly delineating fibroblasts will open the doors for successful targeting of this most abundant and highly critical component of the tumor microenvironment in the future.

BIBLIOGRAPHY

References

1. Hanahan, D., Weinberg, R. A. & Francisco, S. The Hallmarks of Cancer. **100**, 57–70 (2000).
2. Yang, L., Pang, Y. & Moses, H. L. TGF- β and immune cells: an important regulatory axis in the tumor microenvironment and progression. *Trends Immunol* **31**, 227 (2010).
3. Ng, C. P., Hinz, B. & Swartz, M. A. Interstitial fluid flow induces myofibroblast differentiation and collagen alignment in vitro. *J. Cell Sci.* **118**, 4731–4739 (2005).
4. Ostrand-Rosenberg, S. & Sinha, P. MDSCs: Linking Inflammation and Cancer. *J. Immunol.* **182**, 4499–4506 (2009).
5. Hanahan, D. & Coussens, L. M. Accessories to the crime: functions of cells recruited to the tumor microenvironment. *Cancer Cell* **21**, 309–22 (2012).
6. LeBleu, V. S. & Kalluri, R. A peek into cancer-associated fibroblasts: origins, functions and translational impact. *Dis. Model. Mech.* **11**, dmm029447 (2018).
7. Balkwill, F., Charles, K. A. & Mantovani, A. Smoldering and polarized inflammation in the initiation and promotion of malignant disease. *Cancer Cell* (2005) doi:10.1016/j.ccr.2005.02.013.
8. Cirri, P. & Chiarugi, P. Cancer-associated-fibroblasts and tumour cells: A diabolic liaison driving cancer progression. *Cancer Metastasis Rev.* **31**, 195–208 (2012).
9. Erez, N., Truitt, M., Olson, P. & Hanahan, D. Cancer-Associated Fibroblasts Are Activated in Incipient Neoplasia to Orchestrate Tumor-Promoting Inflammation in an NF- κ B-Dependent Manner. *Cancer Cell* **17**, 135–147 (2010).
10. Kalluri, R. & Zeisberg, M. Fibroblasts in cancer. *Nat. Rev. Cancer* **6**, 392–401 (2006).
11. Orimo, A., Gupta, P. B., Sgroi, D. C., Arenzana-Seisdedos, F., Delaunay, T., Naeem, R., Carey, V. J., Richardson, A. L. & Weinberg, R. a. Stromal fibroblasts present in invasive human breast carcinomas promote tumor growth and angiogenesis through elevated

- SDF-1/CXCL12 secretion. *Cell* **121**, 335–348 (2005).
12. Spaeth, E. L., Dembinski, J. L., Sasser, A. K., Watson, K., Klopp, A., Hall, B., Andreeff, M. & Marini, F. Mesenchymal stem cell transition to tumor-associated fibroblasts contributes to fibrovascular network expansion and tumor progression. *PLoS One* **4**, (2009).
 13. Räsänen, K. & Vaheri, A. Activation of fibroblasts in cancer stroma. *Exp. Cell Res.* **316**, 2713–2722 (2010).
 14. Branco-Price, C., Zhang, N., Schnelle, M., Evans, C., Katschinski, D. M., Liao, D., Ellies, L. & Johnson, R. S. Endothelial cell HIF-1 α and HIF-2 α differentially regulate metastatic success. *Cancer Cell* **21**, 52–65 (2012).
 15. Stover, D. G., Bierie, B. & Moses, H. L. A delicate balance: TGF- β and the tumor microenvironment. *J. Cell. Biochem.* **101**, 851–861 (2007).
 16. Plaster, M., Singh, S. & Tavana, H. Fibroblasts Promote Proliferation and Matrix Invasion of Breast Cancer Cells in Co-Culture Models. *Adv. Ther.* **1900121**, 1900121 (2019).
 17. Bergers, G., Brekken, R., McMahon, G., Vu, T. H., Itoh, T., Tamaki, K., Tanzawa, K., Thorpe, P., Itohara, S., Werb, Z. & Hanahan, D. Matrix metalloproteinase-9 triggers the angiogenic switch during carcinogenesis. *Nat. Cell Biol.* **2**, 737–744 (2000).
 18. Iijima, J., Konno, K. & Itano, N. Inflammatory alterations of the extracellular matrix in the tumor microenvironment. *Cancers (Basel)*. **3**, 3189–3205 (2011).
 19. Sieweke, M. H., Thompson, N. L., Sporn, M. B. & Bissell, M. J. Mediation of wound-related rous sarcoma virus tumorigenesis by TGF- β . *Science (80-.)*. **248**, 1656–1660 (1990).
 20. Dolberg, D. S., Hollingsworth, R., Hertle, M. & Bissell, M. J. Wounding and its role in RSV-mediated tumor formation. *Science (80-.)*. **230**, 676–678 (1985).
 21. Sieweke, M. H., Stoker, A. W. & Bissell, M. J. Evaluation of the Cocarcinogenic Effect of Wounding in Rous Sarcoma Virus Tumorigenesis. *Cancer Res.* **49**, 6419–6424 (1989).

22. Li, J. Y., Yang, M., Li, P., Su, Z. Z., Gao, P. & Zhang, J. Idiopathic pulmonary fibrosis will increase the risk of lung cancer. *Chin. Med. J. (Engl)*. **127**, 3142–3149 (2014).
23. Le Jeune, I., Gribbin, J., West, J., Smith, C., Cullinan, P. & Hubbard, R. The incidence of cancer in patients with idiopathic pulmonary fibrosis and sarcoidosis in the UK. *Respir. Med.* (2007) doi:10.1016/j.rmed.2007.07.012.
24. Bugianesi, E., Leone, N., Vanni, E., Marchesini, G., Brunello, F., Carucci, P., Musso, A., De Paolis, P., Capussotti, L. & Salizzoni, M. Expanding the natural history of nonalcoholic steatohepatitis: From cryptogenic cirrhosis to hepatocellular carcinoma. *Gastroenterology* (2002) doi:10.1053/gast.2002.34168.
25. De Kruijf, E. M., Van Nes, J. G. H., Van De Velde, C. J. H., Putter, H., Smit, V. T. H. B. M., Liefers, G. J., Kuppen, P. J. K., Tollenaar, R. A. E. M. & Mesker, W. E. Tumor-stroma ratio in the primary tumor is a prognostic factor in early breast cancer patients, especially in triple-negative carcinoma patients. *Breast Cancer Res. Treat.* **125**, 687–696 (2011).
26. Dekker, T. J. A., Van De Velde, C. J. H., Van Pelt, G. W., Kroep, J. R., Julien, J. P., Smit, V. T. H. B. M., Tollenaar, R. A. E. M. & Mesker, W. E. Prognostic significance of the tumor-stroma ratio: Validation study in node-negative premenopausal breast cancer patients from the EORTC perioperative chemotherapy (POP) trial (10854). *Breast Cancer Res. Treat.* **139**, 371–379 (2013).
27. Moorman, A. M., Vink, R., Heijmans, H. J., Van Der Palen, J. & Kouwenhoven, E. A. The prognostic value of tumour-stroma ratio in triple-negative breast cancer. *Eur. J. Surg. Oncol.* **38**, 307–313 (2012).
28. Xu, K., Tian, X., Oh, S. Y., Movassaghi, M., Naber, S. P., Kuperwasser, C. & Buchsbaum, R. J. The fibroblast Tiam1-osteopontin pathway modulates breast cancer invasion and metastasis. *Breast Cancer Res.* **18**, 14 (2016).
29. Tyan, S. W., Kuo, W. H., Huang, C. K., Pan, C. C., Shew, J. Y., Chang, K. J., Lee, E. Y. H. P. & Lee, W. H. Breast cancer cells induce cancer-associated fibroblasts to secrete

- hepatocyte growth factor to enhance breast tumorigenesis. *PLoS One* **6**, 1–9 (2011).
30. Virchow, R. Die krankhaften Geschwülste - Dreissig Vorlesung, gehalten während des Wintersemesters 1862-1863 an der Universität zu Berlin.
 31. Barcellos-hoff, M. H. & Ravani, S. A. Irradiated Mammary Gland Stroma Promotes the Expression of Tumorigenic Potential by Unirradiated Epithelial Cells Irradiated Mammary Gland Stroma Promotes the Expression of Tumorigenic Potential by Unirradiated Epithelial Cells 1. 1254–1260 (2000).
 32. Barcellos-Hoff, B. H. Radiation-induced Transforming Growth Factor α and Subsequent Extracellular Matrix Reorganization in Murine Mammary Gland. *Cancer Res.* **53**, 3880–3886 (1993).
 33. Moinfar, F., Man, Y. G., Arnould, L., Bratthauer, G. L., Ratschek, M. & Tavassoli, F. A. Concurrent and independent genetic alterations in the stromal and epithelial cells of mammary carcinoma: Implications for tumorigenesis. *Cancer Res.* **60**, 2562–2566 (2000).
 34. Howe, J. R., Roth, S., Ringold, J. C., Summers, R. W., Järvinen, H. J., Sistonen, P., Tomlinson, I. P. M., Houlston, R. S., Bevan, S., Mitros, F. A., Stone, E. M. & Aaltonen, L. A. Mutations in the SMAD4/DPC4 gene in juvenile polyposis. *Science (80-.)*. **280**, 1086–1088 (1998).
 35. Jacoby, R. F., Schlack, S., Cole, C. E., Skarbek, M., Harris, C. & Meisner, L. F. A juvenile polyposis tumor suppressor locus at 10q22 is deleted from nonepithelial cells in the lamina propria. *Gastroenterology* **112**, 1398–1403 (1997).
 36. Bhowmick, N. a, Chytil, A., Plieth, D., Gorska, A. E., Dumont, N., Shappell, S., Washington, M. K., Neilson, E. G. & Moses, H. L. TGF-beta signaling in fibroblasts modulates the oncogenic potential of adjacent epithelia. *Science* **303**, 848–851 (2004).
 37. Barcellos-Hoff, M. H. & Ravani, S. A. Irradiated mammary gland stroma promotes the expression of tumorigenic potential by unirradiated epithelial cells. *Cancer Res.* **60**, 1254–1260 (2000).

38. Manuscript, A. Why don't we get more cancer? A proposed role of the microenvironment in restraining cancer progression. *Changes* **29**, 997–1003 (2012).
39. Harach, H. R., Franssila, K. O. & Wasenius, V. -M. Occult papillary carcinoma of the thyroid. A "normal" finding in finland. A systematic autopsy study. *Cancer* **56**, 531–538 (1985).
40. Chin, K., De Solorzano, C. O., Knowles, D., Jones, A., Chou, W., Rodriguez, E. G., Kuo, W. L., Ljung, B. M., Chew, K., Myambol, K., Miranda, M., Krig, S., Garbe, J., Stampfer, M., Yaswen, P., Gray, J. W. & Lockett, S. J. In situ analyses of genome instability in breast cancer. *Nat. Genet.* **36**, 984–988 (2004).
41. Gurtner, G. C., Werner, S., Barrandon, Y. & Longaker, M. T. Wound repair and regeneration. *Nature* **453**, 314–321 (2008).
42. Schäfer, M. & Werner, S. Cancer as an overhealing wound: An old hypothesis revisited. *Nat. Rev. Mol. Cell Biol.* **9**, 628–638 (2008).
43. Dvorak, H. F. Tumors: Wounds That Do Not Heal - Similarities between Tumor Stroma Generation and Wound Healing. *N. Engl. J. Med.* **315**, 1650–1659 (1986).
44. Ohlund, D., Elyada, E. & Tuveson, D. Fibroblast heterogeneity in the cancer wound. *J. Exp. Med.* **211**, 1503–1523 (2014).
45. Kalluri, R. & Weinberg, R. A. Review series The basics of epithelial-mesenchymal transition. *J Clin. Investig.* **119**, (2009).
46. Raz, Y., Cohen, N., Shani, O., Bell, R. E., Novitskiy, S. V., Abramovitz, L., Levy, C., Milyavsky, M., Leider-Trejo, L., Moses, H. L., Grisaru, D. & Erez, N. Bone marrow-derived fibroblasts are a functionally distinct stromal cell population in breast cancer. *J. Exp. Med.* **215**, 3075–3093 (2018).
47. Serini, G. & Gabbiani, G. Mechanisms of myofibroblast activity and phenotypic modulation. *Exp. Cell Res.* **250**, 273–283 (1999).
48. Ariga, N., Sato, E., Ohuchi, N., Nagura, H. & Ohtani, H. Stromal expression of fibroblast

- activation protein/seprase, a cell membrane serine proteinase and gelatinase, is associated with longer survival in patients with invasive ductal carcinoma of breast. *Int. J. Cancer* **95**, 67–72 (2001).
49. Xing, F., Saidou, J. & Watabe, K. Cancer associated fibroblasts (CAFs) in tumor microenvironment. *Front. Biosci. (Landmark Ed.)* **15**, 166–79 (2010).
 50. Strutz, F., Okada, H., Lo, C. W., Danoff, T., Carone, R. L., Tomaszewski, J. E. & Neilson, E. G. Identification and characterization of a fibroblast marker: FSP1. *J. Cell Biol.* **130**, 393–405 (1995).
 51. Garin-Chesa, P., Oldt, L. J. & Rettig, W. J. Cell surface glycoprotein of reactive stromal fibroblasts as a potential antibody target in human epithelial cancers. *Pnas* **87**, 7235–7239 (1990).
 52. Ramirez-Montagut, T., Blachere, N. E., Sviderskaya, E. V., Bennett, D. C., Rettig, W. J., Garin-Chesa, P. & Houghton, A. N. FAPalpha, a surface peptidase expressed during wound healing, is a tumor suppressor. *Oncogene* **23**, 5435–5446 (2004).
 53. Alves, F., Vogel, W., Mossie, K., Millauer, B., Hofler, H. & Ullrich, A. Distinct structural characteristics of discoidin I subfamily receptor tyrosine kinases and complementary expression in human cancer. *Oncogene* **10**, 609–618 (1995).
 54. Corsa, C. A. S., Brenot, A., Grither, W. R., Van Hove, S., Loza, A. J., Zhang, K., Ponik, S. M., Liu, Y., DeNardo, D. G., Eliceiri, K. W., Keely, P. J. & Longmore, G. D. The action of Discoidin Domain Receptor 2 in basal tumor cells and stromal Cancer Associated Fibroblasts is critical for breast cancer metastasis. *Cell Rep.* **15**, 2510–2523 (2016).
 55. Simpkins, S. A., Hanby, A. M., Holliday, D. L. & Speirs, V. Clinical and functional significance of loss of caveolin-1 expression in breast cancer-associated fibroblasts. *J. Pathol.* **227**, 490–498 (2012).
 56. Goetz, J. G., Minguet, S., Navarro-Lérida, I., Lazcano, J. J., Samaniego, R., Calvo, E., Tello, M., Osteso-Ibáñez, T., Pellinen, T., Echarri, A., Cerezo, A., Klein-Szanto, A. J. P.,

- Garcia, R., Keely, P. J., Sánchez-Mateos, P., Cukierman, E. & Del Pozo, M. A. Biomechanical remodeling of the microenvironment by stromal Caveolin-1 favors tumor invasion and metastasis. **146**, 148–163 (2011).
57. Connell, J. T. O., Sugimoto, H., Cooke, V. G., Macdonald, B. a & Mehta, A. I. VEGF-A and Tenascin-C produced by S100A4+ stromal cells are important for metastatic colonization. (2011) doi:10.1073/pnas.1109493108/-/DCSupplemental.www.pnas.org/cgi/doi/10.1073/pnas.1109493108.
 58. Yu, Y., Xiao, C.-H., Tan, L.-D., Wang, Q.-S., Li, X.-Q. & Feng, Y.-M. Cancer-associated fibroblasts induce epithelial–mesenchymal transition of breast cancer cells through paracrine TGF- β signalling. *Br. J. Cancer* **110**, 724–732 (2014).
 59. Chaffer, C. L. & Weinberg, R. a. A perspective on cancer cell metastasis. *Science* **331**, 1559–64 (2011).
 60. Lo, A., Wang, L.-C. S., Scholler, J., Monslow, J., Avery, D., Newick, K., O'Brian, S., Evans, R. A., Bajor, D. J., Clendenin, C., Durham, A. C., Buza, E. L., Vonderheide, R. H., June, C. H., Albelda, S. M. & Pure, E. Tumor-promoting desmoplasia is disrupted by depleting FAP- expressing stromal cells. *Cancer Res.* **75**, 2800–2810 (2015).
 61. Loeffler, M., Krüger, J. A., Niethammer, A. G. & Reisfeld, R. A. Targeting tumor-associated fibroblasts improves cancer chemotherapy by increasing intratumoral drug uptake. *J. Clin. Invest.* **116**, 1955–1962 (2006).
 62. Yauch, R. L., Gould, S. E., Scales, S. J., Tang, T., Tian, H., Ahn, C. P., Marshall, D., Fu, L., Januario, T., Kallop, D., Nannini-Pepe, M., Kotkow, K., Marsters, J. C., Rubin, L. L. & de Sauvage, F. J. A paracrine requirement for hedgehog signalling in cancer. *Nature* **455**, 406–410 (2008).
 63. Rhim, A. D., Oberstein, P. E., Thomas, D. H., Mirek, E. T., Palermo, F., Sastra, S. A., Dekleva, E. N., Saunders, T., Becerra, C. P., Tattersall, I. W., Westphalen, C. B., Kitajewski, J., Fernandez-barrena, M. G., Fernandez-zapico, M. E., Iacobuzzio-donahue,

- C., Olive, K. P. & Stanger, B. Z. Stromal elements act to restrain, rather than support, pancreatic ductal adenocarcinoma. *Nat. Rev. Cancer* **14**, 735–747 (2014).
64. Ozdemir, B. C., Pentcheva-Hoang, T., Carstens, J. L., Zheng, X., Wu, C-C., Simpson, T. R., Laklai, H., Sugimoto, H., Kahlert, C., Novitskiy, S. V., De Jesus-Acosta, A., Sharma, P., Heidari, P., Mahmood, U., Chin, L., Moses, H. L., Weaver, V. L., Maitra, A., Allison, J. P., LeBleu, V. S., Kalluri, R. Depletion of carcinoma-associated fibroblasts and fibrosis induces immunosuppression and accelerates pancreas cancer with reduced survival. *Cancer Cell* **25**, 719–34 (2014).
 65. Kalluri, R. The biology and function of fibroblasts in cancer. *Nat. Rev. Cancer* **16**, 582–598 (2016).
 66. Pavlides, S., Tsirigos, A., Vera, I., Flomenberg, N., Frank, P. G., Casimiro, M. C., Wang, C., Fortina, P., Addya, S., Pestell, R. G., Martinez-Outschoorn, U. E., Sotgia, F. & Lisanti, M. P. Loss of stromal caveolin-1 leads to oxidative stress, mimics hypoxia and drives inflammation in the tumor microenvironment, conferring the ‘reverse Warburg effect’: A transcriptional informatics analysis with validation. *Cell Cycle* **9**, 2201–2219 (2010).
 67. Moffitt, R. A., Marayati, R., Flate, E. L., Volmar, K. E., Loeza, S. G. H., Hoadley, K. A., Rashid, N. U., Williams, L. A., Eaton, S. C., Chung, A. H., Smyla, J. K., Anderson, J. M., Kim, H. J., Bentrem, D. J., Talamonti, M. S., Iacobuzio-Donahue, C. A., Hollingsworth, M. A. & Yeh, J. J. Virtual microdissection identifies distinct tumor- and stroma-specific subtypes of pancreatic ductal adenocarcinoma. *Nat. Genet.* **47**, 1168–1178 (2015).
 68. Nelson, D. L. & Cox, M. M. *Lehninger Principles of Biochemistry, Fourth Edition*. (2004).
 69. Warburg, O., Wind, F. & Negelein, E. THE METABOLISM OF TUMORS IN THE BODY. *J. Gen. Physiol.* **8**, 519–530 (1927).
 70. Fiaschi, T., Marini, A., Giannoni, E., Taddei, M. L., Gandellini, P., De Donatis, A., Lanciotti, M., Semi, S., Cirri, P. & Chiarugi, P. Reciprocal metabolic reprogramming through lactate shuttle coordinately influences tumor-stroma interplay. *Cancer Res.* **72**,

5130–5140 (2012).

71. Guido, C., Whitaker-Menezes, D., Capparelli, C., Balliet, R., Lin, Z., Pestell, R. G., Howell, A., Aquila, S., Ando, S., Martinez-Outschoorn, U., Sotgia, F. & Lisanti, M. P. Metabolic reprogramming of cancer-associated fibroblasts by TGF- β drives tumor growth: Connecting TGF- β signaling with 'Warburg- like' cancer metabolism and L-lactate production. *Cell Cycle* **11**, 3019–3035 (2012).
72. Pavlides, S., Whitaker-Menezes, D., Castello-Cros, R., Flomenberg, N., Witkiewicz, A. K., Frank, P. G., Casimiro, M. C., Wang, C., Fortina, P., Addya, S., Pestell, R. G., Martinez-Outschoorn, U. E., Sotgia, F. & Lisanti, M. P. The reverse Warburg effect: Aerobic glycolysis in cancer associated fibroblasts and the tumor stroma. *Cell Cycle* **8**, 3984–4001 (2009).
73. Roy, A. & Bera, S. CAF cellular glycolysis: linking cancer cells with the microenvironment. *Tumor Biol.* **37**, 8503–8514 (2016).
74. Yang, L., Achreja, A., Yeung, T-L., Mangala, L. S., Jiang, D., Han, C., Baddour, J., Marini, J. C., Ni, J., Nakahara, R., Wahlig, S., Chiba, L., Kim, S. H., Morse, J., Pradeep, S., Nagaraja, A. S., Haemmerle, M., Kyunghee, N., Derichswiler, M., Plackemeier, T., Mercado-Urbe, I., Lopez-Berestein, G., Moss, T., Ram, P. T., Liu, J., Lu, X., Mok, S. C., Sood, A. K., Nagrath, D. Targeting Stromal Glutamine Synthetase in Tumors Disrupts Tumor Microenvironment-Regulated Cancer Cell Growth. *Cell Metab.* **24**, 685–700 (2016).
75. Fantozzi, A. & Christofori, G. Mouse models of breast cancer metastasis. *Breast Cancer Res.* **8**, 212 (2006).
76. Lin, E. Y., Jones, J. G., Li, P., Zhu, L., Whitney, K. D., Muller, W. J. & Pollard, J. W. Progression to Malignancy in the Polyoma Middle T Oncoprotein Mouse Breast Cancer Model Provides a Reliable Model for Human Diseases. *Am. J. Pathol.* **163**, 2113–2126 (2003).

77. LeBleu, V. S., Taduri, G., O'Connell, J., Teng, Y., Cooke, V. G., Woda, C., Sugimoto, H. & Kalluri, R. Origin and Function of Myofibroblasts in Kidney Fibrosis. *Nat. Med.* **19**, 1047–1053 (2013).
78. Cooke, V. G., LeBleu, V. S., Keskin, D., Khan, Z., O'Connell, J. T., Teng, Y., Duncan, M. B., Xie, L., Maeda, G., Vong, S., Sugimoto, H., Rocha, R. M., Damascena, A., Brentani, R. R. & Kalluri, R. Pericyte Depletion Results in Hypoxia-Associated Epithelial-to-Mesenchymal Transition and Metastasis Mediated by Met Signaling Pathway. *Cancer Cell* **21**, 66–81 (2012).
79. Chytil, A., Magnuson, M. A., Wright, C. V. E. & Moses, H. L. Conditional inactivation of the TGF- β type II receptor using Cre: Lox. *Genesis* **32**, 73–75 (2002).
80. Morsut, L., Yan, K. P., Enzo, E., Aragona, M., Soligo, S. M., Wendling, O., Mark, M., Khetchoumian, K., Bressan, G., Chambon, P., Dupont, S., Losson, R. & Piccolo, S. Negative control of Smad activity by ectodermin/Tif1 γ patterns the mammalian embryo. *Development* **137**, 2571–2578 (2010).
81. Srinivas, S., Watanabe, T., Lin, C. S., William, C. M., Tanabe, Y., Jessell, T. M. & Costantini, F. Cre reporter strains produced by targeted insertion of EYFP and ECFP into the ROSA26 locus. *BMC Dev. Biol.* **1**, 1–8 (2001).
82. Lebleu, V. S., Teng, Y., Charytan, D., Sugimoto, H., Kalluri, R., Israel, B. & Medical, D. Identification of Human Epididymis Protein-4 as a Novel Fibroblast-Derived Mediator of Fibrosis. *Nat. Med.* **19**, 227–231 (2013).
83. Iwano, M., Fischer, A., Okada, H., Plieth, D., Xue, C., Danoff, T. M. & Neilson, E. G. Conditional Abatement of Tissue Fibrosis Using Nucleoside Analogs to Selectively Corrupt DNA Replication in Transgenic Fibroblasts. *Mol. Ther.* **3**, 149–159 (2001).
84. Carstens, J. L., Correa de Sampaio, P., Yang, D., Barua, S., Wang, H., Rao, A., Allison, J. P., LeBleu, V. S. & Kalluri, R. Spatial computation of intratumoral T cells correlates with survival of patients with pancreatic cancer. *Nat. Commun.* **8**, 15095 (2017).

85. Eikesdal, H. P., Sugimoto, H., Birrane, G., Maeshima, Y., Cooke, V. G., Kieran, M. & Kalluri, R. Identification of amino acids essential for the antiangiogenic activity of tumstatin and its use in combination antitumor activity. *Proc. Natl. Acad. Sci. U. S. A.* **105**, 15040–15045 (2008).
86. Sugimoto, H., Mundel, T. M., Kieran, M. W. & Kalluri, R. Identification of fibroblast heterogeneity in the tumor microenvironment. *Cancer Biol. Ther.* **5**, 1640–1646 (2006).
87. Bartoschek, M., Oskolkov, N., Bocci, M., Lövrot, J., Larsson, C., Sommarin, M., Madsen, C. D., Lindgren, D., Pekar, G., Karlsson, G., Ringnér, M., Bergh, J., Björklund, Å. & Pietras, K. Spatially and functionally distinct subclasses of breast cancer-associated fibroblasts revealed by single cell RNA sequencing. *Nat. Commun.* **9**, (2018).
88. Elwakeel, E., Brüggemann, M., Fink, A. F., Schulz, M. H., Schmid, T., Savai, R., Brüne, B., Zarnack, K. & Weigert, A. Phenotypic plasticity of fibroblasts during mammary carcinoma development. *Int. J. Mol. Sci.* **20**, (2019).
89. Ahn, S., Cho, J., Sung, J., Lee, J. E., Nam, S. J., Kim, K. M. & Cho, E. Y. The prognostic significance of tumor-associated stroma in invasive breast carcinoma. *Tumor Biol.* **33**, 1573–1580 (2012).
90. Dennison, J. B., Shahmoradgoli, M., Liu, W., Ju, Z., Meric-Bernstam, F., Perou, C. M., Sahin, A., Welm, A. L., Oesterreich, S., Sikora, M. J., Brown, R. E. & Mills, G. B. High intra-tumoral stromal content defines Reactive breast cancer as a low-risk breast cancer subtype. *Clin. Cancer Res.* (2016) doi:10.1158/1078-0432.CCR-16-0171.
91. Costa, A., Kieffer, Y., Alix Scholer-Dahirel, A., Pelon, F., Bourachot, B., Cardon, M., Sirven, P., Magagna, I., Fuhrmann, L., Bernard, C., Bonneau, C., Kondratova, M., Kuperstein, I., Zinovyev, A., Givel, A-M., Parrini, M-C., Soumelis, V., Vincent-Salomon, A., Mechta-Grigoriou, F. Fibroblast Heterogeneity and Immunosuppressive Environment in Human Breast Cancer. *Cancer Cell* **33**, 463-479.e10 (2018).
92. Sugimoto, H., Mundel, T. M., Kieran, M. W. & Kalluri, R. Identification of Fibroblast

- Heterogeneity in the Tumor Microenvironment. *Cancer Biol. Ther.* 1640–1646 (2006).
93. Morgan-Bathke, M., Harteneck, D., Jaeger, P., Sondergaard, E., Karwoski, R., Espinosa De Ycaza, A., Carranza-Leon, B. G., Faubion, W. A., Oliveira, A. M. & Jensen, M. D. Comparison of Methods for Analyzing Human Adipose Tissue Macrophage Content. *Obesity* **25**, 2100–2107 (2017).
 94. Brend, T. & Holley, S. A. Zebrafish Whole Mount High-Resolution Double Fluorescent In Situ Hybridization. *JoVE* **25**, 3–5 (2009).
 95. Tse, J. C. Functional Heterogeneity of Fibroblasts in Cancer Progression and Metastasis. *Harvard Univ.* (2011) doi:10.16194/j.cnki.31-1059/g4.2011.07.016.
 96. Maeda, T., Alexander, C. M. & Friedl, A. Induction of Syndecan-1 Expression in Stromal Fibroblasts Promotes Proliferation of Human Breast Cancer Cells. *Cancer Res.* **64**, 612–621 (2004).
 97. Sadlonova, A., Novak, Z., Johnson, M. R., Bowe, D. B., Gault, S. R., Page, G. P., Thottassery, J. V., Welch, D. R. & Frost, A. R. Breast fibroblasts modulate epithelial cell proliferation in three-dimensional in vitro co-culture. *Breast Cancer Res.* **7**, (2005).
 98. Gache, C., Berthois, Y., Martin, P. M. & Saez, S. Positive regulation of normal and tumoral mammary epithelial cell proliferation by fibroblasts in coculture. *Vitr. Cell. Dev. Biol. - Anim.* **34**, 347–351 (1998).
 99. Su, S., Chen, J., Yao, H., Liu, J., Yu, S., Lao, L., Wang, M., Luo, M., Xing, Y., Chen, F., Huang, D., Zhao, J., Yang, L., Liao, D., Su, F., Li, M., Liu, Q. & Song, E. CD10+GPR77+Cancer-Associated Fibroblasts Promote Cancer Formation and Chemoresistance by Sustaining Cancer Stemness. *Cell* **172**, 841-856.e16 (2018).
 100. Bissell, M. J. & Radisky, D. Putting tumours in context. *Nat. Rev. Cancer* **1**, 46–54 (2001).
 101. Liao, D., Luo, Y., Markowitz, D., Xiang, R. & Reisfeld, R. A. Cancer Associated Fibroblasts Promote Tumor Growth and Metastasis by Modulating the Tumor Immune Microenvironment in a 4T1 Murine Breast Cancer Model. *PLoS One* **4**, e7965 (2009).

102. Tran, E., Chinnasamy, D., Yu, Z., Morgan, R. A., Lee, C. C. R., Restifo, N. P. & Rosenberg, S. A. Immune targeting of fibroblast activation protein triggers recognition of multipotent bone marrow stromal cells and cachexia. *J. Exp. Med.* **210**, 1065–1068 (2013).
103. Wang, L. C. S., Lo, A., Scholler, J., Sun, J., Majumdar, R. S., Kapoor, V., Antzis, M., Cotner, C. E., Johnson, L. A., Durham, A. C., Solomides, C. C., June, C. H., Puré, E. & Albelda, S. M. Targeting fibroblast activation protein in tumor stroma with chimeric antigen receptor T cells can inhibit tumor growth and augment host immunity without severe toxicity. *Cancer Immunol. Res.* **2**, 154–166 (2014).
104. Serini, G. & Gabbiani, G. Mechanisms of Myofibroblast Activity and Phenotypic Modulation. *Exp. Cell Res.* **250**, 273–283 (1999).
105. Bissell, M. J., Kenny, P. A. & Radisky, D. C. Microenvironmental Regulators of Tissue Structure and Function Also Regulate Tumor Induction and Progression: The Role of Extracellular Matrix and Its Degrading Enzymes. (2010)
doi:10.1101/sqb.2005.70.013.Microenvironmental.
106. Ronnov-jessen, L., Petersen, O. W., Koteliansky, V. E. & Bissell, M. J. The Origin of the Myofibroblasts in Breast Cancer. *J Clin Invest* **95**, 859–873 (1995).
107. Yamashita, M., Ogawa, T., Zhang, X., Hanamura, N., Kashikura, Y., Takamura, M., Yoneda, M. & Shiraishi, T. Role of stromal myofibroblasts in invasive breast cancer: Stromal expression of alpha-smooth muscle actin correlates with worse clinical outcome. *Breast Cancer* **19**, 170–176 (2012).
108. Garin-Chesa, P., Old, L. J. & Rettig, W. J. Cell surface glycoprotein of reactive stromal fibroblasts as a potential antibody target in human epithelial cancers. *Proc. Natl. Acad. Sci.* **87**, 7235–7239 (1990).
109. Lo, a., Wang, L.-C. S., Scholler, J., Monslow, J., Avery, D., Newick, K., O'Brien, S., Evans, R. a., Bajor, D. L., Clendenin, C., Durham, a. C., Buza, E. L., Vonderheide, R. H.,

- June, C. H., Albelda, S. M. & Pure, E. Tumor-promoting desmoplasia is disrupted by depleting FAP-expressing stromal cells. *Cancer Res.* **75**, 2800–2811 (2015).
110. Joyce, J. A. & Fearon, D. T. T cell exclusion, immune privilege, and the tumor microenvironment. *Science* (80-.). **348**, 74–80 (2015).
 111. Joyce, J. A. & Pollard, J. W. Microenvironmental regulation of metastasis. *Nat. Rev. Cancer* **9**, 239–52 (2009).
 112. Gordon, S. R., Maute, R. L., Dulken, B. W., Hutter, G., George, B. M., McCracken, M. N., Gupta, R., Tsai, J. M., Sinha, R., Corey, D., Ring, A. M., Connolly, A. J. & Weissman, I. L. PD-1 expression by tumour-associated macrophages inhibits phagocytosis and tumour immunity. *Nature* **545**, 495–499 (2017).
 113. Öhlund, D., Handly-Santana, A., Biffi, G., Elyada, E., Almeida, A. S., Ponz-Sarvisé, M., Corbo, V., Oni, T. E., Hearn, S. A., Lee, E. J., Chio, I. I. C., Hwang, C.-I., Tiriác, H. Baker, L. A., Engle, D. D., Feig, C., Kultti, A., Egeblad, M., Fearon, D. T., Crawford, J. M., Clevers, H., Park, Y., Tuveson, D. A. Distinct populations of inflammatory fibroblasts and myofibroblasts in pancreatic cancer. 579–596 (2017) doi:10.1084/jem.20162024.
 114. Kim, J., de Sampaio, P. C., Lundy, D. M., Peng, Q., Evans, K. W., Sugimoto, H., Gagea, M., Kienast, Y., Amaral, N. S. do, Rocha, R. M., Eikesdal, H. P., Lønning, P. E., Meric-Bernstam, F. & LeBleu, V. S. Heterogeneous perivascular cell coverage affects breast cancer metastasis and response to chemotherapy. *JCI Insight* **1**, 1–17 (2016).
 115. Keskin, D., Kim, J., Cooke, V. G., Wu, C.-C., Sugimoto, H., Gu, C., De Palma, M., Kalluri, R. & LeBleu, V. S. Targeting Vascular Pericytes in Hypoxic Tumors Increases Lung Metastasis via Angiopoietin-2. *Cell Rep.* **10**, 1066–1081 (2015).
 116. Paulsson, J., Sjöblom, T., Micke, P., Pontén, F., Landberg, G., Heldin, C.-H., Bergh, J., Brennan, D. J., Jirstrom, K. & Ostman, A. Prognostic significance of stromal platelet-derived growth factor beta-receptor expression in human breast cancer. *Am. J. Pathol.* **175**, 334–341 (2009).

117. Barsoum, I. B., Koti, M., Siemens, D. R. & Graham, C. H. Mechanisms of hypoxia-mediated immune escape in cancer. *Cancer Res.* **74**, 7185–7190 (2014).
118. Joyce, J. A. & Pollard, J. W. Microenvironmental regulation of metastasis. *Nat. Rev. Cancer* **9**, 239–252.
119. Kraman, M., Bambrough, P. J., Arnold, J. N., Roberts, E. W., Magiera, L., Jones, J. O., Gopinathan, A., Tuveson, D. A. & Fearon, D. T. Suppression of Antitumor Immunity by Stromal Cells Expressing Fibroblast Activation Protein alpha. *Science (80-.)*. **330**, 827–830 (2010).
120. Arnold, J. N., Magiera, L., Kraman, M. & Fearon, D. T. Tumoral immune suppression by macrophages expressing fibroblast activation protein- α and heme oxygenase-1. *Cancer Immunol. Res.* **2**, 121–126 (2014).
121. Roberts, E. W. , Deonarine, A., Jones, J. O., Denton, A. E., Feig, C., Lyons, S. K., Espeli, M., Kraman, M., McKenna, B., Wells, R. J. B., Zhao, Q., Caballero, O. L., Larder, R. Coll, A. P., O'Rahilly, S., Brindle, K. M., Teichmann, S. A., Tuveson, D. A., Fearon, D. T. Depletion of stromal cells expressing fibroblast activation protein- α from skeletal muscle and bone marrow results in cachexia and anemia. *J. Exp. Med.* **210**, 1137–51 (2013).
122. Tchou, J., Zhang, P. J., Bi, Y., Satija, C., Marjumdar, R., Stephen, T. L., Lo, A., Chen, H., Mies, C., June, C. H., Conejo-Garcia, J. & Puré, E. Fibroblast activation protein expression by stromal cells and tumor-associated macrophages in human breast cancer. *Hum. Pathol.* **44**, 2549–2557 (2013).
123. Ren, M., Liu, F., Zhu, Y., Li, Y., Lang, R., Fan, Y., Gu, F., Zhang, X. & Fu, L. Absence of caveolin-1 expression in carcinoma-associated fibroblasts of invasive micropapillary carcinoma of the breast predicts poor patient outcome. *Virchows Arch.* **465**, 291–298 (2014).
124. Mercier, I., Casimiro, M. C., Wang, C., Rosenberg, A. L., Quong, J., Minkeu, A., Allen, K. G., Danilo, C., Sotgia, F., Bonuccelli, G., Jasmin, J.-F., Xu, H., Bosco, E., Aronow, B.,

- Witkiewicz, A., Pestell, R. G., Knudsen, E. S. & Lisanti, M. P. Human breast cancer-associated fibroblasts (CAFs) show caveolin-1 downregulation and RB tumor suppressor functional inactivation: Implications for the response to hormonal therapy. *Cancer Biol. Ther.* **7**, 1212–1225 (2008).
125. Whitaker-Menezes, D., Martinez-Outschoorn, U. E., Lin, Z., Ertel, A., Flomenberg, N., Witkiewicz, A. K., Birbe, R. C., Howell, A., Pavlides, S., Gandara, R., Pestell, R. G., Sotgia, F., Philp, N. J. & Lisanti, M. P. Evidence for a stromal-epithelial “lactate shuttle” in human tumors: MCT4 is a marker of oxidative stress in cancer-associated fibroblasts. *Cell Cycle* **10**, 1772–1783 (2011).
 126. Martinez-Outschoorn, U. E., Lisanti, M. P. & Sotgia, F. Catabolic cancer-associated fibroblasts transfer energy and biomass to anabolic cancer cells, fueling tumor growth. *Semin. Cancer Biol.* **25**, 47–60 (2014).
 127. Martinez-Outschoorn, U. E., Whitaker-Menezes, D., Pavlides, S., Chiavarina, B., Bonuccelli, G., Trimmer, C., Tsirigos, A., Migneco, G., Witkiewicz, A. K., Balliet, R., Mercier, I., Wang, C., Flomenberg, N., Howell, A., Lin, Z., Caro, J., Pestell, R. G., Sotgia, F., Lisanti, M. P. The autophagic tumor stroma model of cancer or ‘battery-operated tumor growth’: A simple solution to the autophagy paradox. *Cell Cycle* **9**, 4297–4306 (2010).
 128. Pavlides, S., Tsirigos, A., Migneco, G., Whitaker-Menezes, D., Chiavarina, B., Flomenberg, N., Frank, P. G., Casimiro, M. C., Wang, C., Pestell, R. G., Martinez-Outschoorn, U. E., Howell, A., Sotgia, F. & Lisanti, M. P. The autophagic tumor stroma model of cancer: Role of oxidative stress and ketone production in fueling tumor cell metabolism. *Cell Cycle* **9**, 3485–3505 (2010).
 129. Ko, Y. H., Lin, Z., Flomenberg, N., Pestell, R. G., Howell, A., Sotgia, F., Lisanti, M. P. & Martinez-Outschoorn, U. E. Glutamine fuels a vicious cycle of autophagy in the tumor stroma and oxidative mitochondrial metabolism in epithelial cancer cells: Implications for

- preventing chemotherapy resistance. *Cancer Biol. Ther.* **12**, 1085–1097 (2011).
130. Semenza, G. L. HIF-1 - upstream and downstream of cancer metabolism.pdf. **20**, 1–10 (2011).
 131. Zhang, D., Wang, Y., Shi, Z., Liu, J., Sun, P., Hou, X., Zhang, J., Zhao, S., Zhou, B. P. & Mi, J. Metabolic Reprogramming of Cancer-Associated Fibroblasts by IDH3 α Downregulation. *Cell Rep.* **10**, 1335–1348 (2015).
 132. Fiegl, H., Millinger, S., Goebel, G., Müller-Holzner, E., Marth, C., Laird, P. W. & Widschwendter, M. Breast cancer DNA methylation profiles in cancer cells and tumor stroma: Association with HER-2/neu status in primary breast cancer. *Cancer Res.* **66**, 29–33 (2006).
 133. Hu, M., Yao, J., Cai, L., Bachman, K. E., Van Den Brûle, F., Velculescu, V. & Polyak, K. Distinct epigenetic changes in the stromal cells of breast cancers. *Nat. Genet.* **37**, 899–905 (2005).
 134. Shahrzad, S., Bertrand, K., Minhas, K. & Coomber, B. L. Induction of DNA hypomethylation by tumor hypoxia. *Epigenetics* **2**, 119–125 (2007).
 135. Vo, A. P. Glucose Metabolism in Cancer-Associated Fibroblasts. *Harvard Univ.* (2013) doi:10.1029/91JD03139.
 136. Lisanti, M. P., Martinez-Outschoorn, U. E. & Sotgia, F. Oncogenes induce the cancer-associated fibroblast phenotype: Metabolic symbiosis and ‘fibroblast addiction’ are new therapeutic targets for drug discovery. *Cell Cycle* **12**, 2723–2732 (2013).
 137. Koukourakis, M. I., Giatromanolaki, A., Harris, A. L. & Sivridis, E. Comparison of metabolic pathways between cancer cells and stromal cells in colorectal carcinomas: a metabolic survival role for tumor-associated stroma. *Cancer Res.* **66**, 632–637 (2006).
 138. Migneco, G., Whitaker-Menezes, D., Chiavarina, B., Castello-Cros, R., Pavlides, S., Pestell, R. G., Fatatis, A., Flomenberg, N., Tsigos, A., Howell, A., Martinez-outschoorn, U. E., Sotgia, F. & Lisanti, M. P. Glycolytic cancer associated fibroblasts promote breast

- cancer tumor growth, without a measurable increase in angiogenesis: Evidence for stromal-epithelial metabolic coupling. *Cell Cycle* **9**, 2412–2422 (2010).
139. Stincone, A., Prigione, A., Cramer, T., Wamelink, M. M. C., Campbell, K., Cheung, E., Olin-Sandoval, V., Grüning, N.-M., Krüger, A., Tauqeer Alam, M., Keller, M. A., Breitenbach, M., Brindle, K. M., Rabinowitz, J. D. & Ralser, M. The return of metabolism: biochemistry and physiology of the pentose phosphate pathway *Anna*. **90**, 927–963 (2016).
 140. Mitchell, M. I. & Engelbrecht, A. M. Metabolic hijacking: A survival strategy cancer cells exploit? *Crit. Rev. Oncol. Hematol.* **109**, 1–8 (2017).
 141. Diers, A. R., Broniowska, K. A., Chang, C., Hogg, N. & Program, R. B. Pyruvate fuels mitochondrial respiration and proliferation of breast cancer cells. *Biochem. J.* **444**, 561–571 (2016).
 142. Gui, D. Y., Sullivan, L. B., Luengo, A., Hosios, A. M., Bush, L. N., Gitego, N., Davidson, S. M., Freinkman, E., Thomas, C. J. & Heiden, M. G. Vander. Environment dictates dependence on mitochondrial complex I for NAD⁺ and aspartate production and determines cancer cell sensitivity to metformin. **24**, 716–727 (2017).
 143. Nakazawa, M. S., Keith, B. & Simon, M. C. Oxygen Availability and Metabolic Adaptations Michael. *Nat Rev Cancer.* **16**, 663–673 (2016).
 144. Rankin, E. B. & Giaccia, A. J. Hypoxic control of metastasis. *Science (80-.).* **352**, 175–180 (2016).
 145. Branco, M. R., Ficz, G. & Reik, W. Uncovering the role of 5-hydroxymethylcytosine in the epigenome. *Nat. Rev. Genet.* **13**, 7–13 (2012).
 146. Scourzac, L., Mouly, E. & Bernard, O. A. TET proteins and the control of cytosine demethylation in cancer. *Genome Med.* **7**, 1–16 (2015).
 147. Beppu, H., Mwizerwa, O. N., Beppu, Y., Dattwyler, M. P., Lauwers, G. Y., Bloch, K. D. & Goldstein, A. M. Stromal inactivation of BMPRII leads to colorectal epithelial overgrowth

- and polyp formation. *Oncogene* **27**, 1063–1070 (2008).
148. Pickup, M. W., Hover, L. D., Polikowsky, E. R., Chytil, A., Gorska, A. E., Novitskiy, S. V., Moses, H. L. & Owens, P. BMPR2 loss in fibroblasts promotes mammary carcinoma metastasis via increased inflammation. *Mol. Oncol.* **9**, 179–191 (2015).
 149. Massagué, J. TGF β signalling in context. *Nat. Rev. Mol. Cell Biol.* **13**, 616–630 (2012).
 150. Carstens, J. L., Shahi, P., Van Tsang, S., Smith, B., Creighton, C. J., Zhang, Y., Seamans, A., Seethammagari, M., Vedula, I., Levitt, J. M., Ittmann, M. M., Rowley, D. R. & Spencer, D. M. FGFR1-WNT-TGF- β signaling in prostate cancer mouse models recapitulates human reactive stroma. **22**, 233–245 (2011).
 151. Kojima, Y., Acar, A., Eaton, E. N., Mellody, K. T., Scheel, C., Ben-Porath, I., Onder, T. T., Wang, Z. C., Richardson, A. L., Weinberg, R. A. & Orimo, A. Autocrine TGF- and stromal cell-derived factor-1 (SDF-1) signaling drives the evolution of tumor-promoting mammary stromal myofibroblasts. *Proc. Natl. Acad. Sci.* **107**, 20009–20014 (2010).
 152. Levy, L. & Hill, C. S. Alterations in components of the TGF- β superfamily signaling pathways in human cancer. *Cytokine Growth Factor Rev.* **17**, 41–58 (2006).
 153. Lu, S., Herrington, H., Reh, D., Weber, S., Bornstein, S., Wang, D., Li, A. G., Tang, C., Siddiqui, Y., Nord, J., Andersen, P., Corless, C. L. & Wang, X. Loss of transforming growth factor β type II receptor promotes metastatic head-and-neck squamous cell carcinoma. *Genes Dev.* **20**, 1331–1342 (2006).
 154. Teng, Y., Kanasaki, K., Bardeesy, N., Sugimoto, H. & Kalluri, R. Deletion of Smad4 in fibroblasts leads to defective chondrocyte maturation and cartilage production in a TGF β type II receptor independent manner. *Biochem. Biophys. Res. Commun.* **407**, 633–639 (2011).
 155. Boomersshine, C. S., Chamberlain, A., Kendall, P., Afshar-Sharif, A. R., Huang, H., Washington, M. K., Lawson, W. E., Thomas, J. W., Blackwell, T. S. & Bhowmick, N. A. Autoimmune pancreatitis results from loss of TGF β signalling in S100A4-positive

- dendritic cells. *Gut* **58**, 1267–1274 (2009).
156. Österreicher, C. H., Penz-österreicher, M., Grivennikov, S. I. & Guma, M. Fibroblast-specific protein 1 identifies an inflammatory subpopulation of macrophages in the liver. (2010) doi:10.1073/pnas.1017547108/-
/DCSupplemental.www.pnas.org/cgi/doi/10.1073/pnas.1017547108.
 157. Achyut, B. R., Bader, D. A., Robles, A. I., Wangsa, D., Harris, C. C., Ried, T. & Yang, L. Inflammation-Mediated Genetic and Epigenetic Alterations Drive Cancer Development in the Neighboring Epithelium upon Stromal Abrogation of TGF- β Signaling. *PLoS Genet.* **9**, (2013).
 158. Andrae, J., Gallini, R. & Betsholtz, C. Role of platelet-derived growth factors in physiology and medicine. *Genes Dev.* **22**, 1276–1312 (2008).
 159. Lederle, W., Stark, H. J., Skobe, M., Fusenig, N. E. & Mueller, M. M. Platelet-derived growth factor-BB controls epithelial tumor phenotype by differential growth factor regulation in stromal cells. *Am. J. Pathol.* **169**, 1767–1783 (2006).
 160. De Wever, O., Nguyen, Q. D., Van Hoorde, L., Bracke, M., Bruyneel, E., Gespach, C. & Mareel, M. Tenascin-C and SF/HGF produced by myofibroblasts in vitro provide convergent pro-invasive signals to human colon cancer cells through RhoA and Rac. *FASEB J.* **18**, 1016–1018 (2004).
 161. Tlsty, T. D. Stromal cells can contribute oncogenic signals. *Semin. Cancer Biol.* **11**, 97–104 (2001).
 162. Karnoub, A. E., Dash, A. B., Vo, A. P., Sullivan, A., Brooks, M. W., Bell, G. W., Richardson, A. L., Polyak, K., Tubo, R. & Weinberg, R. a. Mesenchymal stem cells within tumour stroma promote breast cancer metastasis. *Nature* **449**, 557–63 (2007).
 163. Kim, J., Stein, R. & O'Hare, M. Tumour-Stromal Interactions in Breast Cancer: The Role of Stroma in Tumourigenesis. *Tumour Biol.* **26**, 173–185 (2005).
 164. Bhowmick, N. A., Neilson, E. G. & Moses, H. L. Stromal fibroblasts in cancer initiation

- and progression. *Nature* **432**, 332–337 (2004).
165. Yang, F., Tuxhorn, J. A., Ressler, S. J., McAlhany, S. J., Dang, T. D. & Rowley, D. R. Stromal expression of connective tissue growth factor promotes angiogenesis and prostate cancer tumorigenesis. *Cancer Res.* **65**, 8887–8895 (2005).
 166. Dean, C., Ito, M., Makarenkova, H. P., Faber, S. C. & Lang, R. A. Bmp7 regulates branching morphogenesis of the lacrimal gland by promoting mesenchymal proliferation and condensation. *Development* **131**, 4155–4165 (2004).
 167. Elenbaas, B. & Weinberg, R. A. Heterotypic signaling between epithelial tumor cells and fibroblasts in carcinoma formation. *Exp. Cell Res.* **264**, 169–184 (2001).
 168. Werner, S., Krieg, T. & Smola, H. Keratinocyte-fibroblast interactions in wound healing. *J. Invest. Dermatol.* **127**, 998–1008 (2007).
 169. Herpin, A. & Cunningham, C. Cross-talk between the bone morphogenetic protein pathway and other major signaling pathways results in tightly regulated cell-specific outcomes. *FEBS J.* **274**, 2977–2985 (2007).
 170. Chen, D., Zhao, M. & Mundy, G. R. Bone morphogenetic proteins. *Growth Factors* **22**, 233–241 (2004).
 171. Grijelmo, C., Rodrigue, C., Svrcek, M., Bruyneel, E., Hendrix, A., de Wever, O. & Gespach, C. Proinvasive activity of BMP-7 through SMAD4 /src -independent and ERK/ Rac /JNK -dependent signaling pathways in colon cancer cells. *Cell. Signal.* **19**, 1722–1732 (2007).
 172. Hu, M. C., Wasserman, D., Hartwig, S. & Rosenblum, N. D. p38MAPK Acts in the BMP7-dependent Stimulatory Pathway during Epithelial Cell Morphogenesis and Is Regulated by Smad1. *J. Biol. Chem.* **279**, 12051–12059 (2004).
 173. Ye, L., Lewis-Russell, J. M., Sanders, A. J., Kynaston, H. & Jiang, W. G. HGF/SF up-regulates the expression of bone morphogenetic protein 7 in prostate cancer cells. *Urol. Oncol. Semin. Orig. Investig.* (2008) doi:10.1016/j.urolonc.2007.03.027.

174. Matsumoto, K. & Nakamura, T. Hepatocyte growth factor and the Met system as a mediator of tumor–stromal interactions. *Int. J. Cancer* **119**, 477–483 (2006).
175. Mueller, M. M. & Fusenig, N. E. Friends or foes - Bipolar effects of the tumour stroma in cancer. *Nat. Rev. Cancer* **4**, 839–849 (2004).
176. Derynck, R. & Zhang, Y. E. Smad-dependent and Smad-independent pathways in TGF- β . **4**, (2003).
177. Derynck, R., Akhurst, R. J. & Balmain, a. TGF-beta signaling in tumor suppression and cancer progression. *Nat. Genet.* **29**, 117–29 (2001).
178. Owens, P., Pickup, M. W., Novitskiy, S. V., Giltane, J. M., Gorska, A. E., Hopkins, C. R., Hong, C. C. & Moses, H. L. Inhibition of BMP signaling suppresses metastasis in mammary cancer. *Oncogene* **34**, 2437–2449 (2015).
179. Aranda, F., Buqué, A., Bloy, N., Castoldi, F., Eggermont, A., Cremer, I., Fridman, W. H., Fucikova, J., Galon, J., Spisek, R., Tartour, E., Zitvogel, L., Kroemer, G. & Galluzzi, L. Trial Watch: Adoptive cell transfer for oncological indications. *Oncoimmunology* **4**, (2015).
180. Garber, K. Driving T-cell immunotherapy to solid tumors. *Nat. Biotechnol.* **36**, 215–219 (2018).
181. Sharma, P. & Allison, J. P. Immune checkpoint targeting in cancer therapy: Toward combination strategies with curative potential. *Cell* **161**, 205–214 (2015).
182. Narra, K., Mullins, S. R., Lee, H.-O., Strzemkowski-Brun, B., Magalong, K., Christiansen, V. J., McKee, P. A., Egleston, B., Cohen, S. J., Weiner, L. M., Meropol, N. J. & Cheng, J. D. Phase II trial of single agent Val-boroPro (Talabostat) inhibiting Fibroblast Activation Protein in patients with metastatic colorectal cancer. *Cancer Biol. Ther.* **6**, 1691–1699 (2007).
183. Hingorani, S. R., Zheng, L., Bullock, A. J., Seery, T. E., Harris, W. P., Sigal, D. S., Braithe, F., Ritch, P. S., Zalupski, M. M., Bahary, N., Oberstein, P. E., Wang-Gillam, A., Wu, W., Chondros, D., Jiang, P., Khelifa, S., Pu, J., Aldrich, C., Hendifar, A. E. HALO

- 202: Randomized phase II Study of PEGPH20 Plus Nab-Paclitaxel/Gemcitabine Versus Nab-Paclitaxel/Gemcitabine in Patients With Untreated, Metastatic Pancreatic Ductal Adenocarcinoma. *J. Clin. Oncol.* **36**, 359–366 (2018).
184. Eager, R. M., Casey, C. C., Senzer, N. N., Stephenson, J., Anthony, S. P., O'Day, S. J., Frenette, G., Pavlick, A. C., Jones, B., Uprichard, M. & Nemunaitis, J. Phase II assessment of talabostat and cisplatin in second-line stage IV melanoma. *BMC Cancer* **9**, 1–11 (2009).
 185. Eager, R. M., Cunningham, C. C., Senzer, N., Richards, D. A., Raju, R. N., Jones, B., Uprichard, M. & Nemunaitis, J. Phase II Trial of Talabostat and Docetaxel in Advanced Non-small Cell Lung Cancer. *Clin. Oncol.* **21**, 464–472 (2009).
 186. Amakye, D., Jagani, Z. & Dorsch, M. Unraveling the therapeutic potential of the Hedgehog pathway in cancer. *Nat. Med.* **19**, 1410–1422 (2013).
 187. Feig, C., Jones, J. O., Kraman, M., Wells, R. J. B., Deonarine, A., Chan, D. S., Connell, C. M., Roberts, E. W., Zhao, Q., Caballero, O. L., Teichmann, S. a & Janowitz, T. Targeting CXCL12 from FAP-expressing carcinoma-associated fibroblasts synergizes with anti – PD-L1 immunotherapy in pancreatic cancer. *Proc Natl Acad Sci U S A* **110**, 20212–20217 (2013).
 188. Yang, X., Lin, Y., Shi, Y., Li, B., Liu, W., Yin, W., Dang, Y., Chu, Y., Fan, J. & He, R. FAP Promotes immunosuppression by cancer-associated fibroblasts in the tumor microenvironment via STAT3-CCL2 Signaling. *Cancer Res.* **76**, 4124–4135 (2016).
 189. Keskin, D., Kim, J., Cooke, V. G., Wu, C. C., Sugimoto, H., Gu, C., De Palma, M., Kalluri, R. & LeBleu, V. S. Targeting Vascular Pericytes in Hypoxic Tumors Increases Lung Metastasis via Angiopoietin-2. *Cell Rep.* **10**, 1066–1081 (2015).
 190. Shen, J., Vil, M. D., Prewett, M., Damoci, C., Zhang, H., Li, H., Jimenez, X., Deevi, D. S., Iacolina, M., Kayas, A., Bassi, R., Persaud, K., Rohoza-Asandi, A., Balderes, P., Loizos, N., Ludwig, D. L., Tonra, J., Witte, L., Zhu, Z. Development of a fully human anti-

- PDGFR β antibody that suppresses growth of human tumor xenografts and enhances antitumor activity of an anti-VEGFR2 antibody. *Neoplasia* **11**, 594–604 (2009).
191. Adhane, L., Trail, P. A., Taylor, I. & Wilhelm, S. M. Sorafenib (BAY 43-9006, Nexavar®), a Dual-Action Inhibitor That Targets RAF/MEK/ERK Pathway in Tumor Cells and Tyrosine Kinases VEGFR/PDGFR in Tumor Vasculature. *Methods in Enzymology* (2006) doi:10.1016/S0076-6879(05)07047-3.
 192. Zhang, R., Qi, F., Zhao, F., Li, G., Shao, S., Zhang, X., Yuan, L. & Feng, Y. Cancer-associated fibroblasts enhance tumor-associated macrophages enrichment and suppress NK cells function in colorectal cancer. *Cell Death Dis.* **10**, (2019).
 193. Mace, T. A., Ameen, Z., Collins, A., Wojcik, S., Mair, M., Young, G. S., Fuchs, J. R., Eubank, T. D., Frankel, W. L., Bekaii-Saab, T., Bloomston, M. & Lesinski, G. B. Pancreatic Cancer-Associated Stellate Cells Promote Differentiation of Myeloid-Derived Suppressor Cells in a STAT3- Dependent Manner. *Cancer Res.* **73**, 3007–3018 (2013).
 194. Wang, Y.-H., Israelsen, W. J., Lee, D., Yu, V. W. C., Jeanson, N. T., Clish, C. B., Cantley, L. C., Vander Heiden, M. G. & Scadden, D. T. Cell state-specific metabolic dependency in hematopoiesis and leukemogenesis Ying-Hua. *Cell* **158**, 1309–1323 (2014).
 195. Israelsen, W. J., Dayton, T. L., Davidson, S. M., Fiske, B. P., Hosios, A. M., Bellinger, G., Li, J., Yu, Y., Sasaki, M., Horner, J. W., Burga, L. N., Xie, J., Jurczak, M. J., DePinho, R. A., Clish, C. B., Jacks, T., Kibbey, R. G., Wulf, G. M., Di Vizio, D., Mills, G. B., Cantley, L. C., Vander Heiden, M. G. PKM2 isoform-specific deletion reveals a differential requirement for pyruvate kinase in tumor cells. **155**, (2014).
 196. Tsutsumi, R., Xie, C., Wei, X., Zhang, M., Zhang, X., Flick, L. M., Schwarz, E. M. & O'Keefe, R. J. PGE2 signaling through the EP4 receptor on fibroblasts upregulates RANKL and stimulates osteolysis. *J. Bone Miner. Res.* **24**, 1753–1762 (2009).
 197. Beloueche-Babari, M., Wantuch, S., Galobart, T. C., Koniordou, M., Parkes, H. G., Arunan, V., Chung, Y. L., Eykyn, T. R., Smith, P. D. & Leach, M. O. MCT1 inhibitor

- AZD3965 increases mitochondrial metabolism, facilitating combination therapy and noninvasive magnetic resonance spectroscopy. *Cancer Res.* **77**, 5913–5924 (2017).
198. Noble, R. A., Bell, N., Blair, H., Sikka, A., Thomas, H., Phillips, N., Nakjang, S., Miwa, S., Crossland, R., Rand, V., Televantou, D., Long, A., Keun, H. C., Bacon, C. M., Bomken, S., Critchlow, S. E. & Wedge, S. R. Inhibition of monocarboxyate transporter 1 by AZD3965 as a novel therapeutic approach for diffuse large B-cell lymphoma and burkitt lymphoma. *Haematologica* **102**, 1247–1257 (2017).
 199. Polański, R., Hodgkinson, C. L., Fusi, A., Nonaka, D., Priest, L., Kelly, P., Trapani, F., Bishop, P. W., White, A., Critchlow, S. E., Smith, P. D., Blackhall, F., Dive, C. & Morrow, C. J. Activity of the monocarboxylate transporter 1 inhibitor AZD3965 in small cell lung cancer. *Clin Cancer Res* **20**, 926–937 (2014).
 200. Guan, X., Rodriguez-Cruz, V. & Morris, M. E. Cellular Uptake of MCT1 Inhibitors AR-C155858 and AZD3965 and Their Effects on MCT-Mediated Transport of L-Lactate in Murine 4T1 Breast Tumor Cancer Cells. *AAPS J.* **21**, 13 (2020).
 201. Benjamin, D., Robay, D., Hindupur, S. K., Pohlmann, J., Colombi, M., El-Shemerly, M. Y., Maira, S. M., Moroni, C., Lane, H. A. & Hall, M. N. Dual Inhibition of the Lactate Transporters MCT1 and MCT4 Is Synthetic Lethal with Metformin due to NAD⁺ Depletion in Cancer Cells. *Cell Rep.* (2018) doi:10.1016/j.celrep.2018.11.043.
 202. Todenhöfer, T., Seiler, R., Stewart, C., Moskalev, I., Gao, J., Ladhar, S., Kamjabi, A., Al Nakouzi, N., Hayashi, T., Choi, S., Wang, Y., Frees, S., Daugaard, M., Oo, H. Z., Fisel, P., Schwab, M., Schaeffeler, E., Douglas, J., Hennenlotter, J., Bedke, J., Gibb, E. A., Fazli, L., Stenzl, A., Black, P. C. Selective Inhibition of the Lactate Transporter MCT4 Reduces Growth of Invasive Bladder Cancer. *Mol. Cancer Ther.* **17**, 2746–2755 (2018).
 203. Sun, R. C., Fadia, M., Dahlstrom, J. E., Parish, C. R., Board, P. G. & Blackburn, A. C. Reversal of the glycolytic phenotype by dichloroacetate inhibits metastatic breast cancer cell growth in vitro and in vivo. *Breast Cancer Res. Treat.* **120**, 253–260 (2009).

204. Verma, A., Lam, Y. M., Leung, Y. C., Hu, X., Chen, X., Cheung, E. & Tam, K. Y. Combined use of arginase and dichloroacetate exhibits anti-proliferative effects in triple negative breast cancer cells. *J. Pharm. Pharmacol.* **71**, 306–315 (2019).
205. Woo, S. H., Seo, S. K., Park, Y., Kim, E. K., Seong, M. K., Kim, H. A., Song, J. Y., Hwang, S. G., Lee, J. K., Noh, W. C. & Park, I. C. Dichloroacetate potentiates tamoxifen-induced cell death in breast cancer cells via downregulation of the epidermal growth factor receptor. *Oncotarget* **7**, 59809–59819 (2016).
206. Rustgi, A. K. & El-Serag, H. B. Esophageal carcinoma. *N. Engl. J. Med.* **371**, 2499–2509 (2014).
207. Zhang, H., Feng, Q., Chen, W. D. & Wang, Y. D. HGF/c-MET: A promising therapeutic target in the digestive system cancers. *Int. J. Mol. Sci.* **19**, (2018).
208. Abdelaziz, A. & Vaishampayan, U. Cabozantinib for the treatment of kidney cancer. *Expert Rev. Anticancer Ther.* **17**, 577–584 (2017).
209. Kazandjian, D., Blumenthal, G. M., Chen, H.-Y., He, K., Patel, M., Justice, R., Keegan, P. & Pazdur, R. FDA Approval Summary: Crizotinib for the Treatment of Metastatic Non-Small Cell Lung Cancer With Anaplastic Lymphoma Kinase Rearrangements. *Oncologist* **19**, e5–e11 (2014).
210. Grugan, K. D., Miller, C. G., Yao, Y., Michaylira, C. Z., Ohashi, S., Klein-Szanto, A. J., Diehl, J. A., Herlyn, M., Han, M., Nakagawa, H. & Rustgi, A. K. Fibroblast-secreted hepatocyte growth factor plays a functional role in esophageal squamous cell carcinoma invasion. *Proc. Natl. Acad. Sci. U. S. A.* **107**, 11026–11031 (2010).
211. Owens, P., Pickup, M. W., Novitskiy, S. V., Chytil, A., Gorska, A. E., Aakre, M. E., West, J. & Moses, H. L. Disruption of bone morphogenetic protein receptor 2 (BMPR2) in mammary tumors promotes metastases through cell autonomous and paracrine mediators. *Proc. Natl. Acad. Sci. U. S. A.* **109**, 2814–2819 (2012).
212. Du, H. & Che, G. Genetic alterations and epigenetic alterations of cancer-associated

- fibroblasts (Review). *Oncol. Lett.* **13**, 3–12 (2017).
213. Rønnov-Jessen, L., Petersen, O. W. & Bissell, M. J. Cellular changes involved in conversion of normal to malignant breast: importance of the stromal reaction. *Physiol. Rev.* **76**, 69–125 (1996).
 214. Skalli, O., Pelte, M. F., Peclet, M. C., Gabbiani, G., Gugliotta, P., Bussolati, G., Ravazzola, M. & Orci, L. Alpha-smooth muscle actin, a differentiation marker of smooth muscle cells, is present in microfilamentous bundles of pericytes. *J. Histochem. Cytochem.* **37**, 315–321 (1989).
 215. Mendoza, F. A., Piera-Velazquez, S., Farber, J. L., Feghali-Bostwick, C. & Jimenez, S. A. Endothelial Cells Expressing Endothelial and Mesenchymal Cell Gene Products in Lung Tissue From Patients With Systemic Sclerosis-Associated Interstitial Lung Disease. *Arthritis Rheumatol. (Hoboken, N.J.)* **68**, 210–217 (2016).
 216. Tchou, J., Zhang, J. P., Yingtao, B. & Pure, E. Fibroblast Activation Protein Expression by Stromal Cells and Tumor-Associated Macrophages in Human Breast Cancer. **44**, 2549–2557 (2013).
 217. Micallef, L., Vedrenne, N., Billet, F., Coulomb, B., Darby, I. A. & Desmoulière, A. The myofibroblast, multiple origins for major roles in normal and pathological tissue repair. *Fibrogenesis Tissue Repair* **5**, S5 (2012).
 218. Ronnov-Jessen, L. & Petersen, O. W. Induction of alpha-smooth muscle actin by transforming growth factor-beta 1 in quiescent human breast gland fibroblasts. Implications for myofibroblast generation in breast neoplasia. *Lab. Invest.* **68**, 696–707 (1993).
 219. Shakhov, A. S., Verin, A. D. & Alieva, I. B. [Endothelial cell cytoskeleton reorganization during functional monolayer formation in vitro]. *Tsitologiya* **56**, 36–47 (2014).
 220. Triolo, D., Dina, G., Taveggia, C., Vaccari, I., Porrello, E., Rivellini, C., Domi, T., La Marca, R., Cerri, F., Bolino, A., Quattrini, A. & Previtali, S. C. Vimentin regulates

- peripheral nerve myelination. *Development* **139**, 1359–1367 (2012).
221. Erez, N., Truitt, M., Olson, P. & Hanahan, D. Cancer-Associated Fibroblasts Are Activated in Incipient Neoplasia to Orchestrate Tumor-Promoting Inflammation in an NF- κ B-Dependent Manner. *Cancer Cell* **17**, 135–147 (2010).
 222. Liu, D., Zhang, X., Chen, G., Lu, C. & Dong, H. [Expression of platelet-derived growth factor receptor alpha and its ligand PDGF- A in breast cancer]. *Xi Bao Yu Fen Zi Mian Yi Xue Za Zhi* **27**, 313-314,316 (2011).
 223. Moawad, E. Y. Predicting Effectiveness of Imatinib Mesylate in Tumors Expressing Platelet-Derived Growth Factors (PDGF-AA, PDGF-BB), Stem Cell Factor Ligands and Their Respective Receptors (PDGFR-alpha, PDGFR-beta, and c-kit). *J. Gastrointest. Cancer* **46**, 272–283 (2015).
 224. Zhou, Q., Wei, L., Zhong, C., Fu, S., Bei, Y., Huica, R.-I., Wang, F. & Xiao, J. Cardiac telocytes are double positive for CD34/PDGFR-alpha. *J. Cell. Mol. Med.* **19**, 2036–2042 (2015).
 225. Hirschi, K. K. & D'Amore, P. A. Pericytes in the microvasculature. *Cardiovasc. Res.* **32**, 687–698 (1996).
 226. Goldsmith, E. C., Zhang, X., Watson, J., Hastings, J. & Potts, J. D. The collagen receptor DDR2 is expressed during early cardiac development. *Anat. Rec. (Hoboken)*. **293**, 762–769 (2010).
 227. Lazarides, E. & Balzer Jr., D. R. Specificity of desmin to avian and mammalian muscle cells. *Cell* **14**, 429–438 (1978).
 228. Diaz-Flores, L., Gutierrez, R., Varela, H., Rancel, N. & Valladares, F. Microvascular pericytes: a review of their morphological and functional characteristics. *Histol. Histopathol.* **6**, 269–286 (1991).
 229. Strutz, F., Okada, H., Lo, C. W., Danoff, T., Carone, R. L., Tomaszewski, J. E. & Neilson, E. G. Identification and characterization of a fibroblast marker: FSP1. *J. Cell Biol.* **130**,

- 393–405 (1995).
230. Levy, M. T., McCaughan, G. W., Abbott, C. a., Park, J. E., Cunningham, a. M., Muller, E., Rettig, W. J. & Gorrell, M. D. Fibroblast activation protein: A cell surface dipeptidyl peptidase and gelatinase expressed by stellate cells at the tissue remodelling interface in human cirrhosis. *Hepatology* **29**, 1768–1778 (1999).
231. Minshall, R. D., Sessa, W. C., Stan, R. V., Anderson, R. G. W. & Malik, A. B. Caveolin regulation of endothelial function. *Am. J. Physiol. - Lung Cell. Mol. Physiol.* **285**, 1179–1183 (2003).
232. Scherer, P. E., Lisanti, M. P., Baldini, G., Sargiacomo, M., Mastick, C. C. & Lodish, H. F. Induction of caveolin during adipogenesis and association of GLUT4 with caveolin-rich vesicles. *J. Cell Biol.* **127**, 1233–1243 (1994).